MODULATION OF VOLTAGE-GATED CALCIUM CHANNEL BY A SYNAPTIC PROTEIN AND GANGLIOSIDE

LIN QINGSHU

NATIONAL UNIVERSITY OF SINGAPORE

2015

MODULATION OF VOLTAGE-GATED CALCIUM CHANNEL BY A SYNAPTIC PROTEIN AND GANGLIOSIDE

LIN QINGSHU

(*B.Sc.*, Shanghai Jiao Tong University)

A THESIS SUBMITTED FOR THE DEGREE OF DOCTOR OF PHILOSOPHY

DEPARTMENT OF PHYSIOLOGY

NATIONAL UNIVERSITY OF SINGAPORE

2015

Declaration

I hereby declare that this thesis is my original work and it has been written by me in its entirety. I have duly acknowledged all the sources of information which have been used in the thesis.

This thesis has also not been submitted for any degree in any university previously.

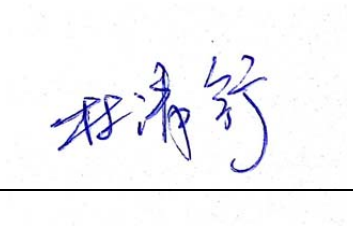

Lin Qingshu

15 January 2015

Acknowledgements

Firstly, I would like to express my special appreciation and thanks to my supervisor Prof Soong Tuck Wah. Among the four years studies and research, Prof Soong has given me constant support and sustainable encouragement to my work. He not only helped me a lot guiding my research journey, but also gave me a lot of useful suggestions for my career.

I would also like to thank all the members of the Ion Channel and Transporter Laboratory for their support, encouragement and friendship, especially Ms. Yu Dejie and Ms. Liang Mui Cheng, who have provided advices and assistances for my projects. Thanks also go to research fellows, Dr. Huang Hua, Dr. Liu Chao, Dr. Katherine Chew and Dr. Wang Juejin for their expertise, precious experiences and critical suggestions to the projects. To my laboratory mates, who are also post-graduate students, Dr. Alex Tai, Dr. Peter Bartels, Dr. Zhai Jing, Mr. Hu Zhenyu, and Mr. Wong Rui Xiong. Thank you very much for the cheerful times we shared. I will always remember the days we did experiments together. Also I would like to thanks lab officer Ms. Yong Tan Fong and research assistant Ms. Wong Yuk Peng and Ms. Chong Pey Rou for their supports on research work and organizing wonderful lab activities.

I want to give gratitude to A/Prof Sanjay Khanna, Dr. Saji Kumar Sreedharan, Dr. Chen Zhi Xiong, Dr. Marc Fivaz and Dr. Shawn Je for the giving me support on research and suggestions to my projects.

Last but not least, I would like to thanks my parents, Lin Ronghao, Wang Ying as well as my girl friend Zhao Ran. Without their support and understanding, this thesis could never have been completed successfully.

I express my sincere thanks to my examiners for making time and effort to examine this thesis.

Table of Content

List of Publications

Lin QS, Yu D, Liang MC, Soong TW, Splice-variant-specific modulation of $Ca_V2.1$ calcium channel by snapin. *(In preparation)*

Lin QS, Miyaji K, Yu D, Chadha A, Soong TW and Yuki N. Effects of Anti-Ganglioside Antibodies on Calcium Influx through the $\alpha_2\delta$ Subunit of $Ca_v2.1$. *(In preparation)*

Abstract

Lin QS, Yu D, Liang MC, Soong TW, Isoform- and Splice-variant-selective Modulation of Voltage-gated Calcium Channels by Snapin: Implications in Synaptic Plasticity, 43th Annual Meeting for Society of Neuroscience; 2013 San Diego.

Lin QS, Chadha A, Soong TW, Yuki N, Anti-ganglioside Antibodies Bidirectionally Modulate the Properties of Voltage-gated Calcium Channel. 8th International Conference of Neurons and Brain Diseases; 2013 Jul 2-4; Singapore.

Summary

Voltage-gated calcium channels play a vital role in triggering the vesicle release in presynaptic terminals. We have identified several molecules in modulating the calcium channel functions. One of our focus is snapin from presynaptic complex, and the other is gangliosides and anti-gangliosides antibodies. We found that snapin could increase current density of voltage-gated calcium channels in an isoform- and splice-variant-selective manner. Notably, the $Ca_V2.1$ and $Ca_V2.2$ channels are mutually exclusively spliced to produce either $Ca_V2.1$[EFa] or $Ca_V2.1$[EFb], and $Ca_V2.2$[EFa] or $Ca_V2.2$[EFb] respectively. Snapin selectively increased the current density of $Ca_V2.1$[EFb] and $Ca_V2.2$[EFa], but not $Ca_V2.1$[EFa] and $Ca_V2.2$[EFb]. Moreover, snapin preferentially modulated $Ca_V1.3$ channel by interacting with the I-II loop region but not on the other calcium channel of Ca_V1 families. In addition, voltage-gated calcium channels were modulated by anti-ganglioside antibodies. The antibodies against ganglioside are found in patient sera of Guillain-Barré syndrome, though the underlying pathogenesis is not clear yet. We discovered that anti-ganglioside antibodies modulated voltage sensing of the Ca^{2+} channel. The opening threshold of voltage-gated calcium channel are either reduced or increased by anti-GM1 and anti-GQ1b antibodies respectively. These interactions between voltage-gated calcium channel and anti-ganglioside antibodies are dependent on the auxiliary $\alpha_2\delta$ subunit of calcium channel.

List of Tables

List of Figures

Abbreviations

AIDP	acute inflammatory demyelinating polyneuropathy
AMAN	acute motor axonal neuropathy
CaM	calmodulin
Ca_V	Voltage-gated calcium channel
CDF	calcium-dependent faciliation
CDI	calcium-dependent inactivation
cDNA	complementary deoxyribonucleic acid
C-terminus	carboxyl-terminus
DAPI	4',6-diamidino-2-phenylindole
DIV	days *in vitro*
DMEM	Dulbecco's Modified Eagle Medium
DNA	deoxyribonucleic acid
EA2	episodic ataxia type 2
E.coli	*Escherichia coli*
EDTA	ethylenediaminetetraacetic acid
EPSC	excitatory post-synaptic current
FBS	fetal bovine serum
FHM1	Familial hemiplegic migraine type 1
GBS	Guillain–Barré syndrome
GST	Glutathione S-transferase
HEK	Human embryonic kidney cell
HBS	HEPES-buffered saline
IHC	inner hair cell
I-V	current-voltage
MAP2	Microtubule-associated protein 2

MFS	Miller Fisher syndrome
mRNA	messenger ribonucleic acid
NMJ	neuromuscular junction
N-terminus	amino-terminus
PBS	phosphate buffered saline
PCR	polymerase chain reaction
PDZ	post-synaptic density protein 95, Drosophila disc large tumour suppressor and zonula occludens-1 protein
PVDF	polyvinylidene difluoride
RIM	Rab3-interacting molecule
SCA6	Spinocerebellar ataxia type 6
SDS-PAGE	sodium dodecyl sulfate Polyacrylamide gel electrophoresis
SNAP-25	synaptosomal-associated protein 25
SNARE	Soluble NSF Attachment Protein Receptor
SSI	steady-state inactivation
sEPSC	spontaneous EPSC
SV	synaptic vesicle
Syt-I	synaptotagmin 1
TBST	Tris-Buffered Saline and Tween 20
VDI	voltage-dependent inactivation
VGCC	voltage-gated calcium channel

Chapter 1 Backgrounds

1.1 Voltage-gated calcium channel

1.1.1 The classification of voltage-gated calcium channel

Voltage-gated calcium channels (VGCC) are a group of pivotal ion channels involved in several cellular functions. VGCCs transduce the electrical input of voltage depolarization into biochemical output of Ca^{2+} ion influx into the cell. These Ca^{2+} ions act as universal messengers to initiate diverse physiological activities such as synaptic transmission, hormone release, muscle contraction, enzymatic activation, gene expression or cellular differentiation (Catterall 2000, Catterall & Few 2008, Evans & Zamponi 2006). The variety of downstream events subsequent to Ca^{2+} influx is achieved by the precise modulations of specific VGCC functions. The voltage-gated calcium channel (Ca_V) is composed of several subunits, forming a hetero-oligometric complex (Takahashi et al 1987). The α_1 subunit is the major pore-forming subunit encoded by 10 distinct genes, which determine the 10 subtypes of Ca_V channels (Tsien et al 1988). Based on genetic homology and pharmacology, these 10 VGCCs could be categorized into three major sub-families, as shown in table 1, and they include Ca_V1 ($Ca_V1.1$, $Ca_V1.2$, $Ca_V1.3$ and $Ca_V1.4$; all are L-type channels), Ca_V2 ($Ca_V2.1$, P/Q type; $Ca_V2.2$, N-type and $Ca_V2.3$ R-type) and Ca_V3 ($Ca_V3.1$, $Ca_V3.2$, $Ca_V3.3$, all are T-type channels) (Ertel et al 2000, Snutch & Reiner 1992).

1.1.2 The subunits of voltage-gated calcium channel

The α_1-subunit is composed of four major domains, called domains I-IV. Each domain contains six trans-membrane segments (S1-S6) and a P-loop region between S5 and S6 forms the selectivity filter that is important for gating ion influx (Heinemann et al 1992, Yu et al 2005). The S4 helix is considered as an important component of the voltage senor and on it is found several positive charged residues including arginine (*R*) and lysine (*K*). The translocation of S4 in response to membrane depolarization is the critical process in opening the voltage-gated calcium channel (Bichet et al 2003, Yi & Jan 2000). The VGCC also contains an intracellular N- and C-terminus and several cytoplasmic loops connecting the domains. These intracellular loops could interact with and be modulated by various proteins including the β subunit, synaptic proteins, calmodulin, G-proteins and various kinases or phosphatases (Catterall 2000).

Table 1.1 Nomenclature and distribution of voltage-gated calcium channels.

Family	Subtype		Distribution
Ca_V1	$Ca_V1.1$		Skeletal Muscle
	$Ca_V1.2$	L-type	Heart, nervous system, smooth muscle, endocrine system
	$Ca_V1.3$		Nervous system, cochlear, endocrine system, sino-atrial node
	$Ca_V1.4$		Retina
Ca_V2	$Ca_V2.1$	P/Q type	Nervous system
	$Ca_V2.2$	N-type	Nervous system
	$Ca_V2.3$	R-type	Nervous system
Ca_V3	$Ca_V3.1$		Nervous system, heart
	$Ca_V3.2$	T-type	Nervous system, heart
	$Ca_V3.3$		Nervous system

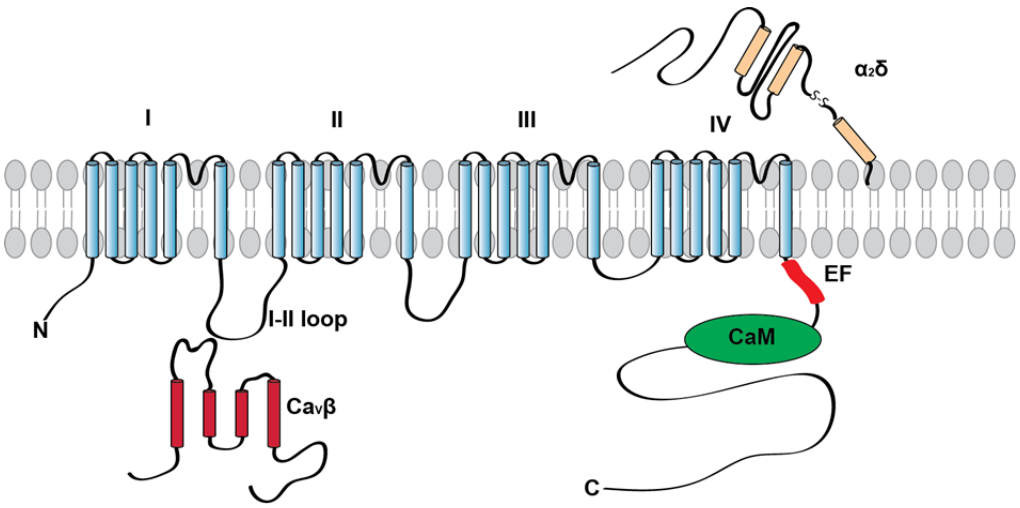

Figure 1.1 Schematic diagrams of the trans-membrane topology and subunit compositions of Ca_V channel.
The α_1 subunit of Ca_V is composed of four major domains (I-IV). Each domain contains six trans-membrane segments (S1-S6). The S4 segment forms the voltage sensor and the loop region between S5 and S6 is responsible for ions gating. The cytoplasmic linkers between the domains are involved in many protein interactions. For example, the I-II loop interacts with $Ca_V\beta$. II-III loop is synaptic protein interaction site (synprint). Pre-IQ, IQ domain and N-terminus of Ca_V1 and Ca_V2 are associated with calmodulin (CaM) binding. Exon 37 of Ca_V1 and Ca_V2 is under alternative splicing and forms EF-hand like domain.
$Ca_V\alpha_2\delta$ subunit is attached to the extracellular membrane and linked with plasma membrane via GPI anchor. The $Ca_V\beta$ binds with the I-II loop of the VGCC. CaM interacts both the N and C-terminus of VGCC in varied local Ca^{2+} concentration. The $Ca_V\gamma$ subunit has been omitted.

Both the Ca_V1 and Ca_V2 sub-families contain auxiliary β- and $\alpha_2\delta$-subunits and/or the γ-subunit (Takahashi et al 1987). Four genes have been found to encode $Ca_V\beta$ subunits (β1-β4) and alternative splicing of these genes generate several $Ca_V\beta$ variants (Buraei & Yang 2010). The $Ca_V\beta$ subunit binds to the I-II loop region of the α_1-subunit and enhances the surface expression of the VGCC (Pragnell et al 1994); (Van Petegem et al 2004). Recent studies from the Zamponi's group have shown that $Ca_V\beta$ influences the ubiquitination of $Ca_V1.2$ channels and therefore regulates the channel's surface expression (Altier et al 2011). $Ca_V\beta$ has been shown to play a role to traffic the Ca_V channel into the cell membrane through binding at the AID domain of the I-II

loop. The absence of the β-subunit would result in the ubiquitination of Ca_V α_1-subunit. Mutations on the β-subunit binding domain (or other proteins competing for the binding of the β-subunit would lead to ubiquitination of the calcium channel and subsequent degradation the channel complex.

The $\alpha_2\delta$-subunit is encoded by four genes ($\alpha_2\delta_1$-$\alpha_2\delta_4$) (Dolphin 2013). The $\alpha_2\delta$ subunit is transcribed by one gene and cleaved into two parts, which is subsequently linked by disulfide bond (Davies et al 2007). The $\alpha_2\delta$-subunit is also involved in trafficking of the calcium channel. Co-expression of $\alpha_2\delta$-subunits augments the calcium channel current in the cell membrane (Arikkath & Campbell 2003). The $\alpha_2\delta$-subunit also plays a crucial role in synaptic vesicle release by recruiting VGCC to the pre-synapse active zone (Hoppa et al 2012). Recent studies have suggested that the $\alpha_2\delta$-subunit is anchored to the plasma membrane by glycerophosphatidylinositol (Davies et al 2010, Kadurin et al 2012).

The γ-subunit is only co-expressed with $Ca_V1.1$, the skeletal muscle L-type channel (Arikkath et al 2003, Campbell et al 1988). It is not clear whether the neuronal type of VGCC also includes the γ-subunit, though the expression of several isoforms of γ-subunit has been found in neuron (Letts et al 1998, Rousset et al 2001).

Several studies have shown that calmodulin (CaM) is associated with VGCC and modulates activity-dependent channel properties, and recently it has been suggested that CaM should be considered as the fourth subunit of the voltage-gated calcium channel complex (Minor &

Findeisen 2010, Peterson et al 1999, Zuhlke et al 1999). The auxiliary subunits are required for the proper function of Ca_V1 and Ca_V2 families, while Ca_V3 families are reconstituted well in the heterologous expression systems with the Ca_V α_1 subunit alone (Perez-Reyes 2003).

1.2 Physiological and pathological properties of voltage-gated calcium channel

1.2.1 $Ca_V2.1$ and $Ca_V2.2$ channels

The $Ca_V2.1$ channel is highly represented in the central and peripheral nervous systems and mediates presynaptic and somatodendritic Ca^{2+} influx (Mori et al 1991, Starr et al 1991). Ca^{2+} influx via the $Ca_V2.1$ channels trigger several Ca^{2+}-related responses. Although $Ca_V2.1$ function could be partially compensated by $Ca_V2.2$, dysfunction of $Ca_V2.1$ has severe consequences. Human *CACNA1A* mutations have been associated with several neurological diseases, including familial hemiplegic migraine type 1 (FHM1), spinocerebellar ataxia type 6 (SCA6) and episodic ataxia type 2 (EA2) (Pietrobon 2010). The $Ca_V2.1$ deficient mice have been reported to suffer from ataxia and motor dysfunction (Jun et al 1999). Over the past ten years, 17 mutations of the *CACNA1A* gene associated with FHM1 have been detected. $Ca_V2.1$ channels with FHM1 related mutations have been shown to exhibit relatively larger currents. The excess Ca^{2+} influx is considered as an underlying mechanism for increased susceptibility of cortical spreading depression (Cao & Tsien 2005, Hans et al 1999, Tottene et al 2002). Other than FHM1, *CACNA1A* mutations associated with EA2

result mostly in the loss-of-function of the channels. The neurodegenerative disease SCA6 is one of the major $Ca_V2.1$ related diseases (Ophoff et al 1996, Zhuchenko et al 1997). It is characterized by late-onset, slow progressive cerebella ataxia and Purkinje cell degeneration in the cerebellum. In patients suffering from SCA6, the expansion of polyglutamine (CAG)n was found in the *CACNA1A* gene. The pathology of SCA6 is closely related with the alternative splicing of $Ca_V2.1$. The CAG repeats are found within the C-terminal alternative exon 47. As such, in human there are two variations of $Ca_V2.1$ channels - with or without exon 47. The expanded (CAG)n repeats will only become toxic when exon 47 is present in the $Ca_V2.1$ channels. As the expression of exon 47 is higher in Purkinje than granule cells, it is proposed that degeneration of cerebellar Purkinje neurons, but not of granule cells, in SCA6 patient results from differential alternative splicing of exon 47 in these neurons.

Similar to $Ca_V2.1$, $Ca_V2.2$ channels are exclusively expressed in the nervous system and Ca^{2+} influx through these channels also triggers synaptic vesicle release in the presynaptic terminals (Nowycky et al 1985, Westenbroek et al 1992, Wheeler et al 1994). The $Ca_V2.2$ knockout mice have mild central nervous system phenotypes due to compensation by $Ca_V2.1$ channels. However, these mice are hyposensitive to pain suggesting the prominent role $Ca_V2.2$ channels play in pain transmission (Hatakeyama et al 2001, Kim et al 2001). The activity of $Ca_V2.2$ could be strongly modulated by a few G-protein

coupled receptors (Bourinet et al 2014, Bourinet et al 1996, Ikeda 1996, Tedford & Zamponi 2006).

1.2.2 Functions and properties of $Ca_V1.3$

The $Ca_V1.3$ channel is differentiated from other L-type of calcium channels by its low-voltage activation threshold. It plays a prominent role in neuronal pace-making in neurons of the suprachiasmatic nucleus (Pennartz et al 2002) and in vesicle release at the ribbon synapse of inner hair cells (IHC) found in the cochlea (Platzer et al 2000).

Deletion of $Ca_V1.3$ gene in the mouse genome resulted in congenital deafness due to the loss of the Ca^{2+} influx into the cochlear inner hair cells. Loss of function of $Ca_V1.3$ due to point mutations have been reported to cause congenital deafness and bradycardia in two families found in Pakistan (Baig et al 2011). More than 90% of the Ca^{2+} current in cochlear IHCs is carried by the $Ca_V1.3$ channels (Platzer et al 2000). These channels are clustered at the ribbon synapse of the inner hair cell and are tethered for synaptic release (Brandt et al 2005). The IHCs are not usually activated by discrete action potentials but by hypo-threshold graded membrane depolarization. Due to its low threshold of activation, the $Ca_V1.3$ mediated Ca^{2+} influx is sensitive to membrane potential change and this ensures the precise response to sound signaling (Goutman 2012) (Striessnig & Koschak 2008).

The $Ca_V1.3$ channels are robustly inactivated by a rise in Ca^{2+} influx. This inactivation effect is mediated via the binding of the Ca^{2+}-sensor

calmodulin to the IQ motif found at the proximal C-terminus of the $Ca_V1.3$ channel. Besides alternative splicing that could remove the expression of the IQ-domain, RNA editing of $Ca_V1.3$ could modify the IQ-domain in a pin-point manner by substituting adenosine to guanosine at the IQ motif. The edited form of $Ca_V1.3$ showed slower Ca^{2+}-dependent inactivation and reduced pace-making spike frequency in the suprachiasmatic nucleus neurons (Huang et al 2012).

1.3 Alternative splicing of voltage-gated calcium channel

1.3.1 Mechanism of alternative splicing

It has been reported that over 70% of genes in the brain are alternatively spliced (Gray et al 2007). Alternative splicing is a process whereby alternative exons of the pre-mRNA combine in multiple arrays to diversify the proteome. That means one gene produces several protein isoforms, which result in the generation of functional diversity.

The common mechanisms for alternative splicing are as follows: (1) One alternative cassette exon could be either included or excluded in the mature mRNA; (2) Two exons of identical size are mutually exclusively included in the transcript; (3) Alternative 5' or 3' of exon could be spliced leading to a relatively longer or shorter exon; (4) Alternative 5' or 3' UTR is included in region that could potentially affect the translation and (5) Intron could be retained in the mature mRNA

transcript. Single pre-mRNA could therefore exhibit multiple splicing patterns (Black 2003, Chen & Manley 2009).

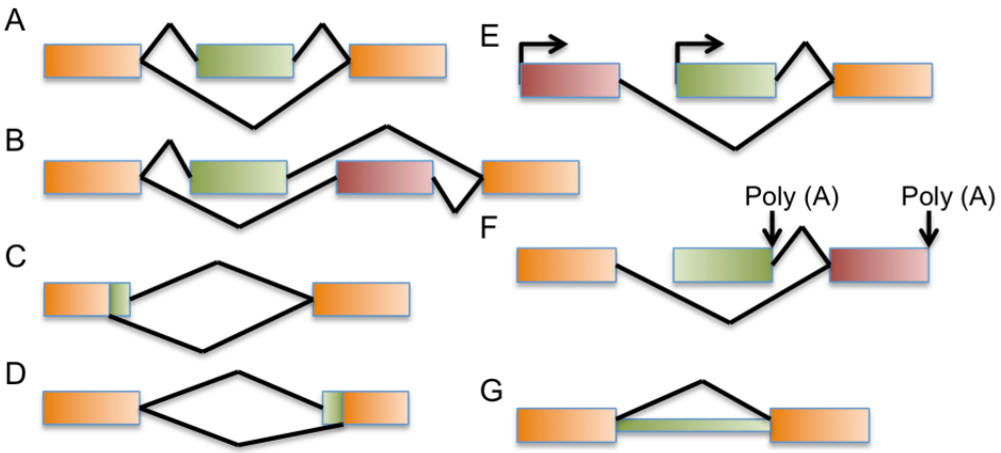

Figure 1.2 Common patterns of alternative splicing.
The constitute exons presence in all mature RNAs were shown in orange box. The alternative RNA segments were shown in green and brown boxes. Multiple splice patterns could happen in one transcript. **A.** Exon can be either included or exclude in mRNA. **B.** Two or more adjacent exons were spliced and only one exon was included in mature RNA. **C, D.** Alternative 5' donor or 3' acceptor splice sites allow the lengthening or shortening of a certain exon. **E, F.** The transcripts may include an alternative 5' promoter or 3' poly (A) site, yielding varied products. **G.** An intron could be either retained or spliced out.

1.3.2 The impact of alternative splicing on voltage-gated calcium channels

Voltage-gated calcium channel is subjected to extensively alternative splicing. The splicing pattern of VGCC has varied impact on the channel physiology and pathology functions (Gray et al 2007, Liao et al 2009).

The C-terminus of $Ca_V1.3$ represents an example of extensive splice sites that have been characterized. The alternative usage of exon 41 acceptor site generates a premature stop codon which skip the IQ motif of $Ca_V1.3$. The truncated $Ca_V1.3$ without IQ domain still conducts the calcium current, but the calcium dependent inactivation is totally abolished (Shen et al 2006). The splicing variant $Ca_V1.3_{\Delta IQ}$ is selectively localized in outer hear cell. The weak CDI of $Ca_V1.3$ found in cochlear support the consistent calcium influx, which is crucial for early development and synaptic transmission (Brandt et al 2005, Yang et al 2006).

In addition, the downstream exon 42 is spliced by exon 42 or 42a, which will generate either long form of $Ca_V1.3$ or short form of $Ca_V1.3$ (Xu & Lipscombe 2001). It is shown that the stop codon found in exon 42a would lead to early truncation immediately after the IQ domain in exon 41, while the $Ca_V1.3$ transcripts carried the exon 42 contains a longer C-terminal. Both long form and short form of $Ca_V1.3$ is ubiquitously found in the nervous system, but the long form and short form of $Ca_V1.3$ exhibits distinct channel properties. The long form of

$Ca_V1.3$ display lower current density and reduced CDI compared to the short-form. The diminished CDI was attributed to CDI-inhibiting region found in the distal C-terminal, which compete the calmodulin binding to IQ domain. This CDI-inhibiting region is only found in long form but not the short form of $Ca_V1.3$ (Liu et al 2010).

Further studies have reported that the alternative splicing variants of $Ca_V1.3$ C-terminals have distinct sensitivity to L-type channel blocker, dihydropyridine. It is shown that full-length $Ca_V1.3_{42}$ and $Ca_V1.3_{\Delta 41}$ channels were associated with higher dihydropyridine sensitivity compared to $Ca_V1.3_{42a}$ (Huang et al 2013).

Alternative splicing of $Ca_V2.1$ has been characterized in rat and human brain or spinal cord (Bourinet et al 1999, Krovetz et al 2000, Soong et al 2002). Studies have reported that several alternative splice sites of $Ca_V2.1$ altered the channel properties. For example, N_{1605}-P_{1606} insertion decreases the sensitivity of $Ca_V2.1$ to specific blocker ω-Aga IVA and the presence of Val_{421} close to I-II loop of $Ca_V2.1$ significantly slowed down the channel inactivation kinetics (Bourinet et al 1999). These splice variants and selective β subunit composition explain the distinct electrophysiological properties between Purkinje cells type (P type) and granule cell type (Q-type) of calcium channel, which are both encoded by *CACNA1A*.

The neurodegenerative disease spinocerebellar ataxia type 6 (SCA6) was one the major related channelopathies (Pietrobon 2010, Zhuchenko et al 1997). It is characterized by the late-onset slow

progressive cerebella ataxia and Purkinje cell degeneration in the cerebellum. In the patient suffered from the SCA6, the expansion of polyglutamine (CAG)n was found. The (CAG)n is 6 times more than the ordinary human which is 8~10.

The pathology of SCA6 is closely related with the alternative splicing of $Ca_V2.1$. The CAG repeats usually attached on the end of exon 47, while there is two version of calcium channel with or with out the exon 47, depending on the splicing site before the exon 47. Such toxic (CAG)n repeats will only occur when the exon 47 is present in the $Ca_V2.1$. Since the expression of exon 47 is higher in Purkinje cell than granule cell, it is proposed that more CAG repeats are found in Purkinje neuron than granule cell which lead to more severe degeneration of Purkinje neuron than that of granule cell in the cerebellum.

Even though, Tsunemi et al (2008) proposed that the extended version of $Ca_V2.1$ with exon 47 and polyglutamine repeat is increased in Purkinje cell of patients, suggested that the splicing factors could be affected by the pathology of diseases. These results might result in SCA-6 associate selective neural degeneration.

The pathological mechanism of $Ca_V2.1$ has been also studied in heterologous expression systems and knock-in mice. The result has shown that the splicing pattern also affects the biophysical properties of the channel. It has been shown that the biophysical properties of $Ca_V2.1$ channel with expanded polyglutamine are altered in the splicing

context. Toru et al (2000) has indicated an opposite effect on two calcium channel splicing variant (+NP and -NP) with expanded polyglutamine repeat in $Ca_V2.1$. It is shown that the voltage dependence of inactivation is reduced (-NP) and enhanced (+NP) through polyglutamine-expanded channel depending on the splicing variant. Strikingly, Saegusa et al (2006) did not show the similar result when they expressed the same -NP human $Ca_V2.1$ isoform under the native cacna1a promoter in knock-in mice (Saegusa et al 2007). There is no difference in the kinetics of voltage activation or inactivation and current density of the $Ca_V2.1$ in the Purkinje neuron with normal or expanded polyglutamine. Similarly, Watase et al (2008) has also suggested that neither voltage dependent activation nor inactivation was altered in the SCA 84Q expanded neurons and the mice expressing hyper expanded polyglutamine developed progressive motor impairment and aggregation of mutant $Ca_V2.1$ channels.

$Ca_V1.2$ plays an important role in calcium signals in multiple tissues, including brain, heart, smooth muscle cells and endocrine system. At least 20 of 56 exons of $Ca_V1.2$ are subject to alternative splicing. It is shown that the $Ca_V1.2$ in varies tissues are linked with specific splicing variants, which contributes to the functional diversity of $Ca_V1.2$. Studies reported that the $Ca_V1.2$ in smooth muscle were more susceptible to inhibition by dihydropyridines than $Ca_V1.2$ in cardiac forms and $Ca_V1.2$ channels in smooth muscle exhibit hyperpolarized shift in activation and inactivation. It is shown that $Ca_V1.2$ in smooth muscle cell exhibit a

combination of splicing pattern with (1/8/9*/32/Δ33) while the cardiac form of $Ca_V1.2$ is (1/8/9*/32/33) (Liao et al 2004, Tang et al 2004).

Recent studies have found that the alternative splicing of $Ca_V1.2$ is associated with Timothy Syndrome. Patients of Timothy Syndrome have severe cardiac arrhythmia and neurological disorders. The point mutations were found in the mutually exclusive exon 8 or 8a, which encode the IS6 region close to I-II loop region. The mutation on cardiac exon 8a has a severe consequence and delay the voltage-dependent inactivation, however, the mutation on neuronal type exon 8 exhibit much less phenotype. It is shown that exon 8a is highly expressed in heart, which explained the more severe consequence in heart than in that brain (Splawski et al 1993, Splawski et al 2004, Splawski et al 2005).

Chapter 2 Splice-variant-selective modulation of Ca_V2 family by snapin

2.1 Introduction

2.1.1 Alternative splicing of Ca_V2

$Ca_V2.1$ exon 37a and 37b

Bourinet *et al* (1999) and Soong *et al* (2002) have identified the splicing patterns of the rat and human $Ca_V2.1$ in brain. Seven splice loci have been identified. In the C-terminus, exon 37 is mutually-exclusively encoded by exon 37a and exon 37b, forming two splice variants of $Ca_V2.1$, named $Ca_V2.1$[EFa] and $Ca_V2.1$[EFb] (Bourinet et al 1999, Krovetz et al 2000). Other splice sites in the C-terminus of $Ca_V2.1$ including exon 43/44, which could be either present or absent, generating four combinations (Soong et al 2002). At the end of the C-terminus, there is an alternatively spliced insertion of GGCAG. With the insertion of the pentanucleotide, exon 47 could be translated in-frame to produce a longer isoform of $Ca_V2.1$. Otherwise, omission of pentanucleotide will result in a frame-shift and a pre-mature stop codon would appear to produce the short-form of $Ca_V2.1$ (Toru et al 2000, Zhuchenko et al 1997).

In the proximal C-terminus of the VGCC, two EF-hand like domains are identified in L-type calcium channel and other VGCCs. Unlike classical EF-hand domain, the EF-hand in VGCC might not bind Ca^{2+} (de Leon et al 1995, Peterson et al 2000). Recent studies suggested that the EF-hand like domain of VGCC is involved in binding to calmodulin. The calmodulin without Ca^{2+} or ApoCaM would bind to the EF-hand region

(Adams et al 2014). Upon Ca^{2+} influx, the calmodulin translocates to bind the IQ motif.

The C-terminus of $Ca_V2.1$ channels modulate channel properties including Ca^{2+}-dependent inactivation (CDI) and Ca^{2+}-dependent facilitation (CDF) ().

The EF-hand like domain of the $Ca_V2.1$ and $Ca_V2.2$ channels are different in that they are encoded by a pair of mutually exclusive exons. The exon 37 is mutually exclusively spliced to generate either exon 37a or exon 37b in the two calcium channels. Several reports have indicated the functional differences of these two splice variants, $Ca_V2.1$[EFa] and $Ca_V2.1$[EFb]. The $Ca_V2.1$ channels undergo dual modulation upon Ca^{2+} influx in different fine-tuning Ca^{2+}-dependent processes such as CDF (τ~ 10 ms) and CDI (τ~ 100- 500 ms) which influence synaptic plasticity in the nervous system (DeMaria et al 2001, Lee et al 2000). Both CDF and CDI have been reported to cause short-term facilitation and depression of synaptic transmission respectively (Borst & Sakmann 1998). It is shown that CDF is associated with local calcium signal, which is mediated by N-lope of CaM, whereas the CDI is mediated by C-lope of CaM and distal calcium signal (Chaudhuri et al 2004). Interestingly, $Ca_V2.1$[EFa] channels with exon 37a could display both the CDI and CDF properties, whilst the mutually exclusive exon 37b-containing $Ca_V2.1$[EFb] channels only displays CDI (Chaudhuri et al 2004, Chaudhuri et al 2007). The CDF process would

cause more Ca^{2+} influx with a pre-pulse and may affect the plasticity of synaptic transmission (Adams et al 2010).

During development, there is an expression-switch between EFa and EFb: EFb variant is expressed predominantly in early development in the fetal rodent brain, and a developmental switch occurred in the first 2-3 weeks after birth when the expression of EFa is increased significantly. A similar scenario is also found in human brain where there is also more EFb variant in the fetal, while in adult brain, there is about a equal distribution of the two variants (Chang et al 2007).

The EFa and EFb variants of $Ca_V2.1$ showed functional diversity and distinct expression patterns. The physiological role of these two splice variants has not been well studied. It will be interesting to determine how these two splice variants could contribute to the synaptic transmission and to determine whether there are some proteins that may modulate their functions.

$Ca_V2.2$ exon 37a and 37b

The $Ca_V2.2$ channel is another voltage-gated calcium channel found at the presynaptic terminal that is involved in synaptic vesicle release (Wheeler et al 1994). Other than $Ca_V2.1$, $Ca_V2.2$ channels are also highly concentrated in the sensory neuron in the dorsal root ganglion and spinal dorsal horn and they play a vital role in pain processing. The $Ca_V2.2$ channels can also be subject to alternative splicing including the EF-hand and two splice variants, $Ca_V2.2$[EFa] and $Ca_V2.2$[EFb], have been reported (Bell et al 2004). The $Ca_V2.2$[EFa] variant is almost

exclusively expressed in $Na_V1.7$-positive neurons and its expression is correlated with higher $Ca_V2.2$ current density in nociceptive neurons compared to the neurons that expressed $Ca_V2.2$[EFb] (Bell et al 2004). The Zamponi's group has shown that only $Ca_V2.2$[EFa] mediates thermal and mechanical nociception. Intrathecal injection of specific siRNA to knockdown $Ca_V2.2$ could effectively relieve pain in mice (Altier et al 2007). Furthermore, studies have provided evidence to support that why $Ca_V2.2$[EFa] is more effective in pain processing than $Ca_V2.2$[EFb] channels. It has been shown that $Ca_V2.2$[EFa] channels' open time is longer than $Ca_V2.2$[EFb] as assessed by single channel recordings, and therefore $Ca_V2.2$[EFa] yielded larger current density as compared to $Ca_V2.2$[EFb] (Castiglioni et al 2006). The $Ca_V2.2$[EFa] channels have higher surface expression as compared to $Ca_V2.2$[EFb] channels, because exon 37b could be preferentially ubiquitinated and therefore more prone to degradation. Mutation of the Y1747 to F1747 in exon 37 promote ubquitination and results in reduction of $Ca_V2.2$[EFa] current density. (Marangoudakis et al 2012). As such, $Ca_V2.2$[EFa] has an advantage for pain processing for its higher conductivity and resistance to ubquitination.

$Ca_V2.2$ is shown to be modulated by G-protein in both a voltage-dependent and a voltage independent way. The prominent effect of $Ca_V2.2$[EFa] is also shown by G-protein dependent modulation. Approximately 0.2-0.3 mM of GTP-γS could inhibit both $Ca_V2.2$[EFa] and $Ca_V2.2$[EFb] and this inhibition could be relived by pre-pulse depolarization. Another voltage-independent inhibition process is

specific to $Ca_V2.2$[EFa]. However, there is additional inhibition on $Ca_V2.2$[EFa] that could be compensated by pre-pulse activation. These voltage-independent inhibitions are dependent on pp60c-src tyrosine kinase and are associated with μ-opioid or $GABA_B$ receptors. The unique tyrosine 1747 in $Ca_V2.2$[EFa] might be a potential target for phosphorylation by pp60c-src tyrosine kinase and be involved in G-protein dependent inhibition of the $Ca_V2.2$ channels (Raingo et al 2007).

2.1.2 Ca_V2 and vesicle release

Voltage-gated calcium channels play a crucial role in mediating the evoked neurotransmitter release upon an action potential. Most of the synapses in the central nervous system rely on $Ca_V2.1$ and $Ca_V2.2$ channels (Wheeler et al 1994).

Synaptic proteins interaction at synprint *modulate VGCC function*

It has been established that SNAP-25 (synaptosome-associated protein 25) and syntaxin interact with the synprint sites of $Ca_V2.1$ and $Ca_V2.2$ channels (Rettig et al 1996, Sheng et al 1996, Sheng et al 1994). Interaction between VGCC and vesicle release machinery promote the voltage-dependent inactivation of channel and G protein regulation (Bezprozvanny et al 1995, Jarvis & Zamponi 2001). It was reported that synprint peptide could compete with the native synprint site in $Ca_V2.1$ and suppress the vesicle release in the chromaffin cell (Mochida et al 1996). The synprint region within the II-III loop of $Ca_V2.1$

is associated with synaptic release and human diseases (Simms & Zamponi 2014, Weiss & Zamponi 2012).

One $Ca_V2.1$ channel splice variant that does not contain the synprint site has been reported in some neuroendocrine cells. This splice variant that lacked most of the synaptic protein-binding site showed reduced Ca^{2+} current and the inactivation potential of the variant was also shifted to the hyperpolarized direction. The $Ca_V2.1$ mutation associated with human migraine, E1015K, has been found in the synprint site. The E1015K mutant channels displayed increased Ca^{2+} channel current because the SNAP-25 did not bind to the mutated synprint site in E1015K $Ca_V2.1$ channel (Condliffe et al 2013)

VGCC localization in the presynaptic terminals and active zone

The VGCCs convert the electrical input of action potential into chemical output of neurotransmitter release. The synaptic vesicle release is mediated by specialized regions in the presynaptic site called the active zones (Augustine et al 2003, Wojcik & Brose 2007). The synaptic vesicle machinery and calcium channels are docked at the active zones. The $Ca_V2.1$ and $Ca_V2.2$ channels are both localized in the active zones and the relative positions for $Ca_V2.1$ and $Ca_V2.2$ are fixed (Cao & Tsien 2005, Cao & Tsien 2010, Jun et al 1999).

Many proteins were reported to regulate the localization of calcium channels such as Mint-1 and CASK (Maximov & Bezprozvanny 2002, Spafford et al 2003). The Sudhof's group has shown that RIM proteins localized calcium channels to the active zones. RIM-deficient neurons

have decreased Ca^{2+} influx and reduced primed vesicles. Two domains of the RIM proteins tether the presynaptic Ca^{2+} channels to the active zones. One is the PDZ domain of RIM and it directly binds to the C-terminus of channels. The PDZ domain of RIM has no selectivity for its binding to either $Ca_V2.1$ or $Ca_V2.2$ channels (Deng et al 2011, Han et al 2011, Kaeser et al 2011). The other is the PXXP domain of RIM. This domain interacts with RIM-binding protein and the presynaptic scaffold protein Bassoon, which specifically recruits $Ca_V2.1$ but not $Ca_V2.2$ channels to the active zones (Davydova et al 2014).

2.1.3 Functions of snapin

Snapin is one of the critical proteins involved in the presynaptic complex important for neurotransmission. It has been identified to interact with many proteins in the axon terminals to affect vesicle fusion and transmitter release. Snapin was first identified as a SNAP-25 binding protein. Human and rodent snapin share about 98% protein sequence identity (Ilardi et al 1999).

Structures of snapin (coil-coil domain, phosphorylation site and dimerization)

Snapin has a short hydrophobic N-terminus and a cytosolic C-terminus. The hydrophobic N-terminus is likely to be responsible for attachment to the vesicle membrane. The C-terminus is predicted to form a coil-coil domain and is the critical binding region for SNAP-25 and synaptotagmin 1 (Syt-I) (Chheda et al 2001, Ilardi et al 1999).

Snapin could be phosphorylated at Ser-50 and Thr-117. Phosphorylation at Ser-50 has been shown to increase the binding between snapin and SNAP-25. Overexpression of S50D, which mimicked phosphorylated snapin led to increase in the readily-releasable pool of synaptic vesicles in chromaffin cells and in cultured primary neurons, while the S50A mutant snapin, which lacked the phosphorylation site, resulted in reduced number of readily-releasable pool number (Chheda et al 2001). In addition to Ser-50, recent studies have identified Thr-117 as another phosphorylation site of Leucine-rich repeat kinase 2 and phosphorylated snapin at Thr-117 decreased the interaction between snapin and SNAP-25 leading to instability of the VAMP2-syntaxin-SNAP25 complex. Thus, snapin phosphorylation at Thr-117 reduced the readily releasable pool and the extent of vesicle release (Yun et al 2013). Snapin might also be phosphorylated by Casein kinase 1 delta (CK1δ), while the exact phosphorylation site has not yet been found (Wolff et al 2006).

Snapin has been shown to function as a dimer, formed through disulfide bond linkage at Cys-66. Snapin mutant C66A that disrupts dimer formation has a low affinity for binding to syt-1 and SNAP-25. Further studies have suggested that snapin could form tetramers in solutions. Snapin will preferentially form dimer when interacting with SNAP-25 (Navarro et al 2012).

Snapin and synaptic transmission

Neurotransmitter release is triggered by presynaptic Ca^{2+} influx (Meir et al 1999, Stanley 1997). The major Ca^{2+} sensor for fast vesicle release has been shown to be synaptotagmin I (Syt-I) (Zhang et al 2002a). Upon Ca^{2+} influx, Syt-I interacts with SNARE complex to trigger vesicle fusion (Chapman 2008). Biochemical studies have shown that snapin interact with both SNAP-25 and Syt-I (Ilardi et al 1999, Tian et al 2005). These interactions stabilize the Syt-I-SNARE complex. The chromaffin cell from snapin knockout mice showed reduced exocytosis burst and could be rescued by snapin overexpression in the snapin-deficient cells (Tian et al 2005). It has been demonstrated that snapin-deficient mice did not affect the basal expression level of the three SNARE complex components and Syt-I. But the interaction between Syt-I and SNARE was reduced, resulting in suppressed vesicle release. Further reports have indicated that snapin is involved in synchronizing synaptic vesicle fusion. Upon high-frequency stimulus of 50 Hz, snapin-deficient neurons do not maintain precision and efficacy as the wild-type neurons do (Pan et al 2009). Before Ca^{2+} influx, it is believed that snapin help to stabilize the apoSyt I-SNARE, when the apoSyt-I does not sense Ca^{2+}. In snapin deficient cells, Syt-I is disassociated with SNARE and the presynaptic machinery could not respond to the transient Ca^{2+} that was elevated upon with in high-frequency stimulus (Pan et al 2009).

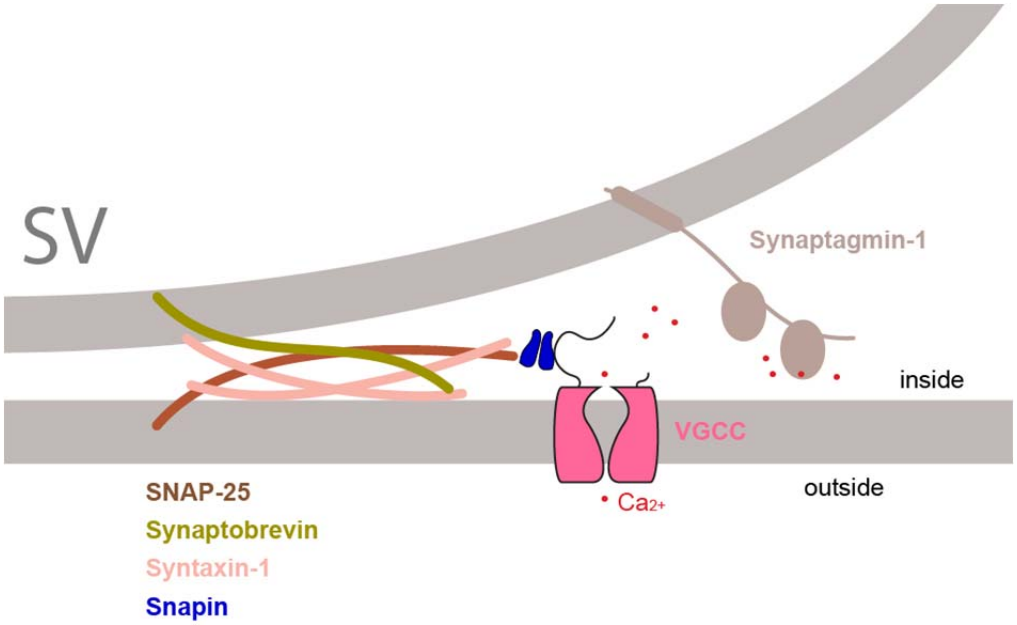

Figure 1.3 Model of presynaptic machinery.
The drawing illustrates the VGCC, snapin, SNARE complex (composed SNAP-25 and
Syntaxin-1 on the plasma membrane and synaptobrevin linked with synaptic vesicles) and Ca^{2+} sensor synaptotagmin-1. Snapin forms a dimmer and has been shown to interact with SNAP-25, synaptagmin-1 and VGCC in our studies.

Snapin and protein transport

In addition to the critical role synchronizing vesicle release, snapin also mediates retrograde transport through binding with dynein. It has been shown that the transport of late-endosome from the distal axon terminal to soma was significantly impaired in snapin-deficient neurons, resulting in the accumulation of endosome and apoptosis of the cells. The motor protein dynein binds the snapin DIC domain (Cai et al 2010). The retrograde transport system has been shown to be involved in several pathological conditions. For example, snapin-dynein machinery mediates transportation of β-site amyloid precursor protein cleaving enzyme and facilitate amyloid precursor protein processing (Ye & Cai 2014). Up to now, several proteins has been reported to transported via the snapin-dynein machinery, including TRPM7, BDNF-TrkB and TMPAP (Krapivinsky et al 2006, Quintero et al 2013, Zhou et al 2012).

2.1.4 Objectives and rationale

The proximal C-terminus of VGCCs contains elements that are important for Ca^{2+}-dependent regulatory processes such as CDI and/or CDF. Two $Ca_V2.1$ splice variants $Ca_V2.1$[EFa] and $Ca_V2.1$[EFb] have functional differences in eliciting Ca^{2+} dependent facilitation that will affect synaptic transmission (Chaudhuri et al 2004, Chaudhuri et al 2007). The spatial and temporal expression patterns of $Ca_V2.1$[EFa] and $Ca_V2.1$[EFb] might influence Ca^{2+} influx and synaptic function (Chang et al 2007). Despite the current findings, the functional

differences of these two variants of $Ca_V2.1$ have not been fully elucidated. It is interesting therefore to investigate how these splice variants contribute to synaptic function and whether there is any factor that could preferentially modulate their functions.

From our work, we have first identified using yeast-two hybrid assay that snapin interacts with $Ca_V2.1$ exon 37b that was used as bait. From biochemical and functional characterizations, we have discovered that snapin preferentially bind to $Ca_V2.1$ exon 37b than to exon 37a. Snapin is one of SNAP-25 binding proteins found in the presynaptic terminal (Ilardi et al 1999), and is involved in synchronizing synaptic vesicle fusion (Cai et al 2010), In addition, snapin mediated retrograde transport by interacting with dynein (Pan et al 2009). Here, we aimed to examine the interaction between $Ca_V2.1$ and snapin by biochemical and electrophysiological methods. Firstly, we determined the binding region between snapin and $Ca_V2.1$. Secondly, we examined the functional effect on $Ca_V2.1$ upon binding of snapin. Thirdly, we strived to examine the potential impact on the synaptic transmission upon snapin binding to $Ca_V2.1$ channels.

2.2 Materials and methods

2.2.1 Materials

The experiments were carried out on C57BL mice as approved by NUS IACUC. The full-length human $Ca_V2.1$[EFa, 47-], $Ca_V2.1$[EFb, 47-], and $Ca_V2.1$[EFb, 47+] subunits were reported in previous studies (Chang et al 2007, Soong et al 2002).$Ca_V2.2$[EFa] and $Ca_V2.2$[EFb] were reported in Lipscombe's group (Bell et al 2004, Castiglioni et al 2006).

2.2.2 Construction of snapin plasmids

The human snapin is amplified from human brain cDNA library (Marathon-Ready Clontech, CA) and Elongase DNA polymerase (Life Technologies, CA) using

Snapin-Fw ATGGCGGGGGCTGGTTCC

Snapin-Rs- TTATTTGCCTGGGGAGCCAG

-for a 411 bp amplicons, according to the standard PCR procedure for Elongase DNA polymerase.

The PCR protocol for cloning the snapin using Elongase is

Pre-denaturation 95°C 5 min

Denaturation 95°C 30 sec

Annealing 62°C 30 sec

Extension 68°C 30 sec

Repeat for 35 cycles

Final extension 68°C for 5 min

Snapin amplicons were sub-cloned into pGEM®-T Easy vector (Promega, WI) and the ligation products were transformed into DH10B *E.coli*. The snapin sequence was confirmed by sequencing according to AF086837.

Subsequently, a myc tag were add on the N-terminals of snapin by PCR using

Snapin-myc-fw
GGATCCGAACAAAAACTCATCTCAGAAGAGGATCTGATGGCGGG
GGCTGGTT

Snapin-re2 GCGAATTCTTATTTGCCTGGGGAGCCAG

The PCR products were double digested by BamHI and EcoRI, and subcloned into pIRES-DsRed2 expression vector (PT3775-5).

The standard digestion reaction were performed for 2 hour incubation at 37°C as suggested by the manufacturer (New England Biolabs, MA). The digested product were purified using agarose gel electrophoresis and Gel Extraction Kit (QIAGEN, Germany). The DNA fragment were ligated at 16 °C overnight by T4 ligase (New England Biolabs, MA) and transformed into DH10B *E.coli.*

Snapin-C66A mutation was generated by site directed mutagenesis (QuickChange II XI site-directed mutagenesis kit, Stratagene) employing the two complimentary primers

C66A forward AGCCACAGAACTGGCCCGCATAAATGAGGATC

C66A reverse GATCCTCATTTATGCGGGCCAGTTCTGTGGCT

The snapin-C66A was sub-cloned into pIRES-DsRed vector as previously described.

2.2.3 Construction of exon 37a/37b chimeras and GST fusion proteins

The GST-fusion protein with EFa and EFb fragment were generated by cloning the proximal C-terminus of $Ca_V2.1$ with exon 37a or exon 37b into the pGEX4T1 vector. The 300 bp amplicons spanned from the end of IV-S6 segment (part of exon 35) to exon 38 as indicated in the alignment of 2.9. The fragments included the two predicted EF-hand like domain but did not contained IQ domain. The PCR were performed using two following primers

hA1A-C ter EcoRI GGAATTCATGGACAACTTTGAGTACC

hA1A-exon38SalI-sh GCGTCGACTCATCCCTTGGCAATCTT

using the standard touch down PCR procedures.

The PCR protocol for cloning the snapin using GoTag was

Pre-denaturation 95°C for 5 min

Denaturation	95°C 30 sec
Annealing	59°C to 53°C decrement
	and 53°C for the rest cycle
Extension	72°C 30 sec

Repeat for 35 cycles

Final extension 72°C for 5 minutes

The annealing temperature may vary in different studies and the extension time would be extended for longer fragments (1kb/min).

The PCR products of EFa and EFb fragment were double digested with EcoRI and SalI and ligated with pGEX4T1 vectors.

Three chimera constructions of exon 37a/37b were generated by overlapping PCR (Fig. 2.2). The overlapping complementary primer pairs spanned the exon 37a and exon 37b sequences. Two pairs of PCR reaction with upstream and downstream primer amplified the 1/3 of up-streaming exon 37a and down-streaming 2/3 of exon 37b. These two DNA fragments were joined with denaturing by 95 for 5 min followed by slowly annealing in room temperature for 4 hours.

The complementary primer pairs for chimera 1

hA1A-hybEFa-0.3EFb fw

TAGGCAAGAAATGTCCGGCCAGAGTGG

hA1A-hybEFa-0.3EFb re

CCACTCTGGCCGGACATTTCTTGCCTA

and chimera 2

hA1A-hyb0.3EFa-EFb Fw

TTCATTATAAGGATATGTATCAGATGCTGA

hA1A-hyb0.3EFa-EFb Re

TCAGCATCTGATACATATCCTTATAATGAA

were used for overlapping PCR.

The chimera 3 with (37b-37a-37b) was generated from EFb and chimera 2 as a template using the following complementary primers.

hA1A-hyb0.3EFb-EFa Fw

ACCTGGACATGTACAGTTTATTACGAGTAA

hA1A-hyb0.3EFb-EFa Re

TTACTCGTAATAAACTGTACATGTCCAGGT

The overlapping PCR products for hybrid EFa and EFb were subsequently amplified by the PCR using hA1A-Cter-EcoRI and hA1A-exon38SalI-sh. The chimeras of $Ca_V2.1$ were sub- cloned into pGEX4T-1 by EcoRI/SalI as previously stated. The $Ca_V2.1$ mutations, $Ca_V2.1$[WMPL-AAAA], $Ca_V2.1$[MPL-AAA], $Ca_V2.1$[W-A], $Ca_V2.1$[M-A], $Ca_V2.1$[P-A], $Ca_V2.1$[L-A], were cloned with the help of Ms. Liang Mui

Cheng. The GST-fusion proteins with the EF-hand domains of $Ca_V2.1$ mutations were cloned in pGEX4T-1 similarly as previously described.

2.2.4 GST pull-down assays and western blot

GST pull-down assays were conducted by using glutathione sepharose beads (GE-Health UK) to isolate the purified GST fusion protein linked with fragment of $Ca_V2.1$ (EFa/EFb and chimeras) and examine the interaction between snapin and proximal C-terminus of $Ca_V2.1$ (Wang et al 2011).

The GST-fusion protein was prepared using isopropyl β-D-1-thiogalactopyranoside (IPTG) induction system. The plasmids were transformed into BL21 *E. coli*. The bacterial was cultured in 200 ml LB media in 37°C until the O.D. value reached 0.8-0.9, before adding isopropyl IPTG (0.5 mM). After 5 hours of induction in 30°C, the bacterial was spun down by 6000 rpm for 20 minutes and washed with PBS. The bacterial pullets were suspended with 10 ml of PBS with 1% Triton X-100 and 1X proteinase inhibitor (Roche). After sonication for 5 minute, the bacterial lysis was spun down in 13,000 rpm for 30 min and the supernatant with GST-fusion protein was incubated with glutathione sepharose beads 3 hours at 4°C. GST-beads were washed with PBS for more than 5 times and stored in -20°C.

The immobilized GST fusion proteins were incubated with HEK 293 cell lysis with transfected snapin for 1h at 4°C. After washing with PBS for 3 times, glutathione-bound proteins were eluted by boiling at 95°C in Laemmli buffer for 10 minutes, and detected by western blot analysis

with anti-snapin (SYSY; 1:1000 dilution) or anti-GST (Santa Cruz; 1:5000 dilution) antibodies.

Total protein for western blot was extracted from culture cell in RIPA buffer. The protein concentration was measured by Bradford assay (Bio-Rad). Protein samples were denatured at 95°C for 5 minutes in 5XSDS-sampling buffer with 2-mercaptoethanol. The SDS-PAGE was performed using 8% to 12% polyacrylamide gel. Equal amount protein were loaded for SDS-PAGE, The protein was electrically transferred to polyvinylidene difluoride (PVDF) membranes (Millipore) using standard transfer buffer.

The PVDF membrane was then blocked by 5% milk in Tris-Buffered Saline and Tween 20 (TBST) buffer and incubated with primary antibodies overnight at 4°C and following HRP-linked secondary antibody for 1 hour at room temperature (Sigma, 1:5000 dilutions). The blots were visualized with either Pierce ECL Western Blotting Substrate or SuperSignal West Pico Chemiluminescent Substrate enhanced (Thermo Scientific, IL) before exposing to an X-ray film (Kodak).

2.2.5 Mammalian cell culture and transient transfection

Human embryonic kidney (HEK) 293 cell were maintained in Dulbecco's Modified Eagle Medium (DMEM) with 10% fetal bovine serum (FBS) and grown in 37°C incubator with 5% CO_2. 1% Pen/strip were added to avoid contamination. All the culture media were from Life Technologies. Cells were passaged every 4-5 days when reaching

80-90% confluency. The cells were plating in 4-6 $X10^4$ cells/cm^2 each time.

Transient expression of calcium channel in HEK293 cell for electrophysiology

For cell transfection by electrophysiological studies, HEK cell were seeded on 12 mm X 12 mm poly-D-lysine coated coverslips in 35 mm culture dishes. The seeding density was low with approximately $1X10^4$ cells/cm^2 and therefore, isolated cell would be available in further whole cell patch clamp studies. The cells were incubated for 16-24 hours to ensure the cells are attached to the coverslips. The growth media are aspirated and replaced with fresh media without antibiotics one hour before transfection. Calcium phosphate transfection was applied to transient expressing the voltage-gated calcium channel and pIRES-DsRed-snapin or snapin-C66A (1 μg) for patch clamp studies. The pIRES-DsRed was used as transfection control for the following studies. Approximately equal-molar ratio of α_1 pore-forming units (1.7 μg), β_{2a} (1.25 μg) and $\alpha_2\delta_1$ (1.25 μg) DNA plasmid as well as T-antigen (0.25 μg) were mixed with 75 μl of $CaCl_2$ and 75 μl of 2XHBS buffer (280 mM NaCl, 50 mM HEPES and 1.5 mM NaH_2PO_4).

The rat β_{2a} and rat $\alpha_2\delta_1$ subunit clones were reported in previous studies (Liao et al 2007, Tang et al 2008). The mixture was incubated in room temperature for 15-20 minutes to allow the DNA-calcium phosphate precipitate to form. We gently added the mixture into culture dishes with HEK293 cell drop by drop and incubated in 37°C incubator.

Calcium phosphate precipitant could be found 3-5 hours after transfection. Afterward, fresh DMEM media without antibiotic were applied to remove the transfection reagent. The cells were maintained for 36-72 hours for electrophysiology studies. Noted that the β_{2a} was cloned into pIRES-AcGFP vector and snapin was cloned pIRES-DsRed vector. The appearance of GFP and DsRed in cells indicated that the calcium channels and snapin were both expressed in cells.

Transient expression in HEK293 cell by lipofectamine

For HEK cell transfection for biochemical studies, the HEK cell were transfected using lipofectamine™ 2000 (Life Technologies). The cells were reach 90% confluency before transfection. One hour before the transfection, the used media was aspirated and fresh media without antibiotics was introduced. 4 µg of plasmid DNA and 10 µl of lipofectamine™ 2000 were diluted in 250 µl of Opti-MEM® I Reduced Serum Media separated. After 5 min incubation, we mixed the DNA plasmid and lipofectamine and incubated in room temperature for 30 minutes to allow the DNA-lipofactamine mixture form. The mixture was then added into the cell culture. After 5-6 hours, the spent media with transfection reagent was aspirated and replaced with fresh media without antibiotics. The cells were grown for 24 hours before harvested.

2.2.6 Primary hippocampal neuron culture

The primary hippocampal neuron was prepared according to establish protocols (Kaech & Banker 2006). The mice hippocampal neurons were cultured on the coverslip supported by the astroglial feeder.

The astroglial feeder was prepared from P1 mice cortex 2 weeks before the neuron culture. The cortex was separated from mice pups and the meninges were removed carefully with forceps to avoid fibroblast cell contamination. The brain tissue was washed by dissecting solution (Hank's Balanced Salt Solution, HBSS with 10 mM HEPES) and cut down into small pieces After dissociated by 0.25% trypsin (Life Technologies) and 1% DNase (Roche), the brain tissues were triturated by pipetting the solution and filtered through cell strainer (BD). The cells are plating in $1.5X10^5$ cell/cm^2 with glial medium (Basal Medium Eagle, 10% Horse Serum, 1% Pen/Scripts, 1 X GlutaMax, and 1 μM Sodium Pyruvate, 1 mM HEPES, 0.6% glucose). The media were changed 1 day after the plating and every 3 days later. The astroglial feeder would reach about 20-40% confluence before neuron culture.

The hippocampi or cortex were dissected from P0 mice. The meninges were carefully removed and the hippocampi was digested by 0.25% trypsin and 1% DNase (Roche) in HBSS for 15 minutes. The hippocampi were then washed by HBSS to removed trypsin and the tissue is dissociated by pipetting the solution with polished tips. The dissociated neurons are plated on poly-D-lysine-treated (Sigma) coverslips (Marienfeld, Germany) with neural plating medium (Basal Medium Eagle, 10% Horse Serum, 1 X GlutaMax, 0.6% glucose and 1 mM HEPES) for 3 hours. The cultured neuron were supported by astroglial feeder and maintained in neural basal medium with B27 supplements. 3 days after plating, cytosine arabinoside was added to

final concentration of 5 μM to inhibit glial proliferation. All media were obtained from Life Technologies.

2.2.7 Lentivirus preparation and transduction on neurons

ShRNA to snapin was packaged using ViraPower™ Lentiviral Expression Systems (Life Technologies CA). HEK 293FT cells were maintained according to standard procedures by DMEM and FBS. The viral plasmid were transfected to the HEK 293FT cells, when it reach 90-95% confluence (10 cm dishes). The viral plasmid pLP1 (3 μg), pLP2 (3 μg) and pLP-VSVG (1 μg) as well as shRNA plasmid (3 μg) were diluted in Opti-MEM media and then mixed with 25μl of lipofactamine 2000. After 30 minutes of incubation, the mixture was added into cell culture. Fresh media was added to replace the media with transfection reagent.

The virus-containing supernatants were harvested two times at 48 and 72 hours post-transfection by transferring the medium into to a 50 ml sterile, capped, conical tube.

The supernatants were spin down at 3000 rpm for 15 minutes at 4°C to remove pellet debris and filtered through Millex-HV 0.45 μm. The viral containing supernatants were spin down at 30,000 rpm for 2 hours at 4°C using ultra-centrifuge. The viral pellet could be found in the bottom of the tube and was re-suspended by 400 μl of DMEM and stored at -80 °C.

In order to determine the tittering ratio for lentivirus, the cells were plating about 30–50% confluent 1 day before transduction. The lentiviral stock was thawed and 10-fold serial dilutions of lentiviral stock ranging from 10-2 to 10-6 were prepared and added in to cell culture. One day after the transduction, the media-containing virus was replaced with fresh DMEM and incubates for 48-72 hours before fixation. The titer rated was determined by counting the transfected cells with fluorescence versus total cell number.

Transducting the lentivirus in primary neuron.

The primary neurons were cultured for DIV7 before transduction. 20 ul of lentiviral stocked was diluted in to and added in to final volume of 1 ml in the neuron culture media. The media with virus was removed and replaced with 1 mL of complete culture medium.

2.2.8 Snapin shRNA

Snapin-shRNA vectors with GFP tag and control vector were purchased from Sigma. (TRCN0000176557, TRCN0000277451, TRCN0000277452, TRCN0000277457, TRCN0000277- 526 and SH003), targeting on the coding sequence of snapin.

2.2.9 Whole cell patch-clamp electrophysiology on mammalian cell culture and primary neuron

Whole cell patch-clamp recording on HEK293 cell channel were performed within 36-72 hours after the calcium phosphate transfection. The external solution contained (in mM) 10 HEPES, 140 TEA-$MeSO_3$ 5

$CaCl_2$ or 5 $BaCl_2$ (pH was adjusted to 7.4 with TEA-OH and osmolarity was adjusted to 300-310 mOsm with glucose). The pipette solution for recording $Ca_V2.1$ and $Ca_V2.2$ channel current contained (in mM) 10 HEPES, 5 CsCl, 138 Cs-$MeSO_3$, 0.5 EGTA, 1 MgCl2, 2 mg/ml MgATP, pH 7.3 (adjusted with CsOH), Osmolarity is between 290 and 300 mOsm.

The borosilicate glass pipette (WPI, FL) were prepared using P97 (Sutter, CA) and polished with microfuge (Narishege, Japan). The pipette solution is backfilled in the glass pipette. The resistance of glass is within 1.5-2 MΩ.

The 293 cells were held at -90 mV by voltage clamp using Axopatch 700B or Axopatch 200B (Molecular Devices, CA). The series resistance for recording was typically less than 5 MΩ, 70-80% compensation on serial resistance and cell membrane capacitance was applied. A P/4 protocol was applied to subtract the leakage current. All data are obtained with Digidata 1440A (Molecular Devices, CA), sampled at 5-50 kHz. The 1 kHz or 6 kHz low pass filter are applied for all the data.

In order to study the activation threshold of voltage-gated calcium channel, we performed the studies using tail protocol, which represent the conductivity of channel. Cells were depolarized to a serials of voltages, ranging from -60 to 100 mV, in steps of 10 mV increments, for 20 ms. Following the depolarization, a -50 mV step for 10 ms evokes the tail currents. The tail current was normalized to the

maximum current obtained from each cell and fitted through single Boltzmann equation:

$$G = G_{min} + (G_{max} - G_{min})/(1 + e^{\frac{V_{1/2act} - V}{k_{act}}})$$

where *G* represents the tail current, *V* is the membrane potential of the test pulse. The following parameters were determined by curve fitting. G_{max} is the maximum tail current recorded from each cell, G_{min} is the maximum tail current recorded for fitting curve. k_{act} is the slope factor and $V_{1/2act}$ represent the voltage when the channel current reaches half of the maximum current.

The current-voltage (I-V) relationships of voltage-gated calcium channel were studied by applying a serial of test potentials from -60 mV to 40 mV with 10 mV increments to the transfected 293 cells during voltage clamp. The I-V relationships are fitted by the following equation:

$$I = G_{max}(E_{rev} - V)/(1 + e^{\frac{V_{1/2act} - V}{k_{act}}})$$

where *I* represents the current, *V* is the membrane potential of the test pulse. The G_{max} represent the maximum conductance of the cell, V is the membrane potential of the test pulse, E_{rev} is the reversal potential for the calcium channel, $V_{1/2act}$ represent the voltage when the channel current reach half of the maximum current and k_{act} is the slope co-efficient for the activation.

Steady-state inactivation (SSI) properties were examined by comparing the test current to the initial pre-pulse. The pre-pulse current was evoked by to 0 mV voltage step for 30 ms. A long depolarizing pulse of 15 seconds are applied to inactivate the calcium channel ranging from -120 to 20 mV, with 10 mV increment. The test-pulse current was evoked by 0 mV voltage step for 100 ms. The test current was divided by the pre-pulse current. The values were fitted with a single Boltzmann equation:

$$I = I_{min} + (I_{max} - I_{min})/(1 + e^{\frac{V_{1/2inact} - V}{k_{inact}}})$$

where I is the normalized current for *V* is the membrane potential of the stead-state inactivation, $V_{1/2inact}$ represents the voltage when the channel current reach half of the maximum current and k_{inact} is the slope co-efficient for the inactivation. I_{max} is the maximum tail current recorded from each cell, I_{min} is the maximum tail current recorded for fitting curve.

Calcium dependent inactivation (CDI) was examined by stepwise voltage depolarization for 1 second. The whole cell current was obtained using Ba^{2+} or Ca^{2+} as charge carrier to distinguish the Ca^{2+} dependent component to voltage dependent component. This idea was derive from selective affinity of calmodulin to Ca^{2+} than Ba^{2+}, From the initial holding of -90 mV, a family of depolarization steps from -60 mV to 50mV was applied on the cell.

The fraction of inhibition was calculated by the remaining current after 300 ms (r_{300}) or 800 ms (r_{800}) recorded in Ba^{2+} or Ca^{2+}. The r_{300} and r_{800}were plotted against the voltage. The curves for CDI were fitted by nonlinear poly regression. The pure calcium dependent inactivation, *f*-index was obtained from deducting the r_{300} or r_{800} recorded in Ca^{2+} from that Ba^{2+} in 10 mV.

Calcium dependent facilitation (CDF) of $Ca_V2.1$ was elicited by a step depolarization followed by a family of pre-pulse (-80 mV to 60 mV with 20 mV increments) recorded in Ba^{2+} and Ca^{2+} solution, to distinguished the pure Ca^{2+} dependent component. It is known that the VGCC also under calcium dependent inactivation. In order to separate the facilitation (CDF) part from the inactivation component (CDI), we have exploited two crucial features. First, the kinetics for CDF is much faster than CDI, (CDF, 10 ms versus CDI, 100 ms to seconds). Second, the occurrence of CDI inactivated a portion of channels, leaving the other channels available for CDF. Therefore, the 20 ms pre-pulse was sufficient to induce CDF and short enough to minimize the inactivation. The diagram of the protocol was shown in figure 2.7.

Without the pre-pulse, the normalized test pulse could be approximately described by the following equation:

$$I_{norm}(t,\ _{nopre}) = F_{fast} + (1 - F_{fast})(1 - e^{-t/\tau})$$

where F_{fast} is the rapid fraction on the channel current and τ is the time-constant for a slower single-exponential increase of channel current.

After pre-pule, a relative fraction (*RF*) is the pre-pulse induced facilitation. Therefore, the normalized test pulse with pre-pulse was given by:

$$I_{norm}(t, V_{pre}) = F_{fast} + RF + (1 - F_{fast} - RF)(1 - e^{-t/\tau})$$

where *RF* is the pre-pulse induced fraction, and the trace is also dependent on the voltage of prepulse (V_{pre}). Therfore, we have integrated the difference value between normalized waveforms obtained with or without prepulse to obtain *ΔQ*. The *ΔQ* is shown by:

$$\Delta Q = \int_{t=0}^{\infty} [I_{norm}(t, V_{pre}) - I_{norm}(t, _{nopre})]dt = \int_{t=0}^{\infty} RF \cdot e^{-t/\tau} dt = RF \cdot \tau$$

Therefore, the value of Relative fraction (RF) is obtained from (total charge difference) *ΔQ* divided by trace decay time (*τ*).

The *τ* was calculated by fitting the normalized curve to single exponential curve obtained in + 20 mV without pre-pulse. The *ΔQ* is calculated from the area difference with or without pre-pulse obtained in a family voltage steps.

Whole cell patch-clamp recording on primary neuron were performed on DIV10-11. The external solution contained (in mM) 145 NaCl, 10 HEPES, 3 KCl, 2 $MgCl_2$, 2 $CaCl_2$ and 8 glucose (pH was adjusted to 7.3 with NaOH and osmolarity was adjusted to 300-310 mOsm with glucose). The glass pipette was back-filled and tip-filled with pipette potassium based solution contained 146.5 K-gluconate, 10 HEPES, 9 NaCl, 7.5 KCl, 1 $MgCl_2$, 0.2 EGTA, and 2 ATP-Na, (pH was adjusted to

7.3 with KOH, and osmolarity was adjusted to 290-300mOsm with K-gluconate). The whole cell patch was performed using Axopatch 700B and obtained with Digidata 1440A. At least 5 minutes after forming the patch, the spontaneous EPSC was record by gap-free protocol continuously for 8 minute, with sampling rate of (pCLAMP 10.2). The EPSC events were analyzed by MiniAnalysis (Synaptosoft, GA)

2.2.10 Immunocytochemistry and confocal imaging

For immunofluorescence on hippocampal neurons, the following antibodies were used, rabbit anti-MAP2 antibody (ab32454, abcam, UK, 1:100), mouse anti-synapsin antibody (106001, SYSY, Germany, 1:100), rabbit anti-snapin antibody (148002 SYSY, Germany, 1:400). The following Alexa fluo dye conjugated with anti-IgG were used, Alexa is goat anti-rabbit Alexa 594 (1:400), anti-rabbit Alexa 488 and goat anti-mouse Alexa 594 (1:400) (Life Technologies, CA).

The primary hippocampal neurons are stained and analyzed at DIV14-16. The neuron are fixed by 4% paraformaldehyde PBS, pemeablized by 0.1% Trion-X and blocked with blocking buffer (5% goat serum and 1% bovine serum albumin in PBS), Primary antibodies (MAP2/synapsin/snapin) were applied in PBS/BSA/Trixton at 4°C overnight and then incubated with the Alaxa-conjugated secondary antibodies for 1 h. The cells were washed by PBS and stained with DAPI for 10 min. The coverslip is mounted in Fluosave Reagent (Chemicon, Billerica, MA) in glass slice to retard photo bleaching.

2.2.11 RNA extraction and RT-PCR

The efficiency on of snapin knock down was detected by RT-PCR experiments. Total RNA from neuron was isolated using standardized Trizol methods (Invitrogen, Carlsbad, CA).

The cDNA was synthesized with oligo (dT)18 primers and Superscript II reverse transcriptase (Life Technologies, CA). RT(-) control reaction without reverse transcriptase were performed in all RT reactions to exclude the possible contamination by genomic DNA. The subsequent PCR were performed by using primer.

Snapin-mus-Fw ATGGCCGCGGCTGGTTCCG

Snapin-mus-Re TTATTTGCTTGGAGAACCAGG

2.3 Results

2.3.1 Snapin bound to proximal C-terminus of voltage-gated calcium channel

Alternative splicing of exon 37 generates two splice variants $Ca_V2.1$[EFa] and $Ca_V2.1$[EFb] (Bourinet et al 1999, Chaudhuri et al 2004, Krovetz et al 2000, Zhuchenko et al 1997). It has been shown that $Ca_V2.1$[EFa] channels conduct more Ca^{2+} than $Ca_V2.1$[EFb] channels. $Ca_V2.1$[EFa], but not $Ca_V2.1$[EFb] exhibits robust Ca^{2+}-dependent facilitation (Chaudhuri et al 2004, Chaudhuri et al 2007). It was also reported that the Ca^{2+} influx through $Ca_V2.1$ channels is crucial for triggering vesicle release (Catterall & Few 2008, Takahashi

& Momiyama 1993, Wheeler et al 1994). However, how the splice variants of $Ca_V2.1$[EFa] and $Ca_V2.1$[EFb] variants contribute to synaptic plasticity is still obscure. In order to expand on the functional diversities of the two $Ca_V2.1$ EF-hand splice variants, we screened for proteins that might preferentially modulate $Ca_V2.1$[EFa] or $Ca_V2.1$[EFb] function.

Our laboratory has performed yeast-two-hybridization screening and we used bait sequence that spanned end point of IV-S6 to exon 38 with either exon 37a or exon 37b. Yeast-two-hybrid screening was done using the human brain library. Our work has shown that snapin, the SNAP-25 binding protein, could preferentially bind to exon 37b but not exon 37a.

In order to confirm the interaction between snapin and exon 37b of $Ca_V2.1$, GST-fusion proteins containing either exon 37a and exon 37b of $Ca_V2.1$ were generated from clones harbouring the respective proximal C-terminus. The segments of proximal C-terminus of $Ca_v2.1$ were sub-cloned into the GST expression vector, pGEX4T-1 (Fig. 2.2A, B).

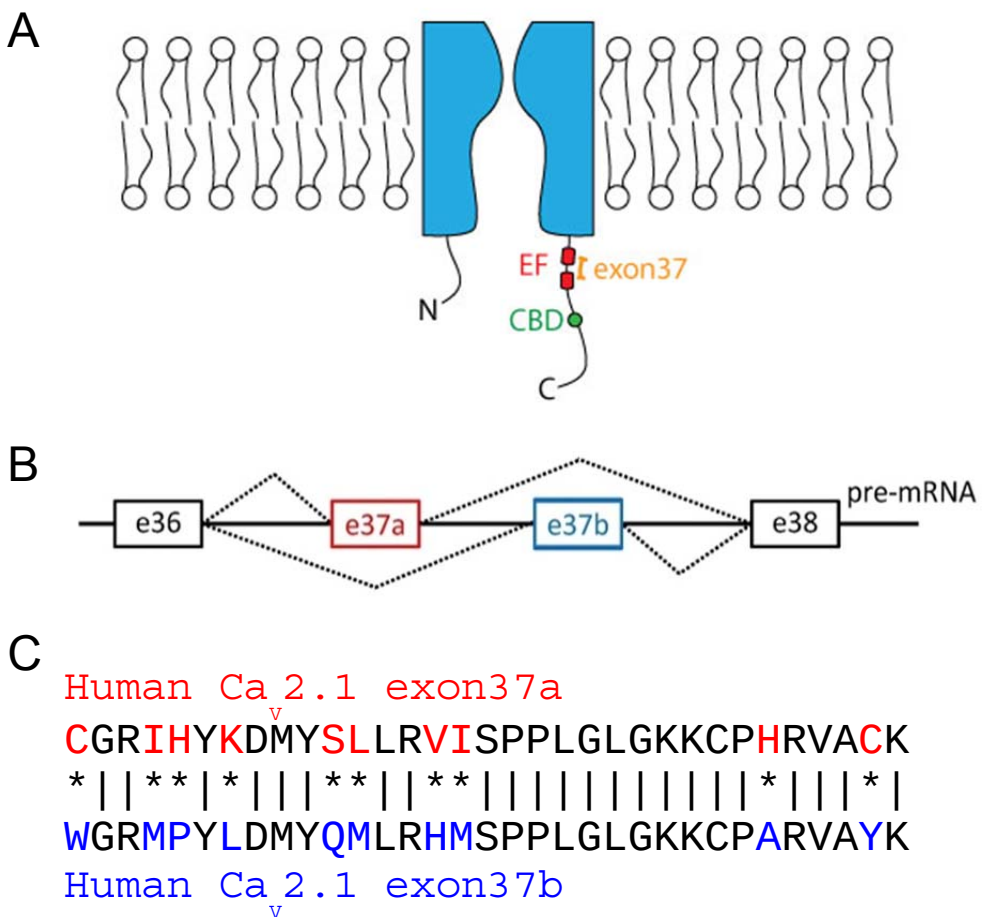

Figure 2.1 Alternative splicing of exon 37 in $Ca_V2.1$.
A. The EF-hand like domain is in the proximal C-terminus of $Ca_V2.1$. Exon 36 and exon 37 (Yellow) form the first EF-hand. Another predicted EF-hand was shown close to the calmodulin-binding domain. **B.** Exon 37a and exon 37b are mutually exclusively expressed in $Ca_V2.1$. **C.** Alignment of amino acid sequences of human exon 37a and exon 37b.

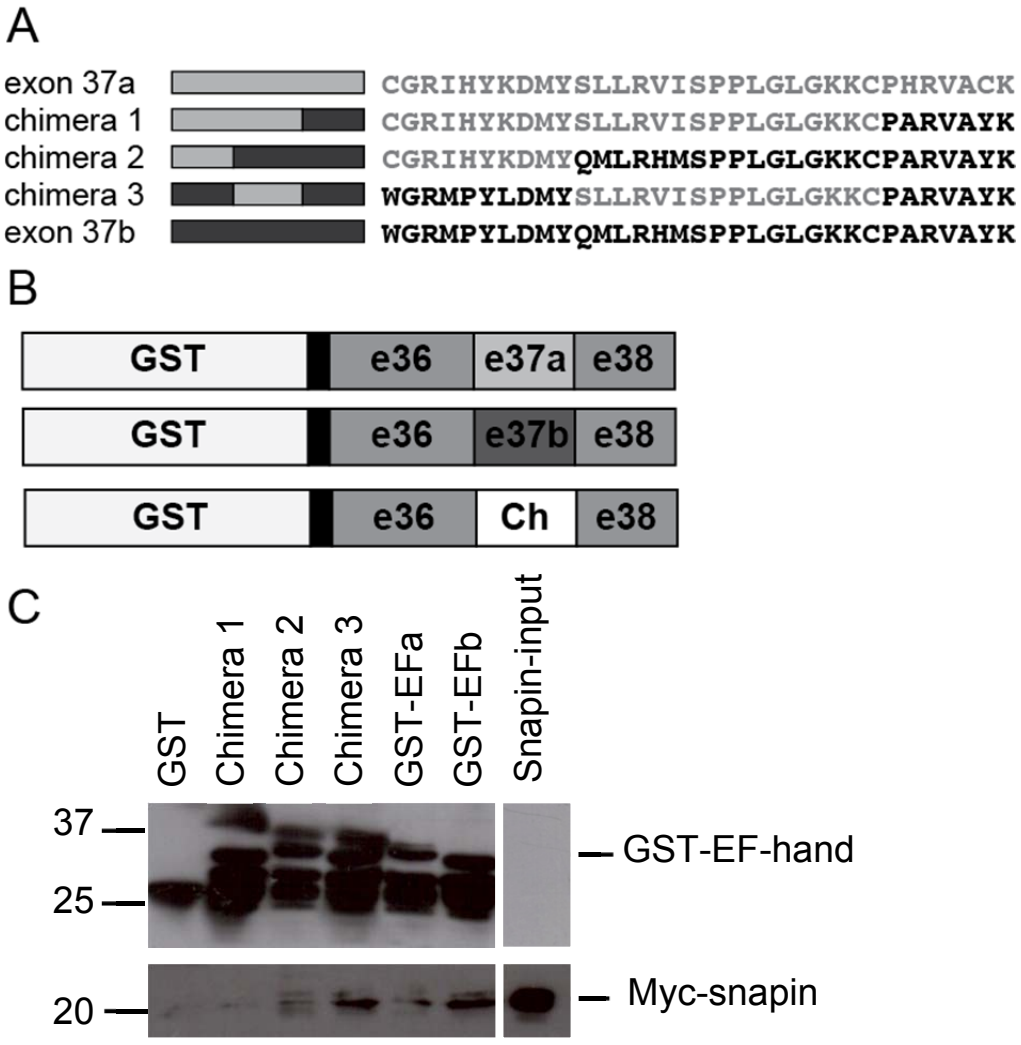

Figure 2.2 GST-pull down assay showed preferential interaction between snapin and EFb variant of $Ca_V2.1$.

A. Alignment of amino acid sequences of EFa, EFb and their chimeras. **B.** Diagrammatic representation of the GST-fusion proteins include part of exon 35, exon 36-38 containing exon 37a, exon 37 b or exon 37a/37b chimeras (Ch). This segment of proximal C-terminus of $Ca_V2.1$ was cloned into pGEX4T-1 to generate GST-fusion proteins. **C.** Western blot analysis of GST pull-down assay indicates snapin has higher affinity of binding to EFb than to EFa fragment of $Ca_V2.1$. Snapin also preferentially pulled down GST-chimera 3. GST-chimera 2 had a relatively weak binding to snapin and almost undetectable binding effect on GST-chimera 1 to snapin

Using these GST-fusion proteins to pull down cell lysis containing snapin, we found that snapin preferentially bound to EFb fragment of $Ca_V2.1$, while there was a faint band of EFa detected. Therefore, snapin was preferentially bound to exon 37b compare to exon 37a of $Ca_V2.1$ (Fig. 2.2C). Further studies were performed to investigate the specific binding sites for snapin-$Ca_V2.1$ interaction. Among the 33 amino acids of exon 37, there are 10 amino acid differences between exon 37a and exon 37b (Bourinet et al 1999). Therefore, we have generated a few chimeras of EF-hands by arbitrarily dividing exon 37 into three segments as shown in figure 2.2A. Chimera 1 contained 2/3 of exon 37a and 1/3 of C-terminus of exon 37b. Chimera 2 contained 1/3 of exon 37a and 2/3 of C-terminus of exon 37b. Chimera 3 contained 1/3 of N and C- terminus of exon 37b and the middle part is from exon 37a sequences. All the chimeras were cloned into GST-expression vector, pGEX4T-1. The GST-pull down assays showed that chimera 3 bound snapin with the highest affinity compared to the other two chimeras. Chimera 2 had a weak interaction to snapin but the binding of snapin to chimera 1 was hardly detectable. These results suggested that the N-terminal segment of exon 37b is critical for binding with snapin.

Four amino acids in N-terminal exon 37b are different from exon 37a. Therefore, we mutated these critical amino acids to alanine in the N-terminal region of exon 37, i.e. tryptophan (W), methionine (M), proline (P) and lysine (L). The GST-pull down assay results showed that the triple mutations of methionine, proline and lysine of the EFb (MPL-

AAA) resulted in a reduction in binding between snapin and EF-hand fragment (Fig. 2.3). Taken together, snapin preferably bound to exon 37b of $Ca_V2.1$ and the amino acids in the N-terminal of exon 37b are critical for the binding of snapin.

2.3.2 Snapin increased current density of $Ca_V2.1$[EFb] but not $Ca_V2.1$[EFa] channels

We have shown the interaction between snapin and $Ca_V2.1$[EFb]. In order to investigate the functional effects of the interaction between snapin and $Ca_V2.1$, we have examined the possible attribution of Ca^{2+} channel properties of $Ca_V2.1$[EFa] and $Ca_V2.1$[EFb] with snapin. Therefore, we co-transfected snapin and $Ca_V2.1$ into HEK 293 cells and performed whole-cell patch clamp electrophysiology.

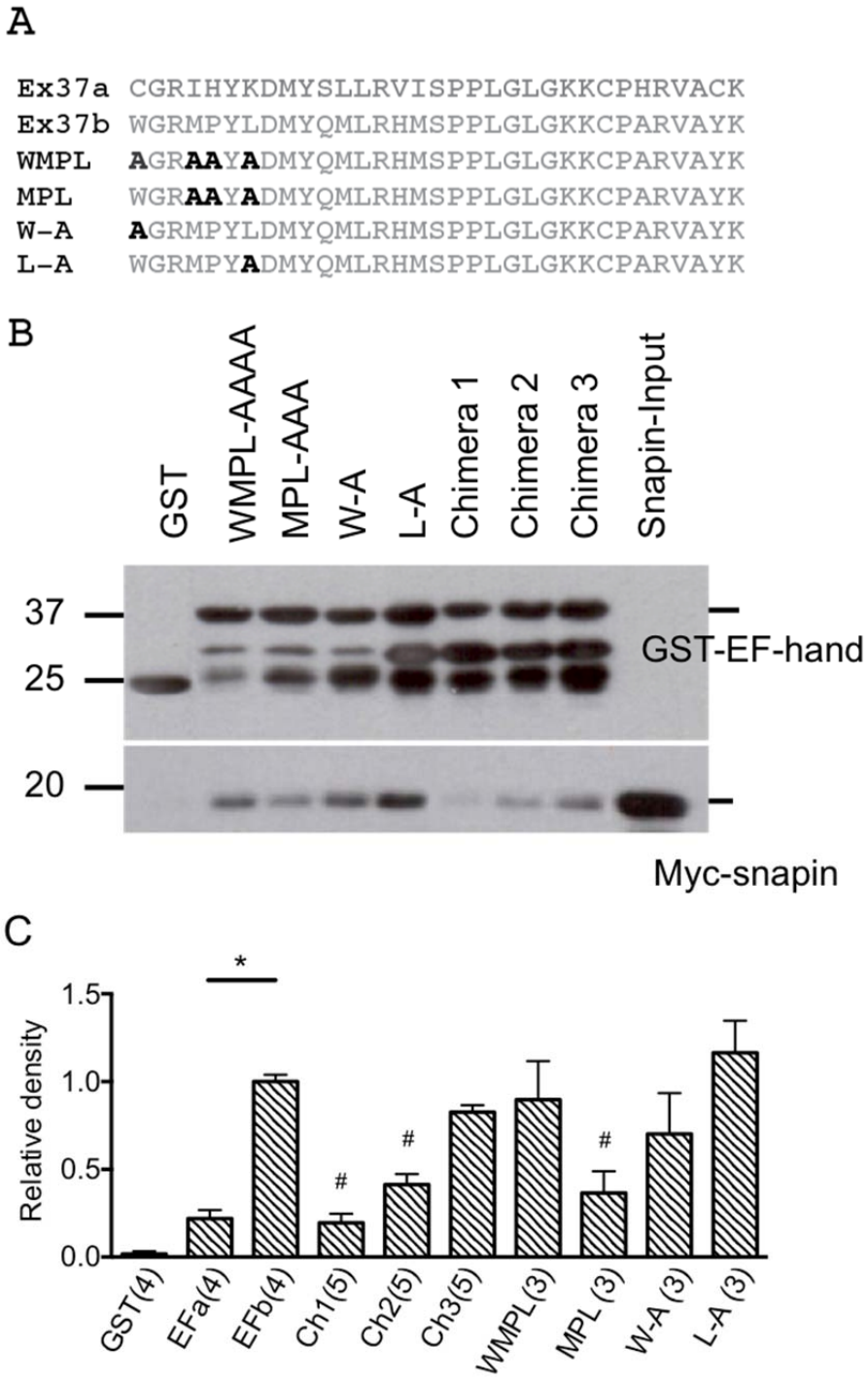

Figure 2.3 GST pull-down assays indicated that N-terminal region of EFb is important for binding of snapin.
A. Several mutations of exon 37b were generated at the critical amino acids in exon 37b, including WMPL-AAAA, MPL-AAA, W-A and L-A. The mutant EFb fragments were then cloned into GST-expression vector. **B**. GST-pull-down assay showed that MPL-AAA triple mutation suppressed the binding between snapin and EFb fragment. **C.** The relative pull down level was determined by western blot. * $p < 0.01$, compared between EFb and EFa, #, $p < 0.05$, compare with EFb. The data were represented as Mean ± SEM and analyzed by Student t-test.

We first briefly examined the by current-voltage (I-V) relationships of snapin co-transfected with the $Ca_V2.1$[EFa] and $Ca_V2.1$[EFb] variants (Liao et al 2004). In this study, a family of depolarization steps were delivered to activate the voltage-gated calcium channel. To obtain results for current density, we divided the currents evoked by each potential by membrane capacitance, which represent cell surface area. The graphs were plotted on the relationships between the holding voltage and current density and the result showed that snapin increased the current density for $Ca_V2.1$[EFb] ($Ca_V2.1$[EFb] + vector 50.97 ± 8.153 pA/pF, n = 19; $Ca_V2.1$[EFb] + snapin 89.06 ± 12.05 pA/pF, n = 14, p = 0.015). But snapin did not affect current density of $Ca_V2.1$[EFa] recorded by I-V protocol.

Further studies were performed using the tail protocol, which is a more accurate way to compare the current-voltage relationships. The tail protocol was generated by a family of 20 ms test-pulse (-60 mV to 100 mV) and -50 mV repolarization, following each step. The results derived from using the tail protocol (Fig. 2.4) showed that snapin significantly increased the current density of $Ca_V2.1$[EFb] channels (from 157.8 ± 7.0 pA/pF, n = 15 to 222.5 ± 6.7 pA/pF, n = 22, p < 0.001). In contrast, snapin did not affect $Ca_V2.1$[EFa] current density (Table 2.1). It is known that the C-terminus of $Ca_V2.1$ undergo alternative splicing and amongst various splice variations could produce a long-form $Ca_V2.1$[47+] and short-form $Ca_V2.1$[47-] (Soong et al 2002, Zhuchenko et al 1997). In view of this, we also examined the effect of snapin on $Ca_V2.1$[EFb, 47+]. The results showed that snapin

increased current density of the long-form $Ca_V2.1$[EFb, 47+] even larger as shown in tail protocol (vector, -168.7 ± 6.2, pA/pF, n = 14; snapin, 283.9 ± 11.4 pA/pF, n = 24, $p < 0.001$) and I-V protocols (vector, 168.7 ± 6.2 pA/pF, n = 22; snapin, -108.2 ± 12.86 pA/pF, n = 19, $p = 0.028$).

Table 2.1 Electrophysiological properties of $Ca_V2.1$ interacting with snapin

	$Ca_V2.1$[EFa] 47- vector	**$Ca_V2.1$[EFa] 47- snapin**	**$Ca_V2.1$[EFb] 47- vector**	**$Ca_V2.1$[EFb] 47- snapin**
Tail: I_{max} (pA/pF)	299.6 ± 11.0 (17)	298.5 ± 7.7 (16)	157.8 ± 7.0 (15)	222.5 ± 6.7* (22)
$V_{1/2act}$ (mV)	-7.51 ± 0.42 (20)	-9.67 ± 0.43 (26)	-7.15 ± 0.60 (15)	-8.66 ± 0.52 (14)
$V_{1/2inact}$ (mV)	-28.59 ± 0.77 (10)	-32.37 ± 0.77 (10)	-32.09 ± 1.61 (7)	-32.00 ± 1.21 (8)

	$Ca_V2.1$[EFb] 47+ vector	**$Ca_V2.1$[EFb] 47+ snapin**
Tail: I_{max} (pA/pF)	168.7 ± 6.2 (22)	283.9 ± 11.4* (24)
$V_{1/2act}$ (mV)	-7.65 ± 0.56 (22)	-4.41 ± 0.75 (22)
$V_{1/2inact}$ (mV)	-22.80 ± 0.44 (8)	-22.79 ± 0.91 (7)

The number of experiments is indicated in parentheses. $V_{1/2act}$ and $V_{1/2inact}$ represent potential of half activation and half inactivation. $V_{1/2act}$ was derived from tail-activation curves recorder in Ba^{2+} solution and $V_{1/2inact}$ was derived from SSI recorded Ba^{2+} solution (Fig. 2.4). For statistics, * $p < 0.001$, compared with same group between snapin and vector (Student's t test, unpaired, two tails).

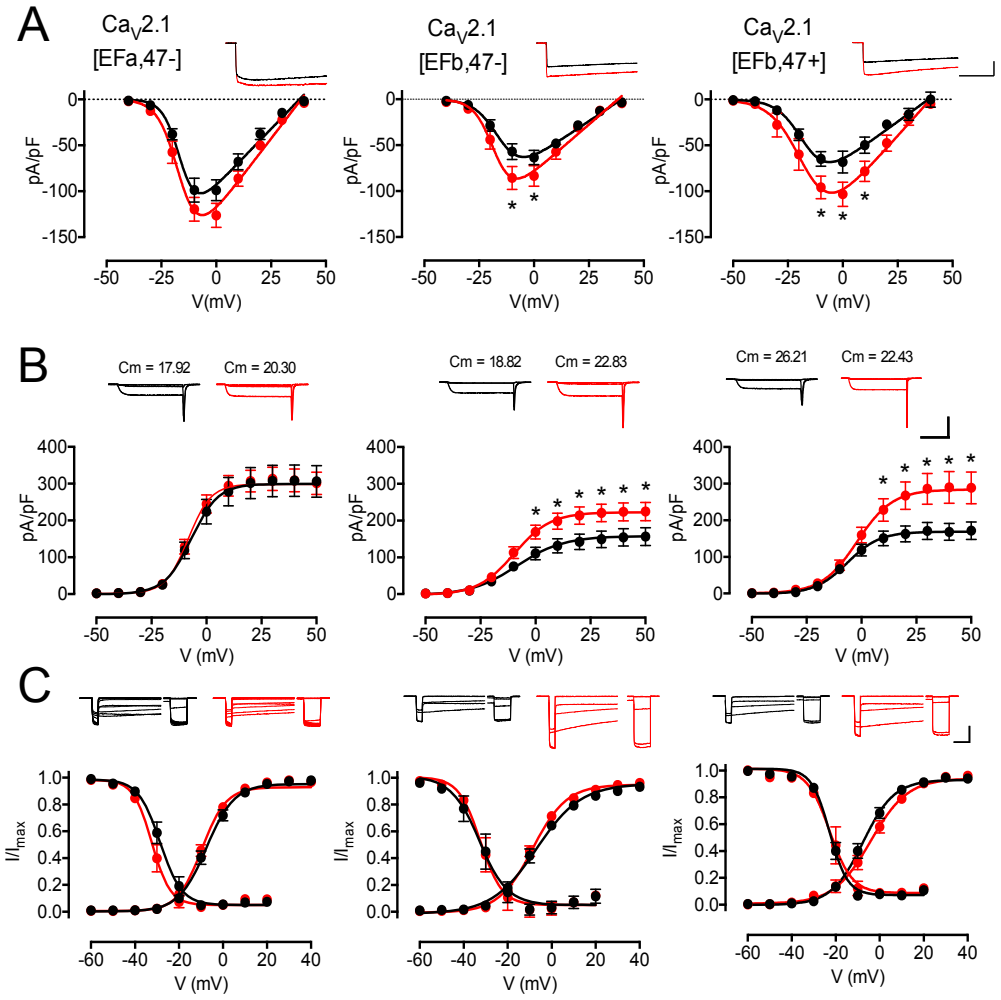

Figure 2.4 Snapin enhanced current density of Ca$_V$2.1[EFb,47±] channels.
A. I-V curve properties of Ca$_V$2.1[EFa,47-], Ca$_V$2.1[EFb,47-] and Ca$_V$2.1[EFb,47+], with (red) or without snapin (black). *Upper panel*, exemplary traces of channel current were shown in 0 mV. Calibration bar: 1 nA, 100 ms. **B.** Channel current activated by tail protocol of Ca$_V$2.1[EFa,47-], Ca$_V$2.1[EFb,47-] and Ca$_V$2.1[EFb,47+] with (red) or without snapin (black). *Upper panel*, exemplary traces of the tail currents activated at -20 mV, +10 mV and +50 mV. Calibration bar: 1 nA, 10 ms. **C.** Activation curve and inactivation curve were obtained from a tail protocol and steady-state inactivation protocol. The two curves of Ca$_V$2.1[EFa,47-], Ca$_V$2.1[EFb,47-] and Ca$_V$2.1[EFb,47+] with (red) or without snapin (black) were plotted in the same chart. *Upper panel*, exemplary traces of the stead-state inactivation of normalization pulse and test pulse. Calibration bar: 0.5 nA, 100 ms. *p < 0.001. Each group was compared with and without snapin by Student t-test.

Together, the electrophysiological results indicate that snapin has a stronger effect on increasing the current density of $Ca_V2.1$[EFb, 47+] (68%) compared to the $Ca_V2.1$[EFb, 47-](41%). These results showed that snapin preferentially increased the current density on $Ca_V2.1$[EFb] but not on $Ca_V2.1$[EFa] through preferential binding to exon 37b. In addition, the inclusion of exon 47 of the distal C-terminus augmented $Ca_V2.1$ current while interacting with snapin.

In addition to current density, we compared the activation and inactivation threshold of $Ca_V2.1$ currents by examining the activation and inactivation potential using the Tail and steady-state inactivation (SSI) protocols. The activation curves were obtained from a tail protocol. The currents obtained at different depolarization steps were normalized to the peak current of each cell. By fitting with single Boltzmann equations, the activation curves is quantified by $V_{1/2act}$, where, half of the channels were open at this voltage. The steady-stated inactivation protocol was conduced by 15s depolarization with a family of voltage. The inactivation ratio was obtained from the ratio of a test pulse before and after this steady-state depolarization. The SSI results were also fitted with single Boltzmann equations and $V_{1/2inact}$ refer to the voltage, where half of the channels were inactivated. The interception of $V_{1/2act}$ and $V_{1/2inact}$ provide the window current for the VGCC (Liao et al 2009). Our results showed that snapin did not significantly affect either $V_{1/2act}$ or $V_{1/2inact}$ of $Ca_V2.1$[EFa] and $Ca_V2.1$[EFb] (Figure 2.4C and Table 2.1). These results suggested that snapin did not affect the voltage sensing or gating of the $Ca_V2.1$

channels.

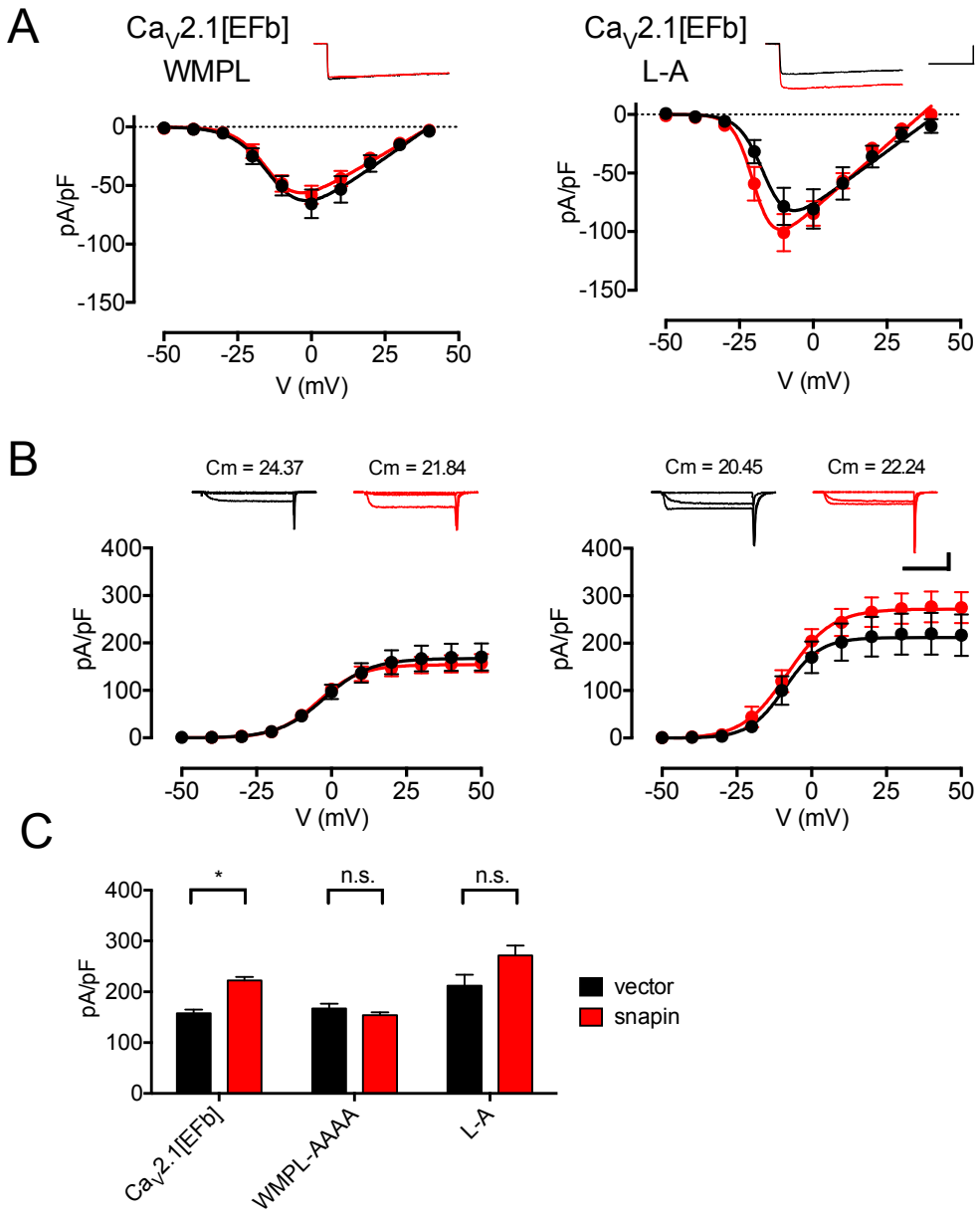

Figure 2.5 Characterization of the interaction between mutant $Ca_V2.1$ and snapin. **A.** I-V curve properties of $Ca_V2.1$[EFb] WMPL-AAAA and $Ca_V2.1$[EFb] L-A and with (red) or without snapin (black). *Upper panel*, exemplary traces of channel current evoked at 0 mV. Calibration bar: 1 nA, 100 ms. **C.** Channel current activated by tail protocol of $Ca_V2.1$[EFb] WMPL-A and $Ca_V2.1$[EFb] L-A with (red) or without snapin (black). *Upper panel*, exemplary traces of the tail current activated at -20 mV, +10 mV and +50 mV. Calibration bar: 1 nA, 10 ms. **D.** Summary chart on the channel current density. * $p < 0.001$. Each group is compared by Student t-test.

The GST pull-down results have indicated that the N-terminus of exon 37b is crucial for binding with snapin. The replacement the N-terminus of exon 37b and the MPL-AAA mutation of exon 37b disrupted the interaction between snapin and $Ca_V2.1$. We generated the full-length channel with MPL-AAA and chimera (1/3e37a+2/3e37b) and examined the electrical properties of the channel. However, these mutated channels were non-functional for unknown reason to us and as a result we could hardly record the channel's current. Therefore, we have tried the WMPL-AAAA quadruple mutation by substituting tryptophan (W), methionine (M), proline (P) and lysine (L) of exon 37b into alanine and examined whether the current densities are altered in the mutant channels as compared to the wild-type reference $Ca_V2.1$[EFb] channel. Therefore we compared the function of WMPL-AAAA and L-A of $Ca_V2.1$[EFb] channels in their interaction with snapin. The data shows that WMPL-AAAA abolished the binding of snapin to $Ca_V2.1$ (WMPL-AAAA + vector, 167.1 ± 10.3 pA/pF, n = 10; WMPL-AAAA + snapin, 154.1 ± 5.8 pA/pF, n = 14; p = 0.25), while the L-A substitution partially impaired the functional effects of snapin binding (L-A + vector, 211.8 ± 21.9 pA/pF; n = 8; L-A + snapin 271.9 ± 18.9 pA/pF, n =15; p = 0.053) (Fig. 2.5). These function results support the idea that snapin-$Ca_V2.1$ interaction is dependent on exon 37b.

Overall, our results suggest that snapin binds to the N-terminus of exon 37b and increases the Ca^{2+} channel current. Mutations of the amino acids found on the N-terminal segment of exon 37b disrupted the binding of $Ca_V2.1$ channel with snapin. Single and multiple amino acid

mutations may disrupt channel functions. WMPL-AAAA of $Ca_V2.1$[EFb] mutant channels conducted normal current but they could not be modulated by snapin. Therefore, the interaction between snapin and $Ca_V2.1$[EFb] offer another level of splice-variant selective modulation to enhance Ca^{2+} influx via $Ca_V2.1$ channel.

2.3.3 Snapin functioned as a dimer in modulating $Ca_V2.1$

It has been reported that snapin forms dimer via disulfide bond of cysteine 66 (Pan et al 2009). In order to determine whether snapin dimerization affects the interaction between snapin and $Ca_V2.1$, we generated the snapin-C66A mutant by substituting the cysteine for alanine. As shown in figure 2.6A, the snapin-C66A mutants could not form dimers as examined under reducing conditions, without addition of 2-mercaptoethanol in the preparation of protein samples for SDS-PAGE. To examine whether the snapin-C66A proteins could still act on $Ca_V2.1$[EFb] channels as monomers, we co-expressed snapin-C66A with $Ca_V2.1$[EFb] in HEK 293 cells. We found that snapin did not increase the current density of the $Ca_V2.1$[EFb] ($Ca_V2.1$[EFb] + snapin-C66A, 156.8 ± 6.8 pA/pF, n = 16; compared with $Ca_V2.1$[EFb] + vector, p = 0.9). Similarly, snapin-C66A also did not affect the current density of $Ca_V2.1$[EFa] channels (Fig 2.6B and 2.6C). Therefore, snapin dimerization is crucial for interacting with EFb segment of $Ca_V2.1$ channel.

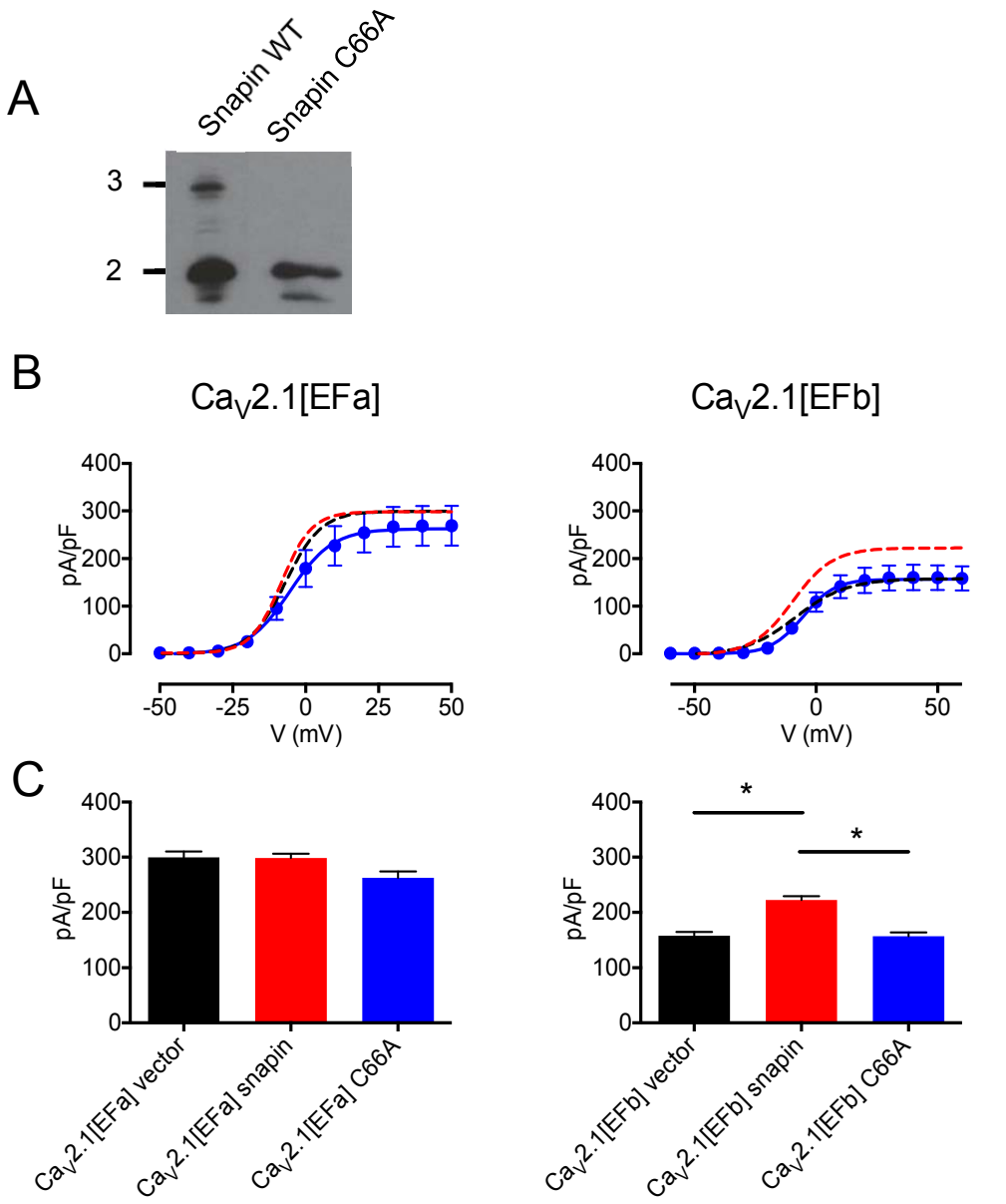

Figure 2.6 Snapin function as a dimer in modulating calcium channel current.
A. Snapin but not snapin C66A form dimers as shown under reduced SDS-PAGE with addition of 2-Mech. **B.** *left panel*, Channel current activated by tail protocol of $Ca_V2.1$[EFa] with snapin-C66A (blue). Previous results of the $Ca_V2.1$[EFa] with (black) or without snapin (red) current are shown in dash line. Exemplary traces are shown. *Right panel*, Channel current activated by tail protocol of $Ca_V2.1$[EFb] with snapin-C66A (blue). Previous results of the $Ca_V2.1$[EFb] with (black) or without snapin (red) current are shown in dash line. Calibration bar: 0.5 nA, 100 ms. **C.** Summary chart on the channel current density. *Left panel.* Snapin and snapin C66A did not affect current of $Ca_V2.1$[EFa]. *Right panel.* Snapin C66A mutation did not increase current of $Ca_V2.1$[EFb] as wild -type snapin did. * $p < 0.001$. Each group was compared by Student t-test.

2.3.4 Snapin did not affect CDF and CDI of $Ca_V2.1$

Reports showed that the proximal C-terminus of VGCC is involved in Ca^{2+}-dependent regulation of Ca^{2+} channels including CDI and/or CDF (Chaudhuri et al 2004, Chaudhuri et al 2007, Huang et al 2012, Liang et al 2003, Minor & Findeisen 2010). These modulations are highly dependent on calmodulin binding to the proximal C-terminus of the channel. In order to assess whether the interaction between snapin and $Ca_V2.1$ affects the Ca^{2+}-dependent modulation by calmodulin, we examined the CDI and CDF processes of $Ca_V2.1$ channels. The CDF of $Ca_V2.1$ channels were elicited by a short depolarization followed by a pre-pulse. The facilitation was quantified by integrating the difference between normalized test-pulse with or without the pre-pulse (ΔQ). The Relative fraction (RF) is obtained from ΔQ divided by the trace decay time (τ). A monotonic RF is expected with Ba^{2+} as a charge carrier. Therefore, CDF was calculated by the difference of RF between Ba^{2+} and Ca^{2+}. As shown in figure 2.7, $Ca_V2.1$[EFa] showed robust CDF, but snapin did not augment or suppress the facilitation of $Ca_V2.1$[EFa] channels. In contrast, CDF was essentially non-existent in the presence of exon 37b and snapin likewise did not change this outcome in $Ca_V2.1$[EFb] channels.

The $Ca_V2.1$[EFa] and $Ca_V2.1$[EFb] channels usually show robust inactivation as recorded within 1 second depolarization. The CDI (*f* value) of the channels was obtained by subtracting the fraction of inactivation as recorded in Ba^{2+} solution. When examined as the

residual amount of current left after 800 ms or 300 ms, r_{800} and r_{300}, snapin did not alter the CDI of $Ca_V2.1$[EFa] and $Ca_V2.1$[EFb] channels (Fig 2.8). As both CDF and CDI of $Ca_V2.1$ are highly dependent on calmodulin, our results showed that binding with snapin and the proximal C-terminus of $Ca_V2.1$ did not affect the interaction between calmodulin and $Ca_V2.1$.

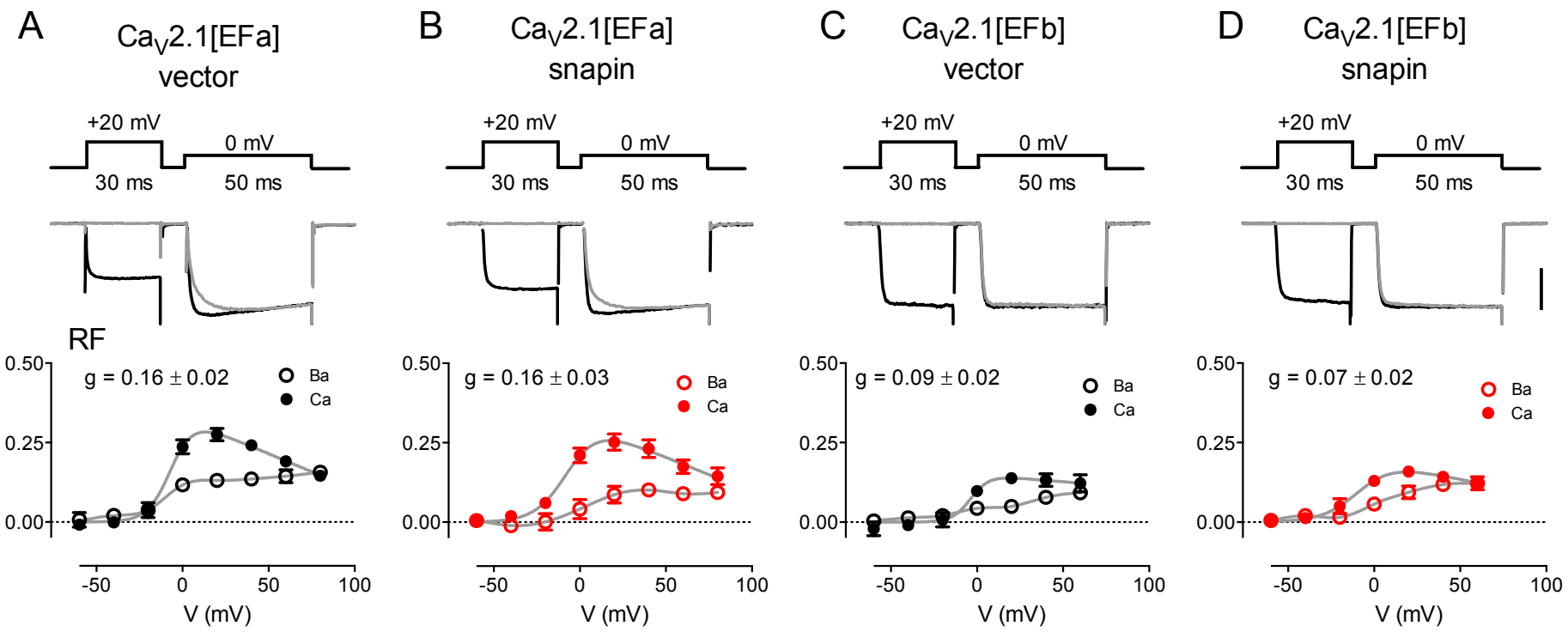
A
$Ca_V2.1$[EFa]
vector
B
$Ca_V2.1$[EFa]
snapin
C
$Ca_V2.1$[EFb]
vector
D
$Ca_V2.1$[EFb]
snapin
+20 mV
0 mV
30 ms
50 ms
RF
g = 0.16 ± 0.02
g = 0.16 ± 0.03
g = 0.09 ± 0.02
g = 0.07 ± 0.02
Ba
Ca
0.50
0.25
0.00
-50
0
50
100
V (mV)

Figure 2.7 Snapin did not affect Ca^{2+}-dependent facilitation of $Ca_V2.1$.
The CDF of the $Ca_V2.1$[EFa] + vector (n = 9) **(A),** $Ca_V2.1$[EFa] + snapin (n = 10) **(B)**, $Ca_V2.1$[EFb] + vector (n = 5) **(C)** and $Ca_V2.1$[EFb] + snapin (n = 7) **(D)** indicated that CDF was unaltered in the presence of snapin. *Top* CDF was characterized by a rectangular voltage depolarization paradigms. A short test pulse depolarization (0 mV, 50 ms) was applied after a pre-pulse (+20 mV). *Middle.* Exemplary traces of the corresponding evoked Ca^{2+} currents were shown. The test pulse traces showed slow phase activation without a prepulse (grey), while after the pre-pulse, the Ca^{2+} current was facilitated with a relative fast phase of activation. The traces were normalized to unity at the end of the test-pulse. The increased fraction of the area with or without the pre-pulse was calculated by relative fraction (RF). Calibration bar represented 0.5 units. *Bottom.* The RF was represented as a function of pre-pulse voltage obtained in Ba^{2+} and Ca^{2+} solution. Averaged g value was calculated by the difference of RF recorded in Ca^{2+} and Ba^{2+} solutions. Mean value of g with +20 mV pre-pulse and SEM were shown.

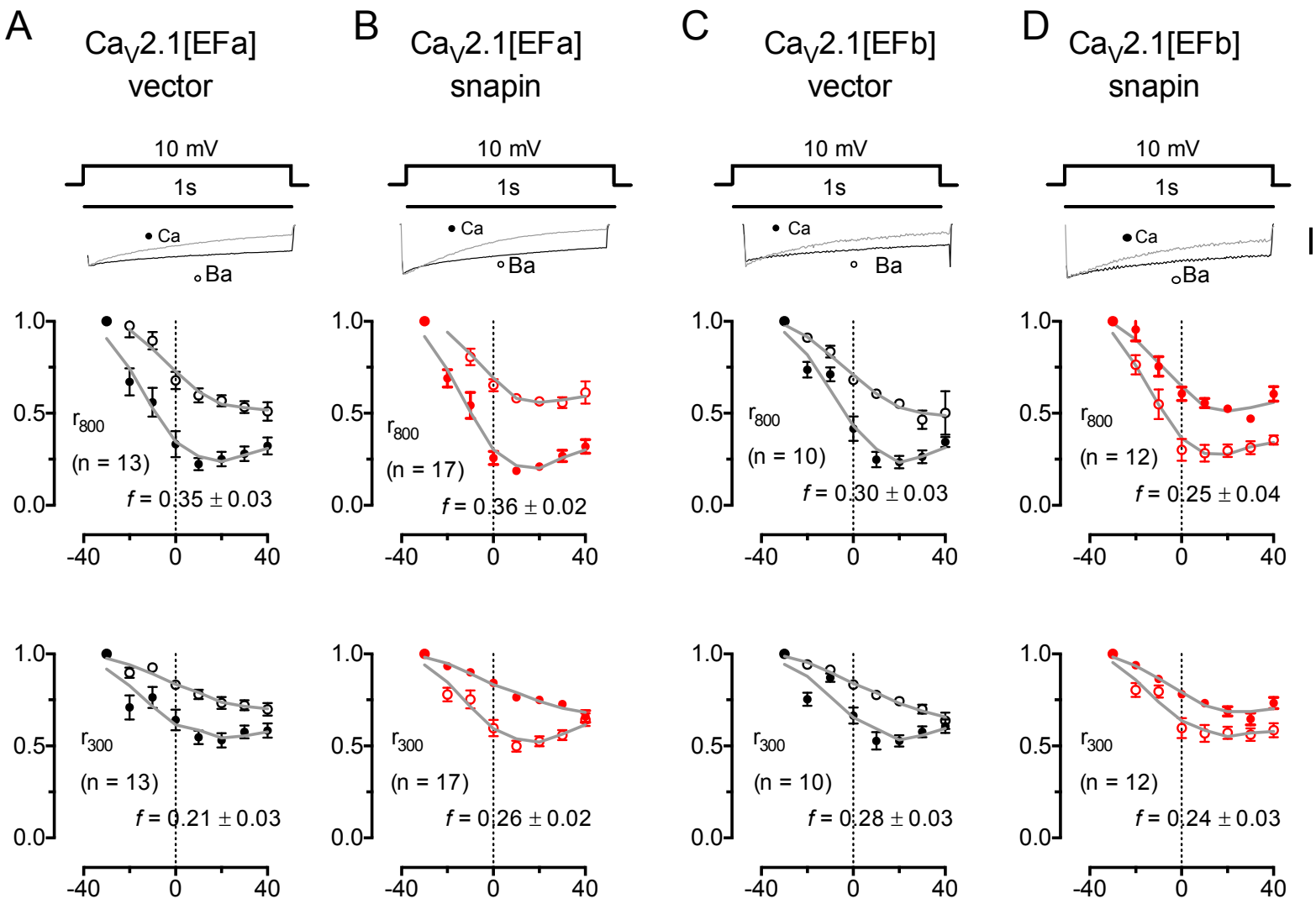
A
$Ca_V2.1$[EFa]
vector
B
$Ca_V2.1$[EFa]
snapin
C
$Ca_V2.1$[EFb]
vector
D
$Ca_V2.1$[EFb]
snapin
10 mV
1s
Ca
Ba
r_{800}
(n = 13)
f = 0.35 ± 0.03
(n = 17)
f = 0.36 ± 0.02
(n = 10)
f = 0.30 ± 0.03
(n = 12)
f = 0.25 ± 0.04
r_{300}
(n = 13)
f = 0.21 ± 0.03
(n = 17)
f = 0.26 ± 0.02
(n = 10)
f = 0.28 ± 0.03
(n = 12)
f = 0.24 ± 0.03
1.0
0.5
0.0
-40
0
40

Figure 2.8 Snapin did not affect the Ca^{2+}-dependent inactivation of $Ca_V2.1$.
The CDI of $Ca_V2.1$[EFa] + vector **(A)** $Ca_V2.1$[EFa] + snapin **(B)**, $Ca_V2.1$[EFb] + vector **(C)** and $Ca_V2.1$[EFb] + snapin **(D)** are shown. *Top.* CDI was characterized by prolonged 1 second depolarization (+10 mV). The $Ca_V2.1$ channels produced faster decay of Ca^{2+} (Grey, filled dot) versus Ba^{2+} currents (Black, open dot). Calibration bar: 0.5 nA. *Middle.* The averaged inactivation profiles were shown by r_{800}, the remaining fraction of current after 800 ms depolarization obtained in Ba^{2+} and Ca^{2+}, corresponding to a depolarizing voltage. The CDI is characterized by a f-value representing the difference between r_{800} of Ca^{2+} and Ba^{2+}. *Bottom.* The averaged inactivation profiles were also shown by r_{300}. The CDI was characterized based on the inactivation after 300 ms depolarization. Mean value of f with +10 mV pre-pulse and SEM are shown.

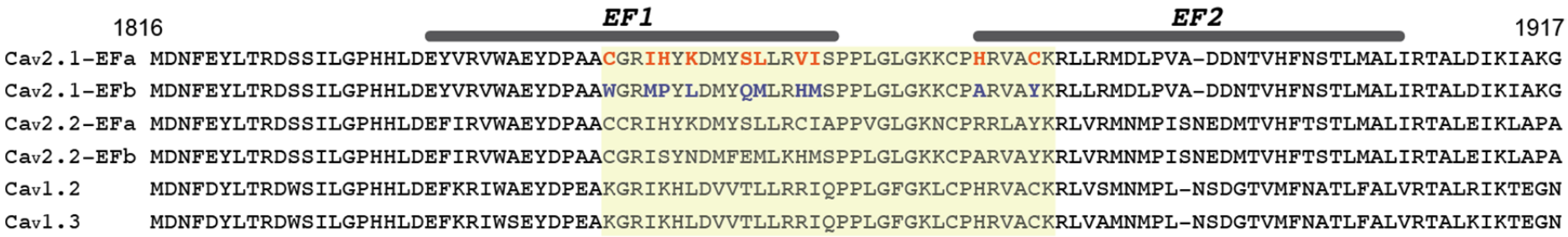

Figure 2.9 Alignment of proximal C-terminus of $Ca_V2.1$[EFa]/[EFb], $Ca_V2.2$[EFa]/[EFb], $Ca_V1.2$ and $Ca_V1.3$.
Exon 37 of $Ca_V2.1$ and homologous sequences from $Ca_V2.2$, $Ca_V1.3$ and $Ca_V1.2$ were highlighted in grey. The critical differences in amino acids sequences between exon 37a and exon 37b are highlighted in bold font. The putative EF-hand domains are predicted as shown. Exon 37 spans the two EF-hands.

2.3.5 Snapin preferentially increased $Ca_V2.2$ [EFa] current

Both $Ca_V2.1$ and $Ca_V2.2$ are highly expressed in the neurons and promote the synaptic transmission (Mochida et al 1996, Wheeler et al 1994). Similar to $Ca_V2.1$, $Ca_V2.2$[EFa] and $Ca_V2.2$[EFb] are found in the nervous system (Bell et al 2004). It would be interesting to evaluate whether snapin could modulate $Ca_V2.2$. Therefore, we co-transfected $Ca_V2.2$[EFa] and $Ca_V2.2$[EFb] with snapin and examined the current density, activation and inactivation potential of $Ca_V2.2$ channels. Surprisingly, we found that snapin preferentially increased the current density of $Ca_V2.2$[EFa] but not of $Ca_V2.2$[EFb] ($Ca_V2.2$[EFa] + snapin, 403.7 ± 2.5 pA/pF, n = 12; compared with $Ca_V2.2$[EFa] + vector, 315.6 ± 2.0 pA/pF, n = 17; $p < 0.001$). Given that $Ca_V2.2$[EFa] channels are critical for pain processing, these studies would suggest a role for snapin in pain processing.

Table 2.2 Electrophysiological properties of $Ca_V2.2$ interacting with snapin.

	$Ca_V2.2$[EFa] vector	**$Ca_V2.2$[EFa] snapin**	**$Ca_V2.2$[EFb] vector**	**$Ca_V2.2$[EFb] snapin**
I_{max} Tail (pA/pF)	315.6 ± 1.9 (15)	407.3 ± 2.5 * (12)	169.8 ± 3.0 (12)	183.9 ± 3.8 (17)
$V_{1/2act}$ (mV)	-2.42 ± 0.45 (15)	-0.81 ± 0.40 (26)	-0.73 ± 0.35 (13)	-4.12 ± 0.52 (19)
$V_{1/2inact}$ (mV)	-29.92 ± 1.52 (7)	-31.20± 0.81 (12)	-25.18 ± 0.70 (11)	-23.43 ± 0.62 (11)

The number of experiments is indicated in parentheses. $V_{1/2act}$ and $V_{1/2inact}$ represent potential of half activation and half inactivation respectively. $V_{1/2act}$ was derived from tail-activation curves recorder in Ba^{2+} solution and $V_{1/2inact}$ was derived from SSI recorded Ba_{2+} solution (Fig. 2.10). For statistics, * $p < 0.001$, compared with same group between snapin and vector (Student's t test, unpaired, two tails).

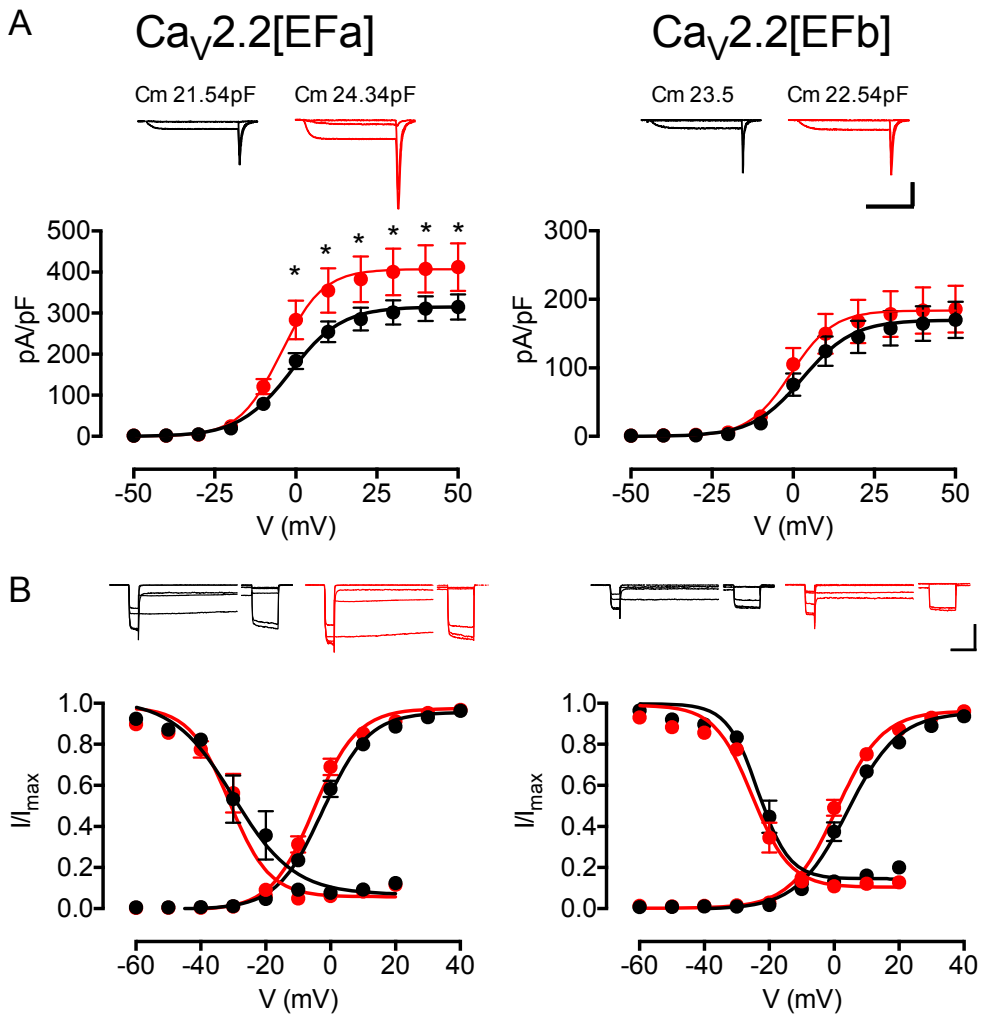

Figure 2.10. Modulation on $Ca_V2.2$ current by snapin.
A. Channel current activated by tail protocol of $Ca_V2.2$[EFa], $Ca_V2.2$[EFb] with (red) or without snapin (black). *Upper panel*, exemplary traces of the tail current activated at -20 mV, +10 mV and +50 mV. Calibration bar: 1 nA, 10 ms. **B.** Activation and inactivation curves were obtained from a tail protocol and steady-state inactivation protocol. The two curves of $Ca_V2.2$[EFa], $Ca_V2.2$[EFb] and $Ca_V2.1$[EFb,47+] with (red) or without snapin (black) were plotted in the same chart. *Upper panel*, exemplary traces of the stead-state inactivation of normalization pulse and test pulse. Calibration bar: 0.5 nA, 100 ms. * $p < 0.001$. Each group was compared with and without snapin by Student t-test.

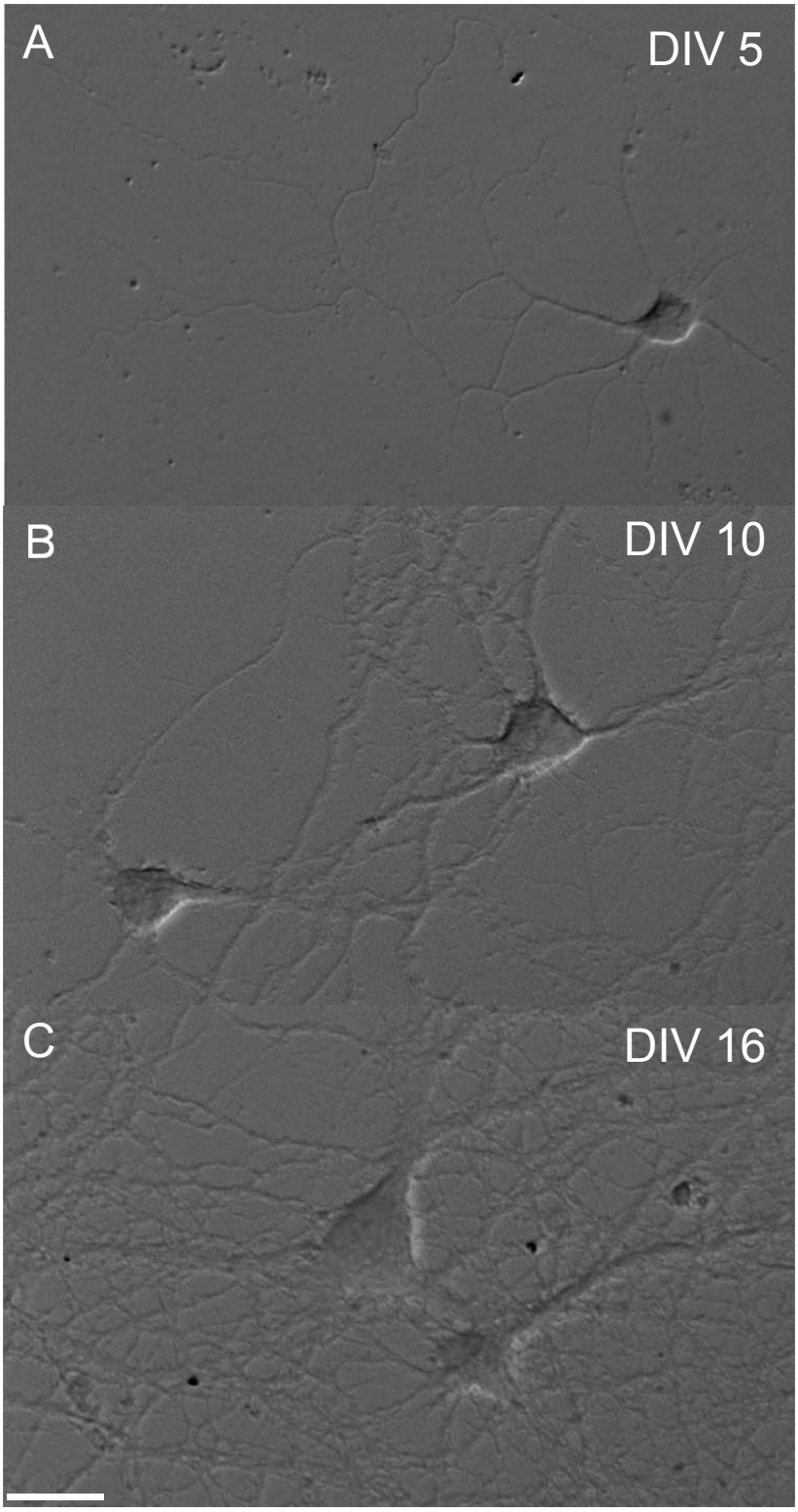

Figure 2.11 Primary hippocampal neuronal culture.
A. 5 days after plating (DIV 5). The dendrites started to grow and many branches could be observed. The axon extended over hundreds of micro-meters and beyond the field of view. **B.** 10 days after plating (DIV 10). Extensive connections had been formed with the nearby neurons. **C.** 16 days after plating (DIV16). The neuron bodies have increased in size. The axon and dendrites forms complicate networks. Scale bar, 10 μm.

2.3.6 Snapin and synaptic transmission

Our studies has revealed that snapin preferentially increased the current density of two splice variants $Ca_V2.1$[EFb] and $Ca_V2.2$[EFa]. Given the crucial role of $Ca_V2.1$ in synaptic transmission, it would be interesting to access whether snapin affects synaptic transmission through interacting with $Ca_V2.1$ channel. Previous works has shown that snapin-deficient neurons did not respond to high-frequency stimulus and synchronizing release was abolished (Pan et al 2009).

We prepared primary hippocampal neurons culture according to Banker's protocol. The hippocampal neurons in various stages of culture were shown in figure 2.11 and 2.12. Snapin is highly expressed in the synapses and co-localized with synapsin, markers of the presynaptic terminals (Fig. 2.13).

In order to examine how snapin affects synaptic transmission, we used shRNA to knockdown snapin expression in the cultured neurons. Two shRNAs targeting the coding sequences of snapin were used in this study. We packaged the shRNA in lentivirus and infected the primary neurons at DIV8 and our results showed that the expression of snapin was suppressed as shown in figure 2.14A.

To examine the functional effects of snapin knockdown, we have recorded the spontaneous EPSC in the cultured neuron by whole-cell patch clamp electrophysiology (Fig. 2.14). Our results indicated that the amplitude of sEPSC was not affected. Taken together our results demonstrated that in primary cultured neuron culture, snapin was co-

localized with synapse marker, synapsin and knocking down snapin did not affect the amplitude of sEPSC.

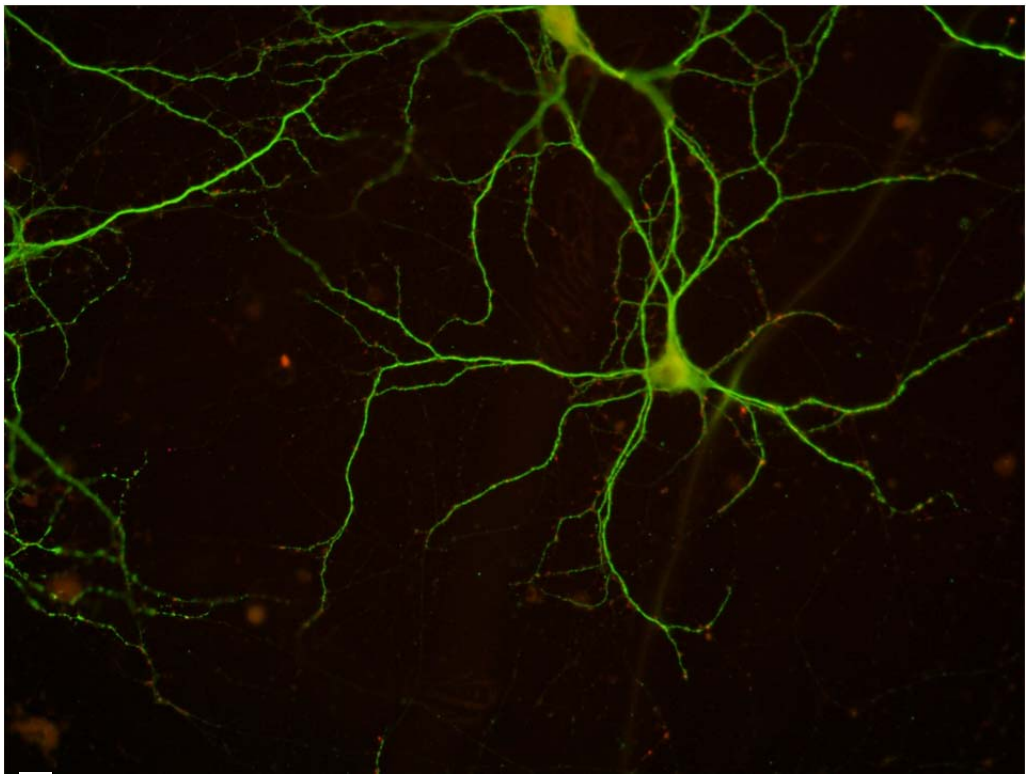

Figure 2.12 The dendrites and synapses are visualized with MAP2 and synapsin antibodies.
The 16-day-old culture was fixed in paraformaldehyde and immunostained with anti-MAP2 and anti-synapsin antibodies. MAP2 decorate the dendritic microtubules and synapsin is exclusively localized in the mature synapse. Scale bar, 10 μm

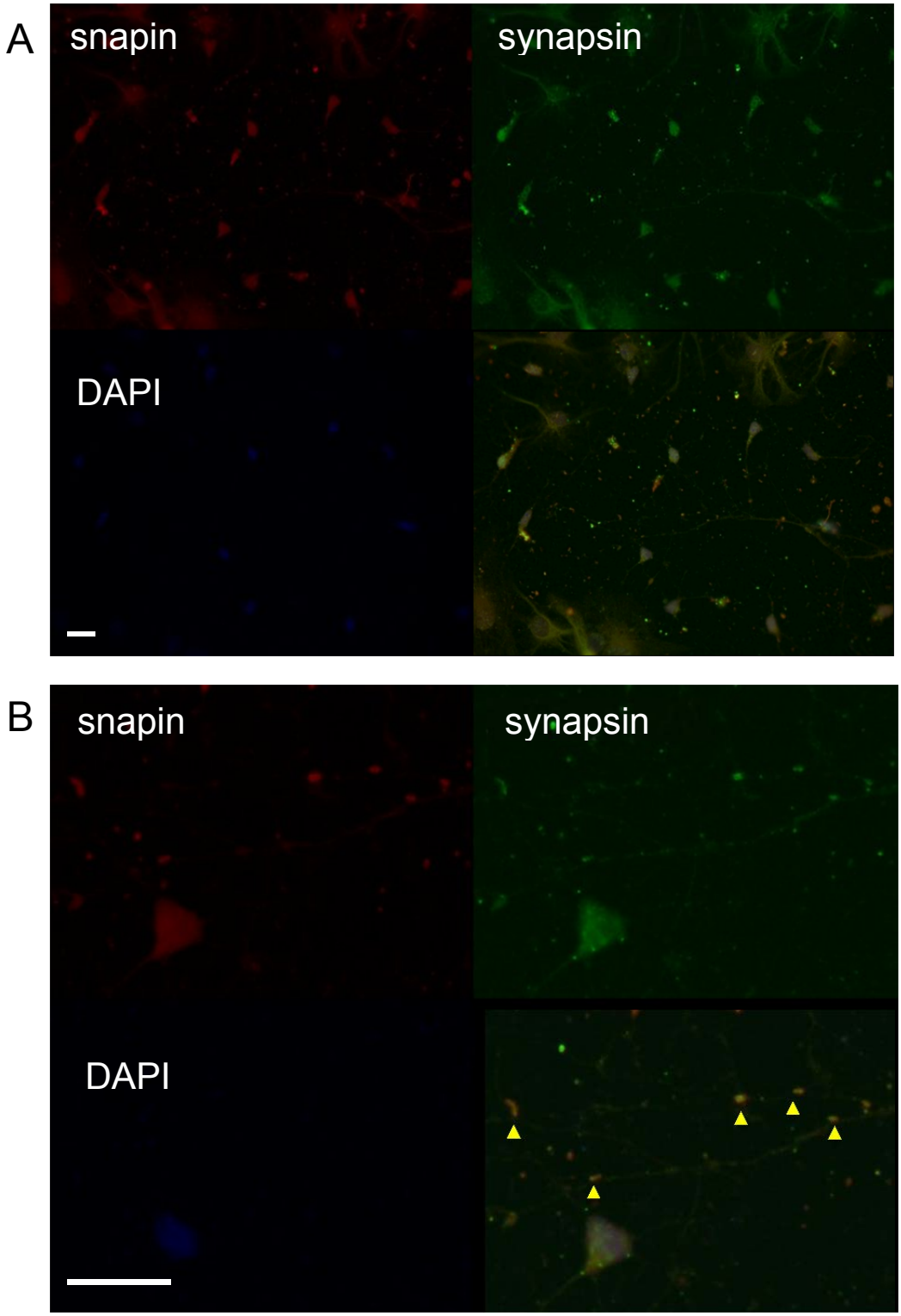

Figure 2.13 Double labeling of snapin (red) and synaptic marker synapsin (green) in primary hippocampal neuron.
A. The primary hippocampal neuron cultures were fixed at DIV 16. Positive immunocytochemical staining for presynaptic marker. Synapsin is labeled in green and snapin is labeled by red. DAPI (blue) stains the nuclears of neurons. Scale bar, 20 μm. **B.** The magnfied photos showed that snapin and synapsin are co-localized in synapse as indicated by yellow arrow head. Scale bar, 20 μm

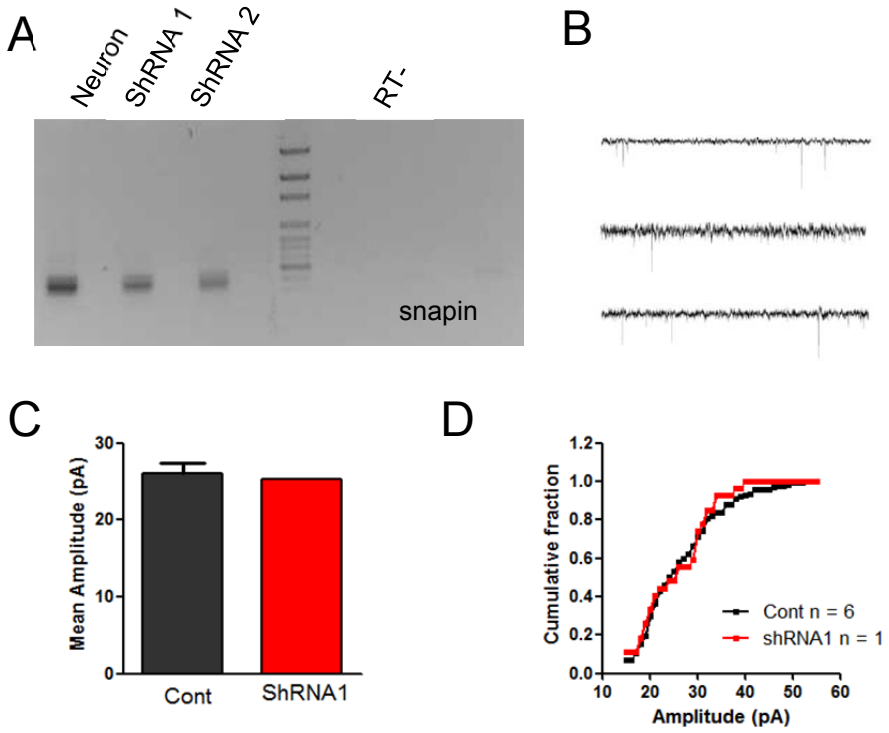

Figure 2.14 Snapin did not affect the spontaneous vesicle release
A. RT-PCR showed expression snapin was reduced by shRNA in neurons. **B.** Exemplary traces by spontaneous EPSC. **C.D.** Knockdown snapin did not affect the spontaneous EPSCs. 73 events of control and 23 events of shRNA were recored

2.4 Discussion

2.4.1 Diversified function of $Ca_V2.1$[EFa] and $Ca_V2.1$[EFb] variants

In these studies, we have examined the interaction between snapin and Ca_V2 channels. We found that snapin could preferentially modulate $Ca_V2.1$ channels containing either exon 37 splice variant. The $Ca_V2.1$[EFa] and $Ca_V2.1$[EFb] are mutually exclusive splice variants. Using yeast-two-hybrid and GST pull-down assays, we have shown that snapin preferentially bound to the N-terminal region of exon 37b. The interaction between snapin and $Ca_V2.1$ increases $Ca_V2.1$[EFb] but not $Ca_V2.1$[EFa] current density. Alanine substitutions of $Ca_V2.1$ exon 37b disrupted the interaction between snapin and calcium channels. Given the important role $Ca_V2.1$ channels play in triggering synaptic vesicle release, the amount of Ca^{2+} influx through the channels will affect synaptic transmission (Catterall & Few 2008). Our studies provide a new insight into the diversified functions of $Ca_V2.1$[EFa] and $Ca_V2.1$[EFb] variants. Alternative splicing events usually occur in tissues and cells with complex functions (Modrek et al 2001, Yeo et al 2005). Mutually exclusive splicing of exon 37 occurs in two similar VGCCs, $Ca_V2.1$ and $Ca_V2.2$, and they are found in most mammals. The $Ca_V2.1$[EFa] and $Ca_V2.1$[EFb] have been shown to display subtle differences in electrophysiological properties such as current density and CDF (Bourinet et al 1999, Chaudhuri et al 2004, Chaudhuri et al 2007, Soong et al 2002). The preferential binding of snapin with $Ca_V2.1$[EFb] would lead to further fine-tuning of $Ca_V2.1$[EFa] and

$Ca_V2.1$[EFb] functions in triggering synaptic transmission and synaptic plasticity. As suggested by previous studies in our laboratory, the expression of $Ca_V2.1$[EFa] and $Ca_V2.1$[EFb] is under spatial and temporal regulations. There are predominant EFb variants in early brain development and after the first two decades of life, there would be about equal expression levels of $Ca_V2.1$[EFa] and $Ca_V2.1$[EFb] (Chang et al 2007). Although the mechanisms underlying the developmentally regulated expression regulation is unknown, our results may help to explain the distinct roles of $Ca_V2.1$[EFb] in early development.

2.4.2 Interaction between snapin and $Ca_V2.1$ potentiates synchronous vesicle release

Snapin is crucial for synchronous vesicle release as snapin-deficient neurons could not respond to high-frequency input precisely and effectively during synaptic transmission (Pan et al 2009). Synchronous release is supported by large and localized Ca^{2+} influx through VGCCs at the active zone (Martens et al 2007). It requires close alignment of Syt-1, SNARE and Ca^{2+} channels. Our results revealed that snapin binds to $Ca_V2.1$ channels and promotes Ca^{2+} influx through VGCCs. Two possible mechanisms may explain the role of snapin binding to Ca_V2 in synchronous release: (1) Snapin facilitates Ca^{2+} influx and simply increases local Ca^{2+} concentration. Elevated transient [Ca^{2+}] leads to more stable Syt I-Ca^{2+} and Ca^{2+}-triggered Syt-I will switch synaptic vesicles from the priming mode to the fusion mode through

interaction with the SNARE complex. Therefore, the higher the local Ca^{2+} concentration, the more efficient it is to trigger synchronous vesicle release; (2) Snapin has been shown to bind to Syt-I, SNAP-25 and VGCC. These multiple protein interactions may form a complicated complex with VGCC-SNARE-Syt-I-snapin. Syt I-Ca^{2+} fused with SNARE during Ca^{2+} influx (Zhang et al 2002a) and snapin could stabilize the Syt-I-SNARE complex before Ca^{2+} influx (Pan et al 2009, Tian et al 2005). The close distance between VGCCs and Syt-I-SNARE complex would be coupled to Ca^{2+} influx and the vesicle fusion process better and then lead to efficient synchronous release.

Studies from our group have shown that pre-synaptically expressed $Ca_V2.1$[EFa] and $Ca_V2.1$[EFb] would differentially affect plasticity of transmitter release upon paired stimulations in cultured neurons. The $Ca_V2.1$[EFa] channels triggered a large initial EPSCs and small EPSC in the following stimulus. While the $Ca_V2.1$[EFb] channels mediated an augmented post-synaptic current upon paired-pulse stimulus (Ng et al unpublished). The repetitive Ca^{2+} influx strengthened the connection between Syt-I-SNARE complex and VGCC and resulted in increasing post-synaptic currents. However, without the interaction between snapin and VGCC, the vesicles are likely to be depleted, resulting in depression of the paired stimuli.

2.4.3 Snapin preferentially recruited EF-hand splice variant of Ca^{2+} channels to the active zones of presynaptic terminals

The active slot for VGCC in mediating synchronous vesicle release is limited. Both $Ca_V2.1$ and $Ca_V2.2$ channels are competing for the active zone of the presynaptic sites (Cao & Tsien 2005, Cao & Tsien 2010). Several proteins such as RIM, Rab3 and Munc 13 have been shown to anchor the $Ca_V2.1$ and $Ca_V2.2$ channels to the active slots (Deng et al 2011, Han et al 2011, Kaeser et al 2011). It has been reported that bassoon selectively controlled $Ca_V2.1$ but not $Ca_V2.2$ recruitment to active zone (Davydova et al 2014). Furthermore, snapin is also reported in SNARE protein retrograde transportation. Deficient snain-dynein interaction impair the autophagic vesicle transportation, which cause vesicle aggregations in synaptic terminals (Cheng et al 2015) The preferential binding of snapin to $Ca_V2.1$[EFb] and $Ca_V2.2$[EFa] may be involved in selective recruitment of the splice variants to presynaptic active zones. Snapin has been shown to be involved in retrograde protein trafficking through interacting with dynein (Cai et al 2010). Studies showed that snapin modulate the transportation of several membrane proteins to cell membrane including TRPM7, BDNF-TrkB and TMPAP, etc. (Krapivinsky et al 2006, Quintero et al 2013, Zhou et al 2012). The availability of VGCC in the presynaptic zone might also be modulated through interacting with snapin.

2.4.4 Exon 37 is crucial for EF-hand like domain structure and channel function

In our studies, we have tried to mutate several amino acids in the EF-hand like domain and examined the functional effects of $Ca_V2.1$-snapin interaction. However, several mutant full-length channels including MPL-triple mutations, W-A, M-A, P-A single mutation, could not conduct Ca^{2+} currents. It has been reported that the truncated VGCC without the EF-hand like domain is non-functional (Graves et al 2008). The alanine substitution in the CaV2.1 exon 37b mutant may be structurally altered and the net result is channel dysfunction (Peterson et al 2000).

2.4.5 Snapin modulated $Ca_V2.2$[EFa] and potential implication in pain processing

In addition to $Ca_V2.1$, our results also showed that snapin preferentially increase the current density of $Ca_V2.2$[EFa] but not $Ca_V2.2$[EFb]. The $Ca_V2.2$ channels have been shown to be involved in the pain processing. In particular, $Ca_V2.2$[EFa] is more efficient in transmitting pain signals than $Ca_V2.2$[EFb] because it is exclusively expressed in small nociceptive neurons and it conducts larger currents. The preferential effects of snapin may facilitate the pain processing mediated by $Ca_V2.2$[EFa] and disruption of the interaction between snapin and $Ca_V2.2$[EFa] may result in the relieved pain sensation.

2.4.6 EF-hand and calmodulin

The EF-hand domain of $Ca_V2.1$ resembles the similar domain in the proximal C-terminus structures in Na_V channels (Chagot et al 2009). The atomic structure of one helical part of EF-hand and the downstream pre-IQ and IQ domain has been resolved in the homologous $Ca_V1.2$ segment. Recent studies have proposed the possible role of EF-hand domain in interacting with apoCaM, the calcium freeform of calmodulin. Mutations on the conserved region of exon 37 in $Ca_V1.3$ attenuate CDI formation. It is suggested that the CaM is pre-associated with EF-hand and IQ domain. Upon Ca^{2+} influx, CaM was trans-located and lead to calcium dependent inactivation. Our studies revealed a novel function of EF-hand in interacting snapin. In additional to the augment on $Ca_V2.1$ current, snapin did not affect the CDF and CDI of $Ca_v2.1$[EFa] or $Ca_v2.1$[EFb]. Therefore, snapin-$Ca_V2.1$ interaction does not affect the calmodulin function. These results could be explained that calmodulin has high affinities to $Ca_V2.1$ upon Ca^{2+} influx. It would replace snapin in interacting with the EF-hand. Therefore, the calmodulin interaction between snapin and $Ca_v2.1$ seems not affected.

Snapin usually forms a dimer with disulfide bond. The snapin dimmer interact with the synaptagmin-1 and snapin monomer, snapin-C66A could not rescue the deficiency of synchronous release in snapin knockout neurons. We find that snapin also interact with $Ca_V2.1$ with dimer, the snapin C66A monomer do not affect the calcium channel

current density, suggesting the widely appearance of snapin dimerization in synaptic function.

2.4.7 Snapin and synaptic transmission

In these studies, we have tried to knock down snapin and examined the synaptic transmission. We knock down the snapin by transfect the shRNA in neurons using lentivirus. It is shown that the expression of snapin was partially inhibited in the neurons with shRNA. In profiling the synaptic transmission, we found that the spontaneous activities of synaptic transmission were not much affected with snapin knocking down. The amplitudes of sEPSC represented the amount of asynchronous vesicle release. Paired stimulus would be considered in future studies to identify the synchronous vesicle release. Therefore, a single neuron would be depolarized and activate the nearby neuron transmitter release.

2.4.8 Conclusion and future studies

Our studies here revealed a novel interaction between the snapin and C-terminus of $Ca_V2.1$. Striking, these interactions were preferentially to $Ca_V2.1$[EFb] splice variant instead of $Ca_V2.1$[EFa]. The N-terminals of exon 37b were crucial for the binding with snapin. Functionally, snapin selectively increased the current density of $Ca_V2.1$[EFb] compared to $Ca_V2.1$[EFa]. Mutation on the N-terminals of exon 37b disrupt the interaction between snapin and $Ca_V2.1$[EFb]. Moreover, the snapin functions as dimer in modulating $Ca_V2.1$ channel properties.

Substituting the cysteine 66 to alanine of snapin disrupted snapin-$Ca_V2.1$ interaction.

$Ca_V2.1$ mediates the Ca^{2+} influx and play a crucial role in triggering vesicle release. Given the crucial role of snapin in interacting several proteins related to vesicle release, including SNAP-25 and Syt-I (Chheda et al 2001, Ilardi et al 1999, Pan et al 2009), would the interaction between snapin and $Ca_V2.1$ affect the synaptic release?

Previous studies have identified the interaction between synprint region VGCC and syntaxin and Syt-I (Bezprozvanny et al 1995, Rettig et al 1996, Simms & Zamponi 2014, Weiss & Zamponi 2012). It is not clear that how does snapin-$Ca_V2.1$ interaction affect the relationships between VGCC and SNARE complex. Does snapin compete for VGCC binding to syntaxin and Syt-I or facilitate the multiple protein interaction in complicated protein complex? We would knockdown snapin or overexpress the dominant-negative mutation snapin C66A in neurons and use immunoprecipation assay to pull down the presynaptic complex. These studies may further elucidate the role of snapin in presynaptic vesicle release machinery.

The preliminary studies have been performed by knocking down snapin in primary neuron. Although the synaptic transmission of snapin deficient neuron has been characterized, the dysfunction of retrograde transportation and altered development may induce wide-ranging effect on neuron (Cai et al 2010, Pan et al 2009, Tian et al 2005). Therefore, we would use shRNA to knock down snapin in culture neuron. It is

shown that synchronized release of synaptic transmission is altered in snapin deficient neurons (Pan et al 2009). In the future studies, we will examine the synaptic transmission under high frequency stimulation and whether the synaptic transmission is altered in snapin knockdown neurons. In addition, since the $Ca_V2.1$[EFa] and $Ca_V2.1$[EFb] display distinct roles in short-term synaptic plasticity, whether the preferential interaction of snapin on $Ca_V2.1$[EFb] would affect the short-term synaptic plasticity. Therefore we would deliver paired stimulus on culture neurons. Two interconnected neuron would be patched at the same time. The depolarization on one neuron would induce post-synaptic current in the other neuron through synapse. We would knock down snapin in one neuron and examine the synaptic current in the other. The fluorescence marker carried by snapin shRNA would help to identify the transfected neuron. It would helpful to explain how snapin affect the synaptic transmission.

Furthermore, we would examine the synaptic vesicle release using VGlut1-pHluorin (Burrone et al 2007). The pH sensitive protein VGlut1-pHluorin displays fluorescence green when it is released from the vesicles to synaptic clefts. The amount of fluorescence represents he amount of vesicle release. We would use this methology to examine the synaptic transmission in neurons with snapin overexpression or snapin knockdown.

Chapter 3 Splice-variant-selective modulation of $Ca_V1.3$ by snapin

3.1 Introduction

$Ca_V1.3$ is one of the L-type voltage-gated calcium channels and it is widely expressed in excitable cells. These channels are highly enriched in the superchrismatic nucleus and substantia nigra of brain, sinoatrial nodes of heart and inner hair cells (IHCs) of cochlea (Brandt et al 2005, Platzer et al 2000, Zhang et al 2002b). Although the sequence is quite similar to $Ca_V1.2$, $Ca_V1.3$ channels display several unique features. The $Ca_V1.3$ channel is characterized by its low activation threshold, independent of the tissue of origin or the auxiliary subunits associated with it. It is usually activated from -45 mV to -60 mV (Xu & Lipscombe 2001). In addition, $Ca_V1.3$ channels are less sensitive to dihydropyridine antagonists as compared to $Ca_V1.2$ (Huang et al 2013). The $Ca_V1.3$ gene can be extensively modified post-transcriptionally. In addition to extensive alternative splicing (Shen et al 2006, Tan et al 2011), $Ca_V1.3$ pre-mRNA could be edited by adenosine deaminase, in the IQ-domain to affect Ca^{2+}-dependent inactivation (Huang et al 2012, Adams et al 2014).

3.1.1 $Ca_V1.3$ in cochlea during development

Calcium currents in cochlea were first described in the chicken hair cells. Whole-cell patch clamp studies in hair cell have recorded voltage sensitive Ca^{2+} currents (Fuchs & Sokolowski 1990). Unlike other synapses in the nervous system, Ca^{2+} channels in the inner hair cells are exclusively $Ca_V1.3$ instead of $Ca_V2.1$ or $Ca_V2.2$ (Kollmar et al 1997a, Kollmar et al 1997b). Deletion of $Ca_V1.3$ in the mice resulted in

a reduction of over 90% of the Ca^{2+} currents in the inner hair cells (Platzer et al 2000). It is known that $Ca_V1.3$ channels play a critical role in inner hair cells during different developmental stages. Prior to hearing onset, $Ca_V1.3$ is essential for cochlea development. $Ca_V1.3$ mediates spontaneous action potential in rodent immature inner hair cells. These spontaneous activity is essential for synapse formation and wiring of the neuronal network in the cochlea (Kros et al 1998). It has been shown that $Ca_V1.3$ channels in immature neurons exhibit larger Ca^{2+} currents and stronger voltage-dependent inactivation than that found in mature neurons, which may shape the activation potential waveforms (Inagaki & Lee 2013). Moreover, $Ca_V1.3$ channels in the immature inner hair cells are rarely associated with synaptic vesicles in the ribbon synapse (Zampini et al 2010). In adult IHCs, $Ca_V1.3$ senses graded voltage depolarization from hair bundle vibration and Ca^{2+} influx through $Ca_V1.3$ would eventually trigger vesicle release (Fuchs 2005, Song et al 2003).

3.1.2 I-II loop region of $Ca_V1.3$

The I-II loop contains the β-subunit binding domain. It is crucial for calcium channel trafficking and protein ubquitination (Altier et al 2011). Several splice sites in the I-II loop have been identified. It was reported that alternative exon 9* and exon 11 of $Ca_V1.3$ are located at the I-II loop (Kollmar et al 1997a, Kollmar et al 1997b). The alternative splicing of a paralogous exon 9* could also be found in the $Ca_V1.2$ channels and its presence shifted the activation potential (Liao et al 2009). The

intracellular I-II loop region may obstruct the calcium channel pore and alter its biophysical properties. The inclusion of additional amino acids through the inclusion of exon 9* may therefore alter the topology of the β-subunit binding region. Exon 11 is unique to $Ca_V1.3$ and the homologous sequences of exon 11 are not found in $Ca_V1.2$ or other L-type calcium channels. Exon 11 contains 20 amino acids, which is a slightly shorter than exon 9*. The inclusion of exon 11 could be found in brain, heart and cochlea, though the functional studies on $Ca_V1.3$ channels containing exon 11 is limited.

3.1.3 $Ca_V1.3$ undergoes feedback modulations

For its vital role in cellular function, $Ca_V1.3$ is subject to negative feedback regulation by a rise in internal Ca^{2+} concentration (Calcium-dependent inactivation, CDI) and by membrane voltage change (Voltage-dependent inactivation, VDI). These feedback regulations are modulated with post-transcriptional modification on $Ca_V1.3$ (e.g. alternative splicing and RNA editing). Similar to Ca_V2 family, Ca^{2+}-dependent inactivation of $Ca_V1.3$ channels is achieved by Ca^{2+}-calmodulin binding to the C-terminus of the $Ca_V1.3$ channels (Adams et al 2014, Peterson et al 1999, Zuhlke et al 1999). Studies from Huang et al have shown that post-transcriptional modification by RNA editing could convert the isoleucine (I) to methionine (M), and glutamine (Q) to arginine (R). The edited channel has significantly reduced CDI as compared to the un-edited channel (Ben Johny et al 2013, Huang et al 2012). The presence or absence of IQ-domain could also be

determined by alternative splicing. Some splice variants found in the cochlea were truncated in the proximal C-terminals without the IQ-domain. The CDI of the truncated $Ca_V1.3_{\Delta IQ}$ was abolished due to the absence of the IQ-domain (Shen et al 2006). In addition, alternative splicing of the $Ca_V1.3$ on the distal C-terminus also affected the strength of CDI. The $Ca_V1.3$ is mutually exclusive spliced by exon 42 and exon 42a. Exon 42a would generate a premature stop codon immediately after the IQ-domain. The $Ca_V1.3_{42a}$ is called the short-form or $Ca_V1.3_{42a}$ compared to the long-form $Ca_V1.3_{42}$ ($Ca_V1.3$ long form). The long-form of $Ca_V1.3$ expresses weak CDI as compared to $Ca_V1.3_{42a}$ channels. It is shown that the distal C-terminus of $Ca_V1.3$ long form contains a CDI inhibiting domain and may occlude the calmodulin-binding domain and diminished the CDI (Liu et al 2010).

The VDI process is initiated by a conformation change of the S1-S4 segment in response to voltage depolarization. The subsequent movements of S6 segment and I-II loop block the gating pore of the calcium channel by a possible “hinge-lid” mechanism (Tadross & Yue 2010). Recent studies found that the S6 in $Ca_V1.3$ repelled the lid closure, which keep the channel open despite the long time voltage depolarization (Tadross et al 2010). The VDI and CDI avoid excessive Ca^{2+} influx through VGCC. Mutation on the S6 segment of $Ca_V1.2$ cause delayed VDI and the excessive Ca^{2+} influx leads to heart failure in Timothy syndrome patients (Splawski et al 1993, Splawski et al 2004, Splawski et al 2005).

3.1.4 Objectives and rationale

The previous works have shown that snapin preferentially increases the current density of the splice variants such as $Ca_V2.1$[EFb] and $Ca_V2.2$[EFa]. The interaction between snapin and calcium channel may increase the efficiency of synaptic transmission. $Ca_V1.3$ triggers the vesicle release in ribbon synapse of inner hair cell. In this study, we would like to examine whether snapin also modulates $Ca_V1.3$ in a similar fashion as for $Ca_V2.1$ or $Ca_V2.2$ channels. Here, we have examined the effects of snapin on three neuronal types of Ca_V1 families: $Ca_V1.2$, $Ca_V1.3$ and $Ca_V1.4$ channels.

In addition, $Ca_V1.3$ can undergo extensive alternative splicing and the splicing pattern could potential change in various developmental stages. We further examined the splicing pattern of $Ca_V1.3$ in the cochlea and how alternative splicing of $Ca_V1.3$ contribute to snapin-$Ca_V1.3$ interaction.

3.2 Materials and methods

3.2.1 Materials

Experiments were carried out on Sprague-Dawley rats with 8 to 9 weeks old, as approved by the NUS IACUC. The full-length human $Ca_V1.2$, $Ca_V1.3$, $Ca_V1.4$ subunits were reported in previous studies (Huang et al 2012, Tan et al 2011, Tan et al 2012, Wang et al 2011).

3.2.2 Construction on the GST-fusion protein

The GST-fusion protein with $Ca_V1.3$ fragments was generated as previously described. The I-II loop, I-III-loop, III-IV loop and C-terminus of $Ca_V1.3$ were amplified by using the following primers.

1.3LF-I-II-Fw GAATTCTCAAAGGAAAGAGAGAAG

1.3LF-I-II-Re GTCGACGACAGACTTCACAGCTGCCC

1.3LF-2/3-Fw GAATTCGACAATTTGGCTGATGCTGA

1.3LF-2/3-Re GTCGACGTGGTGGTTGATGAGTTTGTG

1.3LF-3/4-Fw GAATTCGGCTTCGTCATCGTCACC

1.3LF-3/4-Re GTCGACCGAGGAGTTCACCACGTAC

1.3LF-CT-Fw GGATCCATGGACAATTTTGACTATCTGAC

1.3LF-CT-Re GTCGACCTACAAGGTGGTGATGCA

1.3ShortF-CT GTCGACCTAGAGCATCCGTTCAAG

The $Ca_V1.3_{\Delta E11}$ was given by Huang Hua. The I-II ΔE11 amplified using the primers of 1.3LF-I-II-Fw and 1.3LF-I-II-Re. The PCR products were cloned into pGEX4T-1 as previously described in chapter 2.

3.2.3 Western blot and co-immunoprecipation

The GST-pull down assay was performed similarly as chapter 2, using glutathione sepharose beads (GE Health). Immunoprecipation was performed to examine the interaction between snapin and full-length $Ca_V1.3$. HEK cell lysis transfected with $Ca_V1.3$ and snapin were mixed with 1 μg of anti-$Ca_V1.3$ primary antibodies (Alomone AC-005) and incubated overnight at 4°C. Then the mixture was incubated with 15 μl of Protein A-Sepharose for 3 hr at 4°C. The beads were washed with PBS for three times and the immunoprecipitated protein were detected with SDS-PAGE and immunoblotting. Rabbit anti-$Ca_V1.3$ (1:200) and rabbit anti-snapin (SYSY, 1:1000) were used for blotting.

3.2.4 Total RNA extraction for cochlea

The cochleas from rats were rapidly dissected after decapitation. Total RNA of tissue was isolated using the Trizol (Life Technologies, CA). First strand cDNA was synthesized with Superscript III (Life Technologies, CA) and specific reverse primer at exon 17 of $Ca_V1.3$

according to manufactory instructions.

Rat ex7-17 Re CCAGTCTGGCTGATTGTAGTGCTC

RNA minus control reactions without adding reverse transcriptase were performed in all RT-PCR experiments to exclude genomic DNA contamination.

Subsequent PCR was performed using following primers.

Rat ex7-17 Fw CTTTGCCATGCTCACTGTGT

Rat ex7-17 Re CCAGTCTGGCTGATTGTAGTGCTC

3.2.5 Colony screen for the alternative splicing

Colony screening was performed to determine the splicing ratio of particular splicing sites. The PCR products of I-II loop of $Ca_V1.3$ from cochlea RNA were sub-cloned into pGEM-T easy vector (Promega, WI). The ligation products were then transformed to DH10B *E. coli* competent cell with electronic shock and spread into LB-plate. Isolated clones were picked from LB-plate and colony PCR was performed using

Rat ex9-14 Fw ACCTGGTTCTTGGTGTCCTTAGTG

Rat ex9-14 Re CCAGTCTGGCTGATTGTAGTGCTC

The splicing patterns were determined by the DNA size and the random colony were sent to sequencing to confirm the splicing pattern.

3.2.6 Mammalian cell culture and transfection

HEK293 cells were maintained as previous described (2.3.2). $Ca_V1.3$ channels and snapin was transfected in to HEK cells by calcium phosphate transfection. The DNA plasmids, pIRES-DsRed-Snapin / pIRES-DsRed (1 µg), $Ca_V1.3$ (1.7 µg), β_{2a} (1.25 µg) and $\alpha_2\delta_1$ (1.25 µg) as well as T-antigen (0.25 µg) were used for 35 mm dishes. For biochemical studies, the HEK cell were transfected using lipofectamine™ 2000 according to the standard procesures (Life Technologies, CA).

3.2.7 Whole cell patch clamp electrophysiology

The whole cell patch clamp on the HEK cell was performed as described. The external solution contained (in mM) 10 HEPES, 140 TEA-$MeSO_3$ 5 $CaCl_2$ or 5 $BaCl_2$ (pH 7.4, Osmolarity 300-310 mOsm). The glass pipettes were back- filled with pipette solution contained (in mM) 10 HEPES, 5 CsCl, 138 Cs-$MeSO_3$, 5 EGTA, 1 $MgCl_2$, 2 mg/ml MgATP, (pH 7.3 Osmolarity 290-300 mOsm).

In these studies, Tail, SSI and CDI/VDI were performed to examine the channel properties. The programs and analysis were same as in chapter 2. All data were represented with Mean ± SEM and compared with Student's t-test.

3.3 Results

3.3.1 Snapin bound to I-II loop of $Ca_V1.3$ and increases $Ca_V1.3$ current density

Our previous work showed that snapin preferentially increased $Ca_V2.1$[EFb] and $Ca_V2.2$[EFa] currents (Fig. 2.4 and Fig. 2.10). These two channels from Ca_V2 family are responsible for triggering vesicle release in the central neurons. Other than $Ca_V2.1$ and $Ca_V2.2$, $Ca_V1.3$ is expressed in the cochlear inner hear cells and influx of Ca^{2+} through these channels triggers vesicle release in ribbon synapse (Fuchs 2005, Platzer et al 2000). Therefore, we would like to examine whether snapin, which is found in the presynaptic terminal, could potentially interact with $Ca_V1.3$ channels. To investigate the electrophysiological properties of snapin-$Ca_V1.3$ interaction, we co-expressed $Ca_V1.3$ with snapin in HEK 293 cells and recorded the current density and activation/inactivation potentials of $Ca_V1.3$ channels by the standard tail and steady-state inactivation protocols. As shown in figure 3.1, snapin increased the current density of $Ca_V1.3$ by 30% using Ba^{2+} as the charge carrier ($Ca_V1.3$ + vector, 102.8 ± 3.4 pA/pF, n = 24; $Ca_V1.3$ + snapin, 131.9 ± 5.1 pA/pF, n = 19; $p < 0.001$). Furthermore, Snapin modestly shifted the $V_{1/2act}$ of activation curve of $Ca_V1.3$ to the left ($V_{1/2act}$: $Ca_V1.3$ + vector, -18.75 ± 0.70 mV, n = 18; $Ca_V1.3$ + snapin, -22.27 ± 0.96 mV, n = 26; $p = 0.008$). (Fig. 3.1C and Table 3.1).

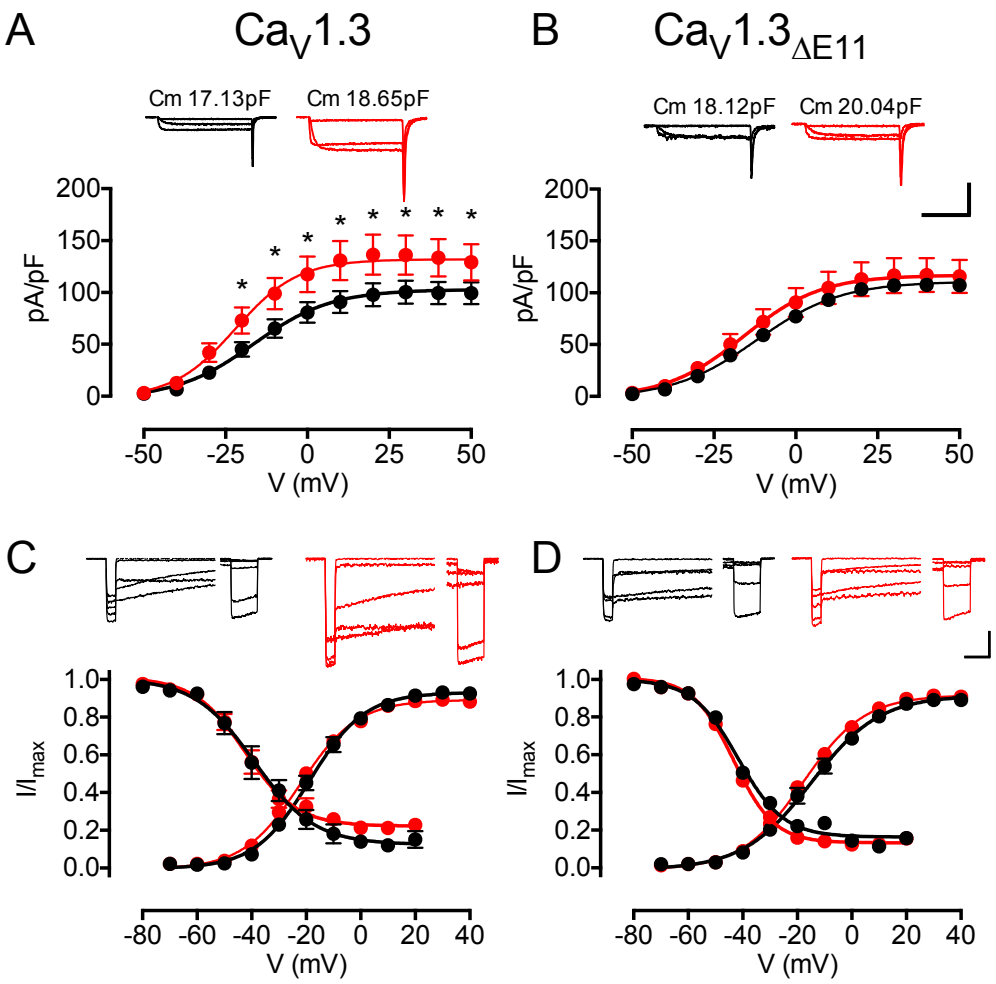

Figure 3.1 Snapin preferentially modulated $Ca_V1.3$ but not $Ca_V1.3_{\Delta E11}$.
A.B. Channel current density of $Ca_V1.3$ recorded by tail protocol **(A)** and $Ca_V1.3_{\Delta E11}$ **(B)** with (red) or without snapin (black). *Upper panel*, exemplary traces of the tail current activated at -20 mV, +10 mV and +50 mV. Calibration bar: 1 nA, 10 ms. **C.D.** Activation curve and inactivation curve were obtained from tail and steady-state inactivation protocols. The two curves of $Ca_V1.3$ **(C)** and $Ca_V1.3_{\Delta E11}$ **(D)** with (red) or without snapin (black) were plotted in the same chart. *Upper panel*, exemplary traces of the steady-state inactivation of normalization pulse and test pulse. Calibration bar: 0.5 nA, 100 ms. * $p < 0.001$. Each group was compared with and without snapin by Student t-test.

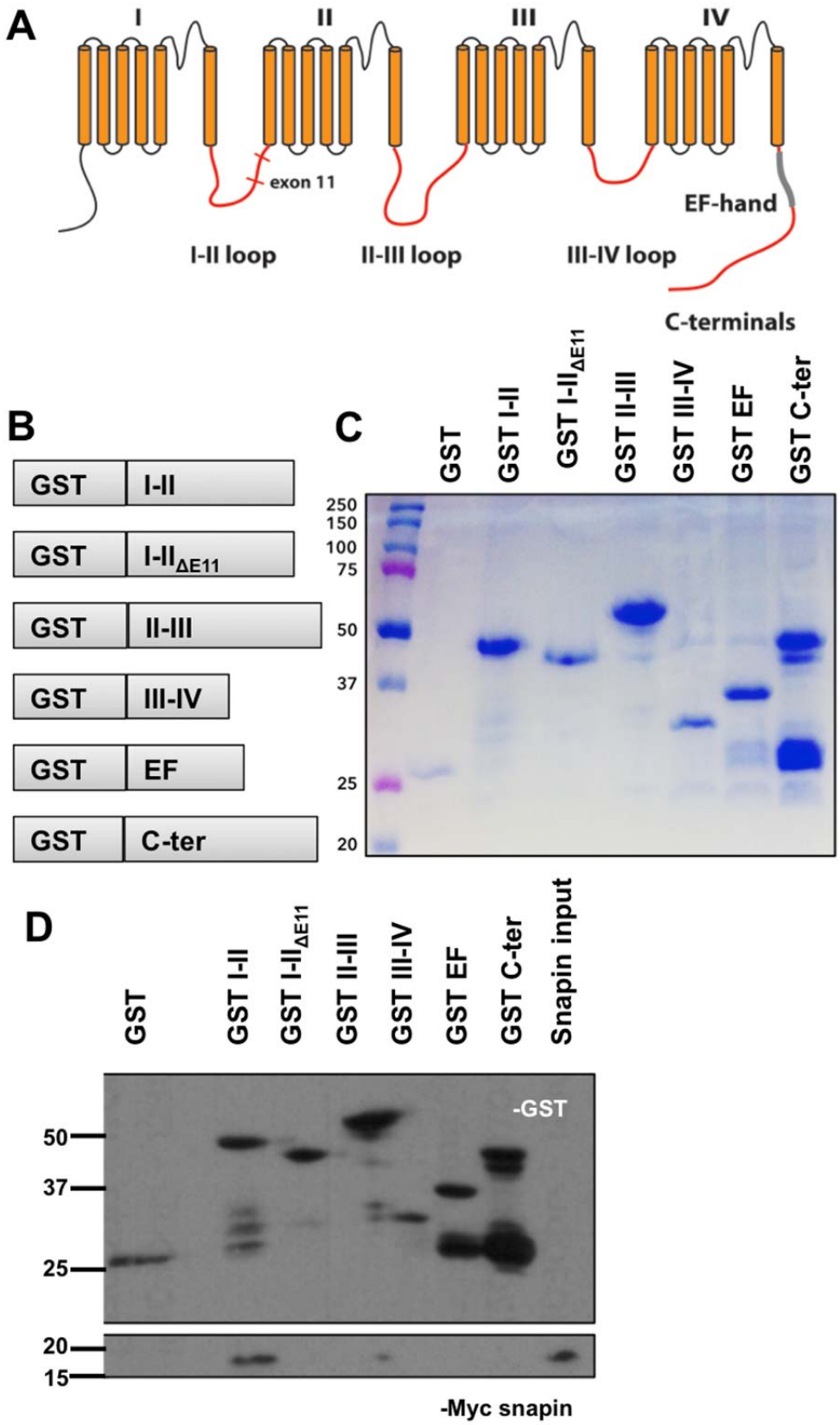
A
I
II
III
IV
exon 11
EF-hand
I-II loop
II-III loop
III-IV loop
C-terminals
B
GST
I-II
GST
I-II ΔE11
GST
II-III
GST
III-IV
GST
EF
GST
C-ter
C
GST
GST I-II
GST I-II ΔE11
GST II-III
GST III-IV
GST EF
GST C-ter
250
150
100
75
50
37
25
20
D
GST
GST I-II
GST I-II ΔE11
GST II-III
GST III-IV
GST EF
GST C-ter
Snapin input
-GST
50
37
25
20
15
-Myc snapin

Figure 3.2 Snapin preferentially bound to $Ca_V1.3$ I-II loop containing exon 11.
A. Schematic diagrams of $Ca_V1.3$. Several cytosolic regions of $Ca_V1.3$ were labeled in red. Exon 11 is alternatively spliced in the $Ca_V1.3$ I-II loop. **B.** GST fusion protein of I-II loop, I-II loo $_{\Delta E11}$, II-III loop, III-IV loop, EF-hand and 42a short form C-terminus were generated by cloning the respective regions of $Ca_V1.3$ into pGEX4T1 vector. **C.** Coomassie blue staining showed the purified GST-fusion proteins. **D.** GST-pull down assay was performed by incubating the GST-fusion protein beads with cell lysates of HEK 293 cells transfected with snapin. I-II loop of $Ca_V1.3$ pulled down selectively snapin, but I-II loop$_{\Delta E11}$, EF-hand and other cytosolic parts of $Ca_V1.3$ did not pull down snapin.

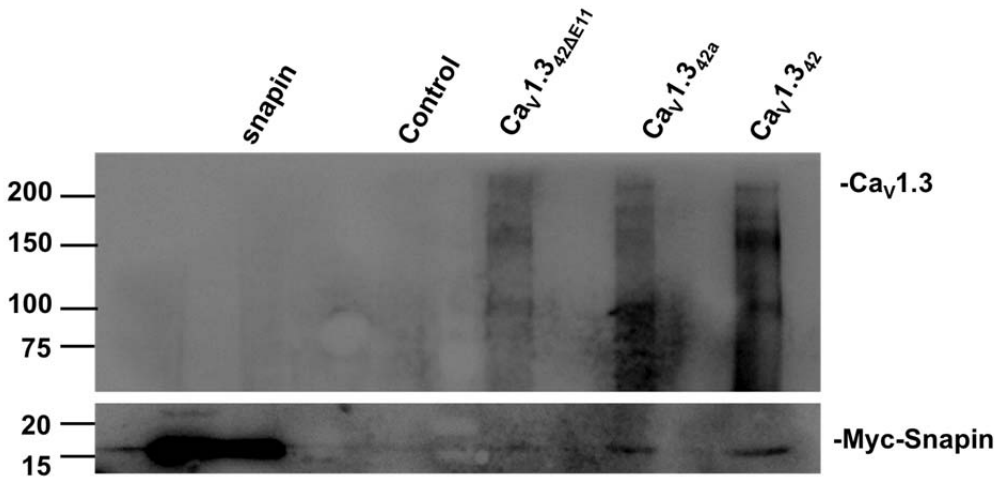

Figure 3.3 Snapin preferentially bound to full-length $Ca_V1.3$ containing exon 11.
Co-IP assay was performed using anti-$Ca_V1.3$ antibody. Full-length $Ca_V1.3_{42a}$, $Ca_V1.3_{42}$, and $Ca_V1.3_{42\Delta E11}$ were used to pull-down snapin. Snapin could be bound to $Ca_V1.3_{42a}$, $Ca_V1.3_{42}$ but not $Ca_V1.3_{42\Delta E11}$.

In order to discover the potential binding regions within $Ca_V1.3$ for snapin, we screened the cytosolic loop regions of $Ca_V1.3$, including I-II loop, II-III loop, III-IV loop, EF-hand like domain and C-terminus. We cloned the cytosolic parts of $Ca_V1.3$ into GST-expression vector (Fig. 3.2A and 3.2B). Unexpectedly, using GST-fusion protein to pull down the cell lysates with snapin, we found that snapin did not interact with the EF-hand like domain in stark contrast to the results obtained for $Ca_V2.1$ channels. However, the results of the pull-down assays indicate that the I-II loop of $Ca_V1.3$ contained the critical binding site (Fig. 3.2D). Therefore, we may have uncovered a novel interaction between snapin and $Ca_V1.3$ in the I-II loop.

The $Ca_V1.3$ I-II loop could be alternatively spliced at exon 9* and exon 11 (Xu & Lipscombe 2001). The reference clone used in our experiments contained Δ9*/E11, which is the most common splice variant in the nervous system. In order to determine whether the inclusion or exclusion of exon 11 affects snapin binding to $Ca_V1.3$, we have assessed the biochemical interactions between snapin and I-II loop lacking exon 11, as well as perform electrophysiological investigations of $Ca_V1.3_{\Delta E11}$ channels. We generated the GST-fusion protein of I-II loop (ΔE11) and our results by GST pull-down assays showed that I-II loop (ΔE11) did not pull down snapin (Fig. 3.2D). Moreover, we have performed immunoprecipitation using anti-$Ca_V1.3$ antibody and found that both the long-form and short-form of $Ca_V1.3$ could pull down snapin. By contrast, $Ca_V1.3_{\Delta E11}$ did not pull down snapin (Fig. 3.3). These results showed that inclusion of exon 11 was

crucial for snapin-$Ca_V1.3$ interactions. In addition to the biochemical studies, we examined the electrophysiological properties of $Ca_V1.3_{\Delta E11}$ channels. Figure 3.1B showed that snapin did not increase the Ca^{2+} current density ($Ca_V1.3_{\Delta E11}$ + vector, 110.7 ± 2.0 pA/pF, n = 13; $Ca_V1.3_{\Delta E11}$ + snapin, 116.9 ± 5.1 pA/pF, n = 16; p = 0.31), suggesting that exclusion of exon 11 abolished the effect of increased current due to binding of snapin. In comparing voltage sensing, snapin could still slightly shifted the $V_{1/2act}$ of $Ca_V1.3_{\Delta E11}$ to the hyper-polarized direction, as compared with the same channel without snapin ($V_{1/2act}$: $Ca_V1.3_{\Delta E11}$ + vector, -14.89 ± 0.96 mV, n = 23; $Ca_V1.3_{\Delta E11}$ + snapin, -17.92 ± 0.81 mV, n = 23; p = 0.020).

In short, our results discovered a novel interaction between $Ca_V1.3$ I-II loop and snapin. Snapin-$Ca_V1.3$ interaction increased the $Ca_V1.3$ current by 30%. These interactions were dependent on the presence of alternative exon 11. Moreover, snapin slightly shifted the activation potential to the hyperpolarized direction of both $Ca_V1.3$ and $Ca_V1.3_{\Delta E11}$ channels. In addition, our electrophysiological data also showed that inclusion of exon 11 shifted the $V_{1/2act}$ of $Ca_V1.3$ slightly to left by 4 mV (Table 3.1, p < 0.001). These results suggested that the exon 11 affects voltage sensing of $Ca_V1.3$.

Table 3.1 Electrophysiological properties of Ca_V1 channels interacting with snapin

	$Ca_V1.3$ vector	**$Ca_V1.3$ snapin**	**$Ca_V1.3_{\Delta E11}$ vector**	**$Ca_V1.3_{\Delta E11}$ snapin**
I_{max} Tail (pA/pF)	102.8 ± 3.4 (24)	131.9 ± 5.1* (19)	110.7 ± 2.0 (13)	116.9 ± 5.1 (16)
$V_{1/2act}$ (mV)	-18.75 ± 0.70 (23)	-22.27 ± 0.70* (26)	-14.89 ± 0.96$^{\#}$ (18)	-17.92 ± 0.81 (16)
$V_{1/2inact}$ (mV)	-42.37 ± 1.19 (11)	-39.06 ± 1.67* (9)	-43.34 ± 0.70 (8)	-41.74 ± 1.30 (7)
	$Ca_V1.2$ vector	**$Ca_V1.2$ snapin**	**$Ca_V1.4$ vector**	**$Ca_V1.4$ snapin**
I_{max} Tail (pA/pF)	310.7 ± 17.4 (20)	294.0 ± 16.8 (14)	22.60 ± 1.26 (11)	24.21 ± 1.08 (15)
$V_{1/2act}$ (mV)	-4.67 ± 0.79 (17)	-4.56 ± 0.86 (20)	-3.76 ± 0.69 (10)	-3.40 ± 1.11 (12)
$V_{1/2inact}$ (mV)	-30.56 ± 0.59 (11)	-33.90 ± 0.33* (11)	-38.07 ± 2.89 (7)	-40.73 ± 2.52 (10)

The number of experiments done is indicated in parentheses. $V_{1/2act}$ and $V_{1/2inact}$ represent potential of half activation of half inactivation. $V_{1/2act}$ was derived from tail-activation curves recorded in Ba^{2+} (Figure 3.1C and 3.4C) and $V_{1/2inact}$ was derived from steady-state inactivation curve recorded Ba^{2+} (Figure 3.1D and 3.4D), $^{*}p < 0.001$, compared with or without snapin, $^{\#}p < 0.001$, compared between $Ca_V1.3$ and $Ca_V1.3_{\Delta E11}$ (Student's t test, two tail, unpaired).

3.3.2 Snapin did not affect $Ca_V1.2$ and $Ca_V1.4$ properties

The alternative exon 11 is distinct to $Ca_V1.3$ and there is no paralogous sequence of exon 11 in $Ca_V1.2$ and $Ca_V1.4$ channels. In order to determine whether snapin preferentially modulates $Ca_V1.3$ but not other L-type channels, we have examined snapin effect on the other two neuronal Ca_V1 channels: $Ca_V1.2$ and $Ca_V1.4$. Therefore, we co-expressed snapin and $Ca_V1.2$ or $Ca_V1.4$ channels in the HEK 293 cells and the results showed that snapin did not significantly affect the current densities of $Ca_V1.2$ and $Ca_V1.4$ channels (Fig 3.4A, 3.4B and Table 3.1). To compare voltage sensing of $Ca_V1.2$ and $Ca_V1.4$ channels, we recorded and analyzed the $V_{1/2act}$ and $V_{1/2inact}$ by tail and steady-state inactivation protocols. The inactivation of $Ca_V1.2$ was slightly hyperpolarized shifted by snapin by 3 mV (Fig 3.4 and Table 3.1). Taken together, among the three neuronal L-type calcium channels, snapin preferentially interacted with $Ca_V1.3$ and snapin binds to $Ca_V1.3$ in the presence of alternative exon 11. The novel interaction mechanism between snapin and $Ca_V1.3$ increased the channel currents and might affect the physiological role of $Ca_V1.3$ in the inner hair cells.

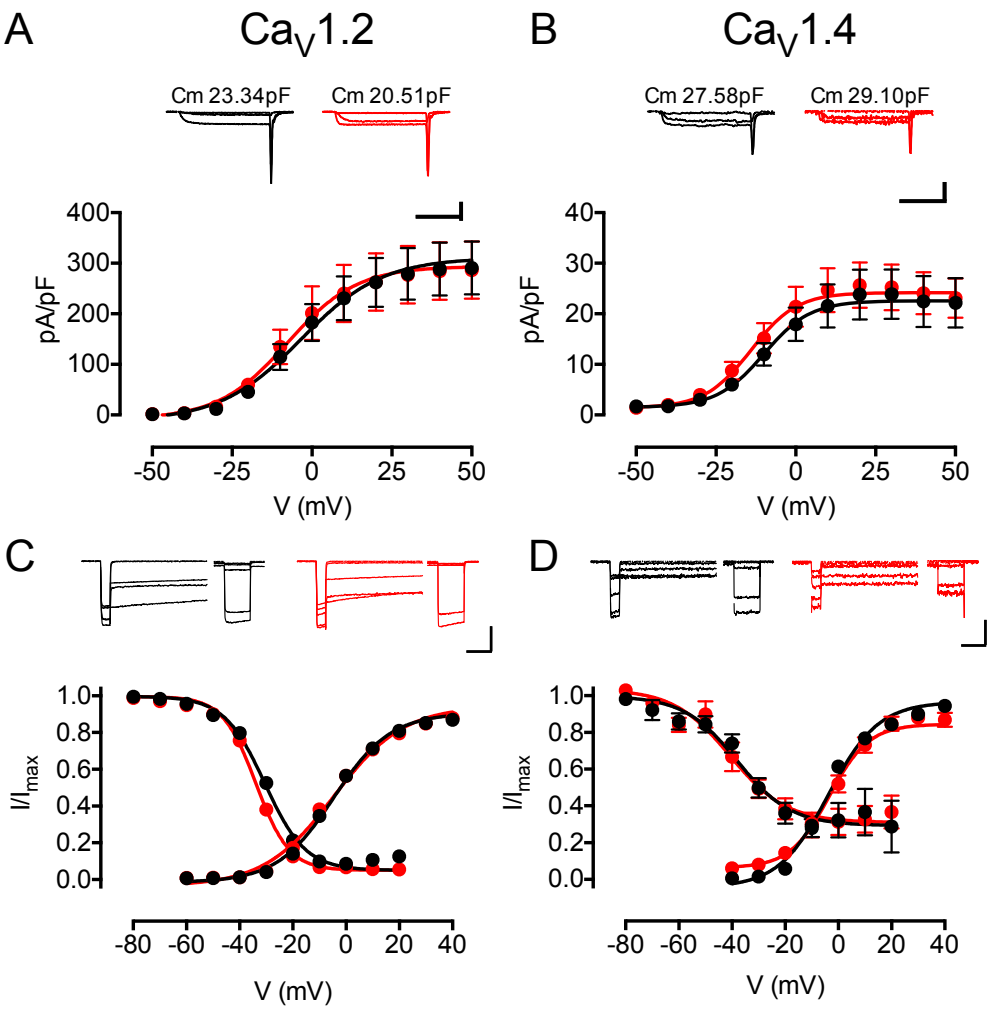

Figure 3.4 Snapin did not alter channel properties of $Ca_V1.2$ and $Ca_V1.4$ channels
A. Channel current density of $Ca_V1.2$ recorded by tail protocol with (red) or without snapin (black). Upper panel, exemplary traces of the tail currents activated at -20 mV, +10 mV and +50 mV. Calibration bar: 0.5 nA, 10 ms. **B.** Channel current density of $Ca_V1.4$ recorded by tail protocol with (red) or without snapin (black). *Upper panel,* exemplary traces of the tail current. Calibration bar: 100 pA, 10 ms. **C.** Activation curve and inactivation curve were obtained from a tail protocol and steady-state inactivation protocol. The two curves of $Ca_V1.2$ with (red) or without snapin (black) were plotted in the same chart. *Upper panel*, exemplary traces of the steady-state inactivation of normalization pulse and test pulse. **D.** Activation curve and inactivation curve of $Ca_V1.4$ were similarly plotted. Calibration bar: 50 pA, 100 ms. Each group was compared with and without snapin by Student t-test.

3.3.3 Snapin modulated the $Ca_V1.3$ VDI

The $Ca_V1.3$ I-II loop has been shown to be involved in voltage-dependent inactivation. The I-II loop blocks the gating pore of channel after voltage depolarization. The inclusion of exon 11 extended the I-II loop length and it is not clear whether exon 11 is involved in voltage-dependent activation. We recorded the VDI by holding the membrane potential with depolarized voltages for 500 ms. The inactivation ratio was determined by the remaining current after 300 ms divided by peak current. Although snapin did not affect the r_{300} obtained at the peak value stimulus (-10 mV), it could modestly reduce the VDI at -40 mV (Fig. 3.5, Table 3.2. p = 0.032). By comparing the r_{300} along with the depolarizing voltage, snapin inhibited the VDI in hyperpolarized voltage but snapin slightly facilitated the VDI in more depolarized voltages. These results suggested that snapin binding to I-II loop of $Ca_V1.3$ might inhibit the VDI processes only in hyperpolarized voltage.

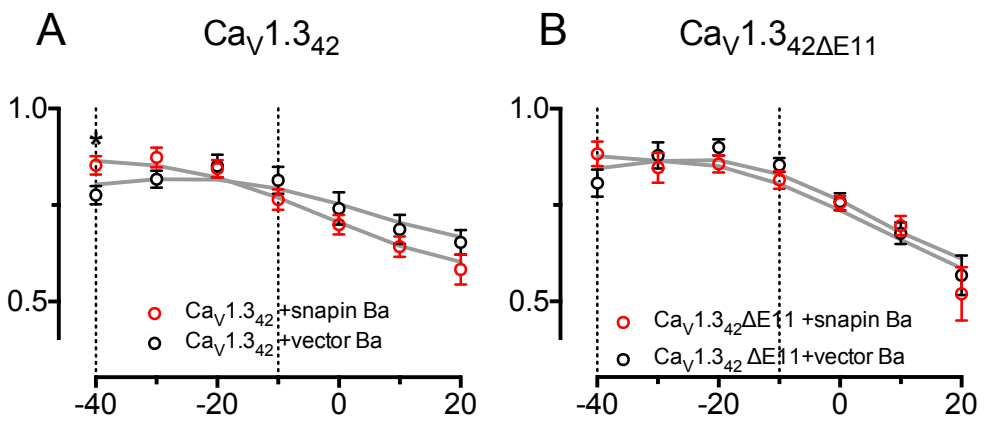

Figure 3.5 Snapin slightly suppressed the VDI in hyperpolarized voltage
A. Snapin suppressed the VDI of $Ca_V1.3_{42}$ in -40 mV, but not the peak current at -10 mV. **B.** Snapin did not significantly affect VDI of $Ca_V1.3_{42\Delta E11}$

Table 3.2 r_{300} of $Ca_V1.3$ and interaction with snapin

Voltage	$Ca_V1.3_{42}$ vector	$Ca_V1.3_{42}$ snapin	$Ca_V1.3_{42\Delta E11}$ vector	$Ca_V1.3_{42\Delta E11}$ snapin
-40 mV	0.776 ± 0.024	0.853 ± 0.024[#]	0.807 ± 0.035	0.883 ± 0.032
-30 mV	0.817 ± 0.022	0.873 ± 0.026	0.879 ± 0.034	0.847 ± 0.039
-20 mV	0.851 ± 0.029	0.844 ± 0.022	0.900 ± 0.021	0.857 ± 0.022
-10 mV	0.814 ± 0.035	0.764 ± 0.027	0.854 ± 0.018	0.815 ± 0.023
0 mV	0.741 ± 0.042	0.699 ± 0.025	0.759 ± 0.022	0.755 ± 0.019
10 mV	0.687 ± 0.038	0.642 ± 0.027	0.677 ± 0.028	0.697 ± 0.025
20 mV	0.653 ± 0.032	0.583 ± 0.039	0.807 ± 0.035	0.568 ± 0.051
n	15	11	12	24

[#]$p < 0.05$, compared between $Ca_V1.3_{42}$ vector and $Ca_V1.3_{42}$ snapin in -40 mV (Student's t test, two tail, unpaired).

3.3.4 Alternative splicing of $Ca_V1.3$ I-II loop in cochlea

Several splice sites in $Ca_V1.3$ I-II loop have been identified, which could generate $Ca_V1.3$ channel functional diversity. Exon 11 has been shown to alternatively splice in the $Ca_V1.3$ I-II loop. In addition to exon 11, exon 9* is also alternatively spliced in the I-II loop.

Here, we investigated the alternative splicing of the I-II loop in adult rat cochlea. The splicing pattern of $Ca_V1.3$ I-II loop was determined by RT-PCR and colony screening (Tang et al 2004, Liao et al 2007). We extracted the cochlear RNA from five 8-9 weeks old rats and obtained the cDNAs using specific reverse primer at exon 17 of $Ca_V1.3$ for the first strand reverse transcription reaction. The sequential PCRs were performed to amplify the amplicons spanning exons 9-14. Multiple bands were shown in 2% agarose gel (Fig. 3.6B), suggesting that exon 9* or exon 11 were alternatively spliced in the I-II loop of $Ca_V1.3$ channels found in the cochlea.

To quantify the inclusion ratio of the alternative exons, we cloned the PCR amplicons into TA vector and transformed them into *E.coli*. Multiple *E.coli* colonies were then picked and colony PCR performed and individual clones were screened in 2% agarose gels. Because the exon 9* (84 bp) is 24-nt longer than exon 11 (60 bp), we were able to identify the presence or absence of an alternative exon by PCR product size. The ΔE9*/E11 amplicons was 24 bp shorter than E9*/ΔE11 and the ΔE9/ΔE11 amplicons were the smallest PCR product (Fig. 3.7A). The splicing pattern of exon 9* and exon 11 was

determined by the PCR product sizes and the ratio. The sequences of randomly selected PCR amplicons were confirmed by direct DNA sequencing (Fig. 3.7B). Our results show that the expression level of exon 11 was 34% and that of exon 9* was 24%. Compared to the previous studies performed in immature rat cochlea, exon 11 expressions was higher in adult than in young rat pups. Exon 9* was much less expressed in adult cochlea than that in young rats. As a summary, the alternative splicing pattern of $Ca_V1.3$ is under developmental regulation in young and adult rat. The temporal regulation of $Ca_V1.3$ alternative splicing may contribute to the physiological role of $Ca_V1.3$ channels in cochlear hair cells.

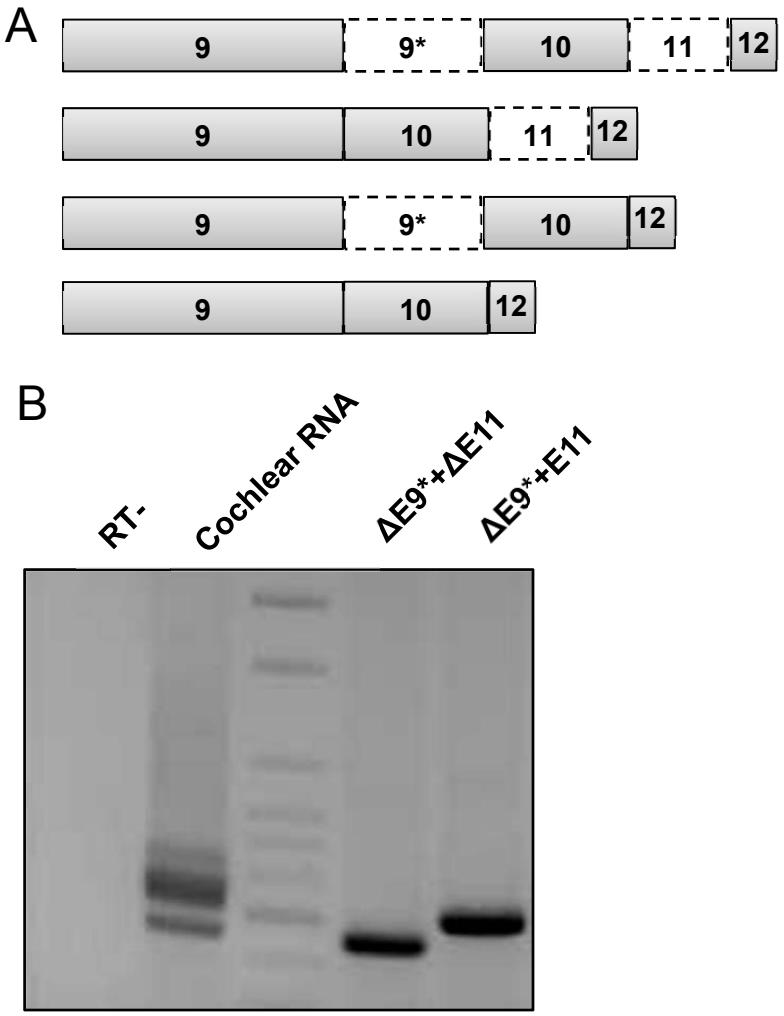

Figure 3.6 Multiple splice variants found in $Ca_V1.3$ I-II loop of adult rat cochlea.
A. Possible combinations of $Ca_V1.3$ I-II loop splicing pattern of exon 9* and exon 11.
B. Agarose gel detected multiple bands (550-700 bp) of PCR products amplified from cochlear RNA, indicating several splice variants of $Ca_V1.3$ I-II loop. PCR products of control plasmid containing ΔE9*/ΔE11 and ΔE9*/E11 are shown.

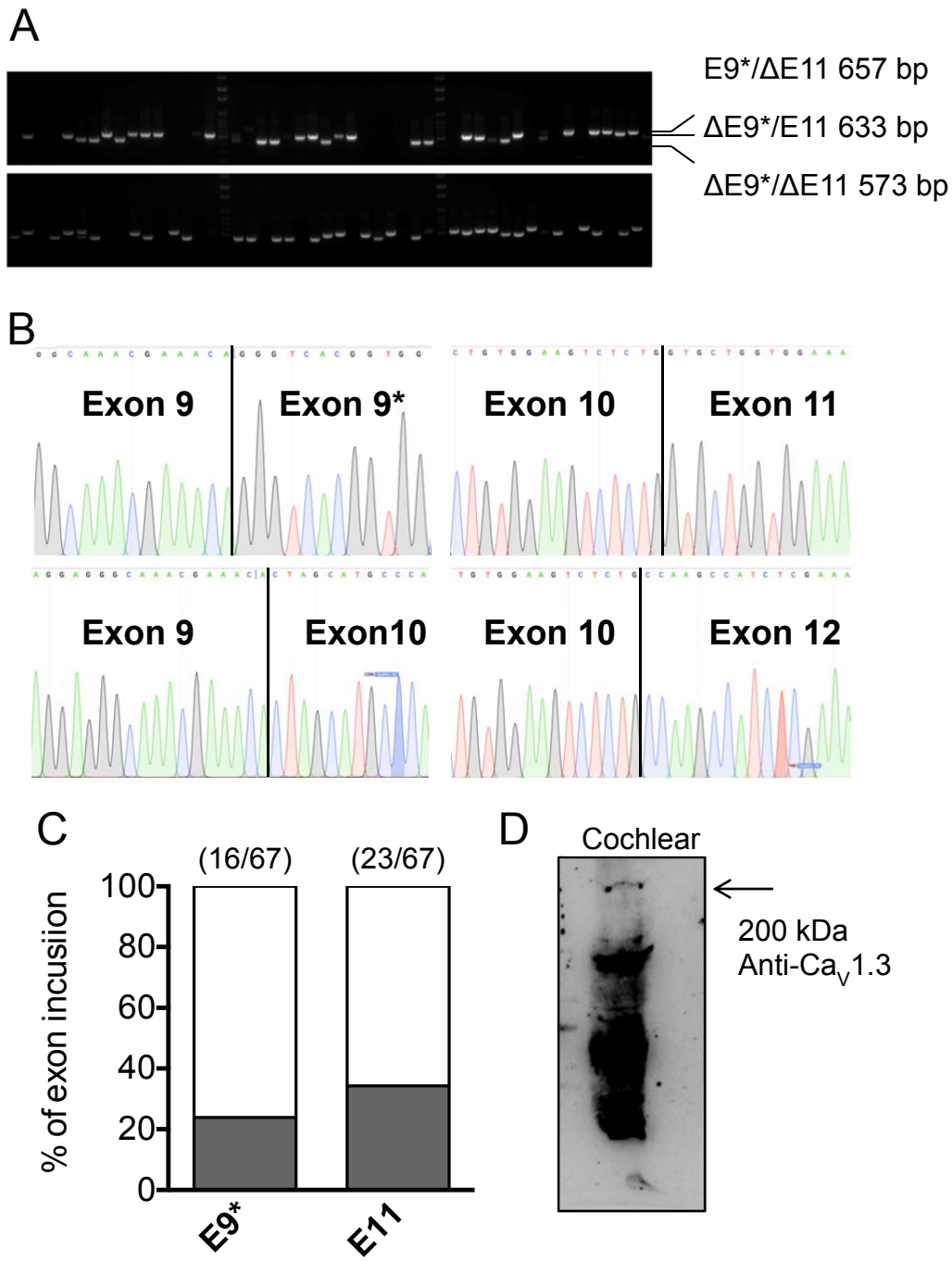

Figure 3.7 Splicing patterns of $Ca_V1.3$ I-II loop.
A. Colony PCR screening of amplicons from mRNA isolated from rat cochlea shows the existence of multiple variants with alternative splicing of exon 9* and exon 11. The expected sizes of ΔE9*/ΔE11 (573 bp), ΔE9*/E11 (633 bp) and E9*/ΔE11 (657 bp) are shown. **B.** The random colonies were sequenced to confirm the splicing pattern. The DNA sequencing results of the transcripts of alternative spliced exon 9* and exon 11 are shown. **C.** Summary bar chart showed the expression levels of exon 9* (24%) and exon 11 (34%) in adult rat cochlea. The percentages of exon 9* and exon 11 are shown in grey. The numbers in parentheses above each bar indicate the number of colonies screened. **D.** Western blot results using anti-$Ca_V1.3$ antibody showed that the $Ca_V1.3$ were expressed in adult rat cochlea.

3.4 Discussion

In this study, we have identified the interaction between snapin and exon 11 of $Ca_V1.3$ and snapin increased the current density of $Ca_V1.3$. However, snapin did not affect voltage sensing of the channels. Exon 11 is an alternative exon and our result showed that 34% of the exon 11 is included in the $Ca_V1.3$ transcripts in cochlea. In addition to $Ca_V1.3$, snapin had no effect on other neuronal VGCCs from the Ca_V1 family, such as $Ca_V1.2$ and $Ca_V1.4$.

3.4.1 Spatial and temporal regulation of $Ca_V1.3$ I-II loop alternative splicing

The onset of hearing is about 2 weeks after birth for most rodents (Fuchs 2005, Safieddine et al 2012). During the period before hearing onset, Ca^{2+} influx from $Ca_V1.3$ mediated spontaneous action potentials. This process supports tonic synaptic activity and maturation of the auditory system. It has been shown that $Ca_V1.3$ in immature IHCs showed increased Ca^{2+} current density and stronger voltage-dependent inactivation as compared to that observed in the mature hair cells (Inagaki & Lee 2013). The coupled Ca^{2+}-activated K^+ channels induced repolarization of the action potential waveforms. It may be required to maintain the proper shape and timing of spontaneous action potentials.

In this study, we have examined the splicing pattern of $Ca_V1.3$ I-II loop in adult rat cochlea. We found that exon 11 is included in about one

third of $Ca_V1.3$ transcripts and exon 9* is found in 24% of the transcripts. Unpublished work from our laboratory also examined the I-II loop splicing pattern of $Ca_V1.3$ in young rat of 1-2 weeks old as well as heart and brain cDNA libraries. To combine these studies together, we found that the alternative splicing at the I-II loop is under spatial and temporal regulation. We showed that exon 11 expression in rat cochlea increased with age. There was less than 6-14% inclusion of exon 11 in immature rats cochlea and our studies showed that exon 11 expression was much higher at 34% in adult rat cochlea. Exon 11 expressions in total brain and heart (30% inclusion) are comparable with that found in cochlea. On the contrary, exon 9* expression in cochlea decreased during development. It decreased from more than 60% at two-week-old rats to 23% in the adult. Exon 9* of $Ca_V1.3$ is expressed at a relatively low level in heart (5.4%) and brain (2.7%). The changing expression of exon 9* and exon 11 of $Ca_V1.3$ channels in cochlea may contribute to the development and function of the auditory system.

3.4.2 Snapin interacted with $Ca_V1.3$

Activation of $Ca_V1.3$ channels followed by Ca^{2+} influx triggers vesicle release in the ribbon synapse. In immature inner hair cells, $Ca_V1.3$ has a lower activation threshold and conducts larger currents compared to $Ca_V1.3$ in adult IHCs. When snapin interacts with $Ca_V1.3$ the net result would be an increase in current density and a shift of the activation threshold to lower potential. Therefore, in the presence of snapin, $Ca_V1.3$ should conduct larger currents and be activated at lower

potentials. The snapin-$Ca_V1.3$ binding may therefore likely shape the channel in the immature pattern. In adult IHCs, snapin binding may lead to more Ca^{2+} influx. It would therefore facilitate neurotransmitter release. Snapin has been identified as a synaptic protein and known to promote the interaction between Ca^{2+} senor, Syt-I and vesicle fusion machinery protein, SNAP-25 (Ilardi et al 1999, Tian et al 2005, Pan et al 2009). Snapin may recruit calcium channels to the active zones in the ribbon synapse it has been shown that $Ca_V1.3$ channels were loosely attached in the active zone. In immature IHCs, most of the $Ca_V1.3$ channels are present outside the presynaptic region and they mediated the firing of spontaneous action potentials instead of triggering vesicle release (Zampini et al 2010). It is not clear what may the underlying mechanisms be for trafficking $Ca_V1.3$ to the ribbon synapse. Since snapin has been shown to be involved in trafficking of several membrane proteins, snapin-$Ca_V1.3$ interaction might be a possible mechanism in locating $Ca_V1.3$ to the pre-synapse.

$Ca_V1.3$ functions have dual roles in immature and mature IHCs. It has not been shown whether snapin in the cochlea is regulated in different developmental stages. However, our findings on the alternative splicing of exon 11 suggested that alternative splicing of exon 11, which is modulated in development, might modulate the snapin-CaV1.3 interaction. If exon 11 is excluded from the transcripts, snapin could not bind to $Ca_V1.3$. Therefore, the alternative splicing of exon 11 may be a switch on snapin-$Ca_V1.3$ interactions.

3.4.3 Essential role of $Ca_V1.3$ I-II loop in channel properties

The I-II loop is critical for interacting with the auxiliary β-subunit by the AID domain in exon 9. In $Ca_V1.2$, exon 9 binds to galectin-1 and compete for the binding of β subunit, which could lead to decreased surface expression of channel. Alternative inclusion of exon 9* disrupt the interaction between galectin-1 and $Ca_V1.2$ (Wang et al 2011). Similar to exon 9*, exon 11 also extended the I-II loop. We would like to determine whether the inclusion of exon 11 or snapin interaction in the I-II loop might also affect I-II loop structure in future studies.

Alternative splicing of exons in the I-II loop of $Ca_V1.3$ has been examined in rat cochlea and chick basilar papilla (Xu & Lipscombe 2001). Our study has revealed that inclusion of exon 11 is crucial for snapin binding to $Ca_V1.3$. We found that snapin slightly suppressed VDI in hyperpolarized voltage. The snapin-binding to I-II loop may obstruct the closure of I-II loop “hinge”. This effect was not found in $Ca_V1.3_{\Delta E11}$. It has been reported that several amino acids in S6 segment repel the “hinge” closure and suppress the VDI (Tadross et al 2010). Therefore, exon 11 and I-S6 of $Ca_V1.3$ may modulate VDI together.

3.4.4 Conclusion and future studies

In this study, we have examined the interaction between snapin and neuronal Ca_V1 channels. Snapin preferentially increased the current density of $Ca_V1.3$ but not on $Ca_V1.2$ and $Ca_V1.4$. In addition, snapin slightly suppress the VDI of $Ca_V1.3$ in low voltage. $Ca_V1.3$ I-II loop was

crucial for snapin-$Ca_V1.3$ interaction and $Ca_V1.3_{\Delta E11}$ did not bind to snapin as shown in GST pull down assay and Co-immunoprecipitation. The inclusion ratio of spliced exon 11 in $Ca_V1.3$ appears higher in adult rat cochlea than immature ones. Therefore, snapin-$Ca_V1.3$ interaction and alternative splicing of $Ca_V1.3$ I-II loop may contributes the functional diversity of $Ca_V1.3$ in cochlea in different developmental stages.

Further studies would be performed to examine how snapin affects the $Ca_V1.3$ in cochlea development. We would first compare the snapin expression in immature and adult cochlea by real time PCR. Then, we would like to knock down snapin expression in cochlea using shRNA and examine whether the cochlea development are altered.

In collaboration with Dr. Tan from University of Melbourne, we aim to examine the expression of snapin and $Ca_V1.3$ in the cochlear whether the snapin and $Ca_V1.3$ is co-localized in the inner hair cell and out hair cell. This study may provide some evidence on the role of snapin-$Ca_V1.3$ interactions in hearing formation or auditory system developments.

In addition, $Ca_V1.3$ is reported to be under extensively alternative splicing. The long form and short form of $Ca_V1.3$ determined by 42/42a splicing are distinct in current density and calcium dependent inactivation. The distal C-terminals also affect the CaM binding (Liu et al 2010). Since we have examine the effects of snapin on long form of $Ca_V1.3$, further studies will be performed to compare how snapin affect

the short form ($Ca_V1.3_{42a}$) with or without exon 11 using electro-physiologies and biochemical studies.

Chapter 4 Modulation of $Ca_V2.1$ by gangliosides

4.1 Introduction

4.1.1 Ganglioside structure and function

Gangliosides are widely expressed on cell membrane and are involved in processes such as cell-cell recognition, cell migration and vesicle releases. Gangliosides are composed of three components: lipophilic fatty acid, sphingosine base and hydrophilic carbohydrate chain. The carbohydrate portion of ganglioside usually contains one or more sialosyl groups that are synthesized by specific glycosyltransferases (GTs). Various subtypes of gangliosides have been identified based on their carbohydrate chains, such as GM GD, GT and GQ, where M, D, T and Q represent mono-, di-, tri-, and quadri-sialosyl groups (Fig 4.1A) (Irie et al 1994).

Gangliosides are abundant in the nervous system. In the plasma membrane, gangliosides and cholesterol are segregated into membrane micro-domains known as lipid rafts. It is one of the critical regions in signal transduction and protein trafficking. Concentration of various proteins in these rafts facilitates protein-protein interactions and the microenvironment of lipid rafts may therefore alter the protein conformation and function (Anderson & Jacobson 2002, Ohmi et al 2012). For example, the potassium channel $K_V2.1$ targets to the lipid raft. The peak current and voltage sensing of the $K_V2.1$ were altered when cholesterol was depleted and the lipid raft formation was disrupted (Martens et al 2000).

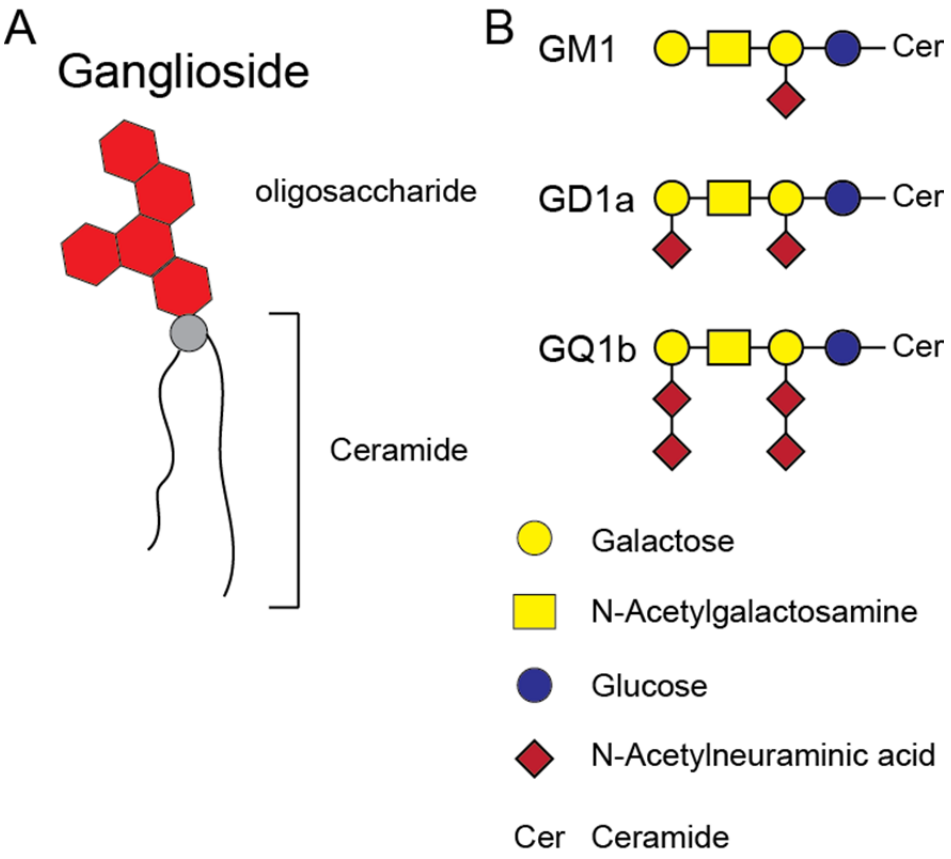

Figure 4.1 Structure of gangliosides including GM1, GD1a and GQ1b.
A. Ganglioside is composed by ceramide and oligosaccharide with one or more sialic acids. The ceramides are linked with sphingosine and a fatty acid, which is a crucial component for cell membranes. The oligosaccharide groups of ganglioside extended beyond the cell surface and could be recognized as surface markers. **B.** The three common gangliosides GM1, GD1a and GQ1b were found to related to GBS. The major differences of these gangliosides are the oligosaccharide groups.

4.1.2 Anti-ganglioside antibody and Guillain-Barré syndrome

Studies have shown that gangliosides were involved in human diseases. Autoantibodies against gangliosides are the major causes of Guillain-Barré syndrome (GBS). GBS is characterized by patients suffering from acute areflexic paralysis that is associated with high protein level in the cerebrospinal fluid. The major symptoms of Guillain-Barré syndrome are progressive limb numbness and paresthesia. Patients usually suffer from hyporeflexia or areflexia as well. It was first described by Guillain, Barré and Strohl in 1916 (Guillain et al 1916, Koga et al 2012, Yuki & Hartung 2012). Guillain-Barré syndrome is now one of the major causes to paralysis with incidence of 1.1 per 100,000 person per years (Sejvar et al 2011). Elevated protein levels could be detected in cerebrospinal fluids obtained by lumbar puncture of patients (Nishimoto et al 2004). It was shown that 30% of GBS patients have a history of infection by *Campylobacter jejuni* (Orlikowski et al 2011). Several other infectious agents including *Mycoplasma pneumonia*, Varicella–Zoster virus and Barr virus have also been identified. It is believed that some antigens of the bacteria or virus share similar structures to ganglioside and induce an abnormal immune response (Jacobs et al 1998, Hadden et al 2001). The current popular treatment for GBS is intravenous immunoglublin injection. The immune globin may neutralize the autoantibodies against gangliosides and reduce nerve injury (van der Meche & Schmitz 1992, Kuitwaard et al 2009).

Guillain-Barré syndrome can be classified as acute inflammatory demyelinating polyneuropathy (AIDP) and acute motor and axonal neuropathy (AMAN) based on the underlying pathologies (Hadden et al 1998, Hiraga et al 2003). The classical pathologies in AIDP are progressive demyelination with inflammatory infiltrates. The demyelinating axons are covered with microphages and subsequently they will result in axonal degeneration. In AMAN pathologies, IgG binds to the nodes of Ranvier of motor fibers and the following immune responses lead to detachment of membrane proteins in the nodes of Ranvier (McKhann et al 1993). The demyelinating form of GBS, AIDP, is prevalent in Europe and North America, whereas, the axonal form, AMAN, accounts for more than 60% of the GBS in Asia (Hadden et al 1998, Islam et al 2010). Miller Fisher syndrome (MFS) appears to be a unique variant of GBS that is characterized by paralysis of the eye muscles and ataxia. This suggests that the underlying pathologies are in the central nervous system. It is commonly found among patients in China and Japan (Fisher 1956, Willison 2005).

Both the AMAN and MFS are highly associated with autoantibodies against gangliosides. In AMAN patients, antibodies against GM1 and GD1a are found in the spinal fluids (Capasso et al 2003, Sekiguchi et al 2012). As GM1 and GD1a are highly expressed in the motor and sensory neurons, this could explain preferential motor axon injury in AMAN patients (Lopez et al 2010, Capasso et al 2011). Anti-GM1 or anti-GD1a, two antibodies associated with AMAN could suppress neuromuscular transmission (Bullens et al 2003). It has been

hypothesized that both patient serum and IgG-GD1a could inhibit acetylcholine evoked synaptic release in rat muscle-spinal cord co-culture (Taguchi et al 2004). As Ca^{2+} influx through VGCCs is crucial to initiate neurotransmitter release, VGCCs have been shown to be involved in the pathology of GBS. Rabbit GD1a-positive sera reversibly inhibit the VGCC currents in PC12 pheochromocytoma cells (Nakatani et al 2007). In addition to anti-GD1a, anti-GM1 has been shown to inhibit quanta release and Ca^{2+} influx into the presynaptic site of the neuromuscular junction (Buchwald et al 2007).

On the contrary, antibodies to GQ1b, which can cross-react with GT1a, are associated with MFS. GQ1b is strongly expressed in ocular motor muscles and limb muscles (Chiba et al 1993, Nagashima et al 2007). Nakatani et al (2009) has found that both AMAN patient serum and anti-GM1 antibody could reversibly inhibit the $Ca_V2.1$ channels expressed in the Purkinje cells of the cerebellum, while anti-GQ1b only inhibited Ca^{2+} currents in granule cells but not in Purkinje cells. These results suggest that altered VGCC function by anti-ganglioside antibody might contribute to ataxia in GBS patients (Nakatani et al 2009a, Nakatani et al 2009b).

4.1.3 Interaction between lipid raft and calcium channel

The Ca^{2+} influx through VGCC triggers a few intracellular events. It is thought that VGCCs are clustered within the lipid raft to facilitate the signal transduction process. Davies *et al*. (2006) has revealed the interaction between calcium channels and lipids, which is dependent

on the auxiliary $\alpha_2\delta$ subunits. The $\alpha_2\delta$ subunits are linked by disulfide bonds between the α_2- and δ-subunit, Four variants of the $\alpha_2\delta$ subunit have been identified in human, namely $\alpha_2\delta$-1, $\alpha_2\delta$-2 $\alpha_2\delta$-3 and $\alpha_2\delta$-4. It has been shown that $\alpha_2\delta$-2 and $Ca_V2.1$ are enriched in the lipid-raft region in mouse cerebellum and tsA-201 cells. The calcium channel current is reduced when the $\alpha_2\delta$ subunit is excluded in the heterologous expression of VGCCs in cell lines. Furthermore, cholesterol depletion could disrupt lipid raft formation leading to attenuation of the enhancing effects of $\alpha_2\delta$ on calcium channel currents (Davies et al 2006). Similar studies by Robinson *et al* (2010) indicated that $Ca_V2.2$ were also clustered with lipid raft and co-localization of $Ca_V2.2$ and lipid raft marker caveolin required the $\alpha_2\delta$-1 subunit. The $\alpha_2\delta$ subunits increase the expression level of various Ca_V channels to affect the physiological function of Ca_V channels (Hoppa et al 2012). The mature $\alpha_2\delta$ subunit can be extensively glycosylated and about 9-12 glycosylation sites from 15 predicted sites can be utilized (Robinson et al 2011). However, how the $\alpha_2\delta$ subunits interact with the lipid raft is not well understood.

4.1.4 Objectives and rationale

The current study revealed that various anti-ganglioside antibodies and VGCC are both expressed at the neuromuscular junction and cerebellum, which may be related to the pathology of the GBS. However, the mechanism of the interaction between calcium channels and anti-ganglioside antibodies is still obscure. Firstly, it has been

shown that several kinds of anti-ganglioside antibodies have been detected in GBS and MFS patient serum. What or which group of anti-gangliosides will be the major component in the pathological process? Secondly, given that VGCC is a hetero-oligomeric complex with a main pore-forming subunit and several auxiliary units, it is not clear which subunit(s) of VGCC is pivotal in interacting with gangliosides or anti-ganglioside antibody. Here, we are interested to investigate whether the main pore-forming unit or the auxiliary subunits interact with antibodies to gangliosides.

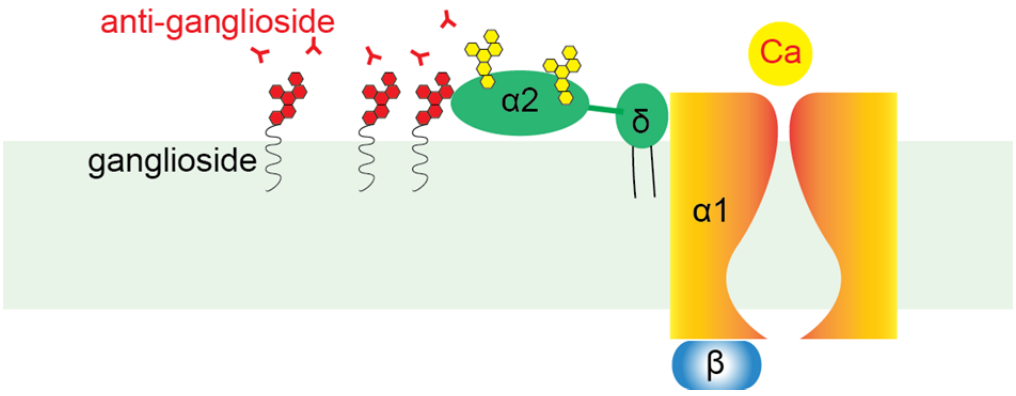

Figure 4.2 The proposed interaction between ganglioside and voltage-gated calcium channel, including α_1, β and $\alpha_2\delta$.
The anti-ganglioside antibodies may recognize the gangliosides in the cell membrane. The $\alpha_2\delta$ subunit is highly glycosylated. There might be potential interaction between the glycosylated $\alpha_2\delta$ and gangliosides.

4.2 Materials and methods

4.2.1 Sera samples

Sera from MFS patients presenting to University Malaya Medical Centre (Kuala Lumpur, Malaysia) and Dokkyo Medical University (Tochigi, Japan) were collected. Informed written consent was obtained from each patient. Normal human sera were prepared from five healthy subjects as a complement source.

4.2.2 Monoclonal anti-ganglioside antibodies

Mouse IgG mono-clone anti-GM1, anti-GD1a and anti-GQ1b antibodies were prepared by Dr. Yuki (Department of Medicine, NUS). It was stored in 4°C until use.

4.2.3 Cell culture and treatments

HEK293 cell were maintained DMEM with 10% FBS and grown in 37°C incubator with 5% CO_2. 1% Pen/strip were added to avoid contamination.

$Ca_V2.1$ and auxiliary subunits was transiently transfect by calcium phosphate methods. The α_1 pore-forming units (1.7 μg), β_{2a} (1.25 μg) and $\alpha_2\delta_1$ (1.25 μg) DNA plasmid as well as T-antigen (0.25 μg) were mixed with 75 μl of $CaCl_2$ and 75 μl of 2XHBS buffer. The mixture was incubated in room temperature for 15-20 minutes and gently added into culture dishes. After 3-5 hours, fresh media without antibiotic were applied to remove the transfection reagent. The antibodies against

gangliosides (5 μg/ml) or patient serum (1:200) were added 24 hours before electrophysiological experiments.

4.2.4 Whole cell patch clamp electrophysiology

Whole cell patch-clamp recording on HEK293 cell channel were performed within 36-72 hours after transfection as previously reported. The external solution contained (in mM) 10 HEPES, 140 TEA-$MeSO_3$ and 5 $BaCl_2$ (pH 7.4, Osmolarity 300-310 mOsm). The glass pipette solution was backfilled with pipette solution (in mM) 10 HEPES, 5 CsCl, 138 Cs-$MeSO_3$, 0.5 EGTA, 1 $MgCl_2$, 2 mg/ml MgATP (pH 7.3 Osmolarity 290-300 mOsm).

HEK cells were held at -90 mV by voltage clamp using Axopatch 700B. The series resistance for recording was typically less than 5 MΩ, 70-80% compensation on serial resistance and cell membrane capacitance was applied. A P/4 protocol was applied to subtract the leakage current. All data were obtained with Digidata 1440A, sampled at 5-50 kHz. The 1 kHz or 6 kHz low pass filter are applied for all the data.

In order to study the activation threshold of voltage-gated calcium channel, we performed the studies using tail protocol, which represent the conductivity of channel. Cells were depolarized to a serials of voltages, ranging from -60 to 100 mV, in steps of 10 mV increments, Following the depolarization, a -50 mV step for 10 ms evoked the tail currents.

4.2.5 Data analysis

The electrophysiology data were analyzed and plotted by using Prism 6 software (San Diego, CA), and were displayed as mean values ± SEM. Statistical significance of differences between two groups were analyzed with unpaired, two-tail Student's *t*-test.

In order to analyze the $V_{1/2act}$, which represent the voltage thresholds for activating the VGCC. The tail current was normalized to the maximum current obtained from each cell and fitted through single Boltzmann equation:

$$G = G_{min} + (G_{max} - G_{min})/(1 + e^{\frac{V_{1/2act} - V}{k_{act}}})$$

where *G* represent the tail current, *V* is the membrane potential of the test pulse. The following parameters were determined by curve fitting. G_{max} is the maximum tail current recorded from each cell, G_{min} is the maximum tail current recorded for fitting curve. k_{act} is the slope factor and $V_{1/2act}$ represents the voltage when the channel current reaches half of the maximum current.

The I-V curve and $V_{1/2inact}$, were analyzed as previously described in chapter 2.

4.3 Results

4.3.1 Antibody of GM1 interacts with calcium channel.

Three major autoantibodies against ganglioside were found to be associated with the GBS. To investigate the relationships between anti-ganglioside, Dr. Yuki (Department of Medicine, NUS) has generated antibodies and the mono-clone antibodies against the ganglioside. The specificity of antibodies was shown in the previous studies and the anti-GM1, anti-GQ1b and anti-GD1a did not cross-react with other epitopes (Lopez et al 2010, Nakatani et al 2007, Nishimoto et al 2004). In order to investigate the interactions between anti-ganglioside antibodies and $Ca_V2.1$, we used whole-cell patch clamp electrophysiology to examine calcium channel properties. We transfected the HEK293 cell with $Ca_V2.1$ and incubated anti-ganglioside antibodies (5 μg/ml) with the HEK cell for 24 hours before electrophysiology experiments.

We first examined the activation voltage $Ca_V2.1$ by both current-voltage (I-V) curve and Tail protocol. For I-V curve, a family of depolarization steps was delivered to activate the voltage-gated calcium channel. Further studies using tail protocol exhibited the effect of anti-GM1 on activation curve. The tail protocol was generated by a family of 20 ms test pulse (-60 mV to 100 mV) and -50 mV repolarization followed by each step. In figure 4.3, we found that the anti-GM1 antibodies shifted the activation voltage of $Ca_V2.1$ channels to hyperpolarized voltage by about 4 mV as represented by $V_{1/2act}$. ($V_{1/2act}$ IgG, -5.33 ± 1.26 mV, n = 10; $V_{1/2act}$ anti-GM1, -9.57 ± 0.93 mV, n = 7; p = 0.025).

Moreover, we compared the inactivation curve by steady-state inactivation. Our results showed that the anti-GM1 has no effect on steady-state inactivation of $Ca_V2.1$ ($V_{1/2inact}$ IgG, -28.75 ± 1.01 mV, n = 11; $V_{1/2inact}$ anti-GM1, -27.01 ± 0.85 mV, n = 7). Therefore, the opening threshold of $Ca_V2.1$ was reduced with the presence of anti-GM1. The anti-GM1 did not affect the current density of $Ca_V2.1$ (IgG, 228.8 ± 6.46, n = 25; anti-GM1, 238.2 ± 8.52, n = 19). These results suggested that the anti-GM1 affected the voltage sensing of $Ca_V2.1$ calcium channels.

Table 4.1 Electrophysiological properties of the $Ca_V2.1$ incubated with anti-GM1.

	w/ $\alpha_2\delta$ IgG	**w/o-$\alpha_2\delta$ IgG**	**w/ $\alpha_2\delta$ anti-GM1**	**w/o-$\alpha_2\delta$ anti-GM1**
$V_{1/2act}$ (mV)	-5.33 ± 1.26 (10)	-4.48 ± 1.58 (10)	-9.57 ± 0.93 (7)	-0.37 ± 0.88* (9)
I_{max} Tail (pA/pF)	215.2 ± 5.2 (25)	205.7 ± 4.9 (15)	227.6 ± 5.6 (19)	227.3 ± 6.6 (18)

The number of experiments is indicated in parentheses. $V_{1/2act}$ represent potential of half activation, which $V_{1/2act}$ was derived from tail-activation curves recorder in Ba^{2+} solution (Fig. 4.4). For statistics, *p < 0.001, compared with same group with or without $\alpha_2\delta$ (Student's t test, unpaired, two tails).

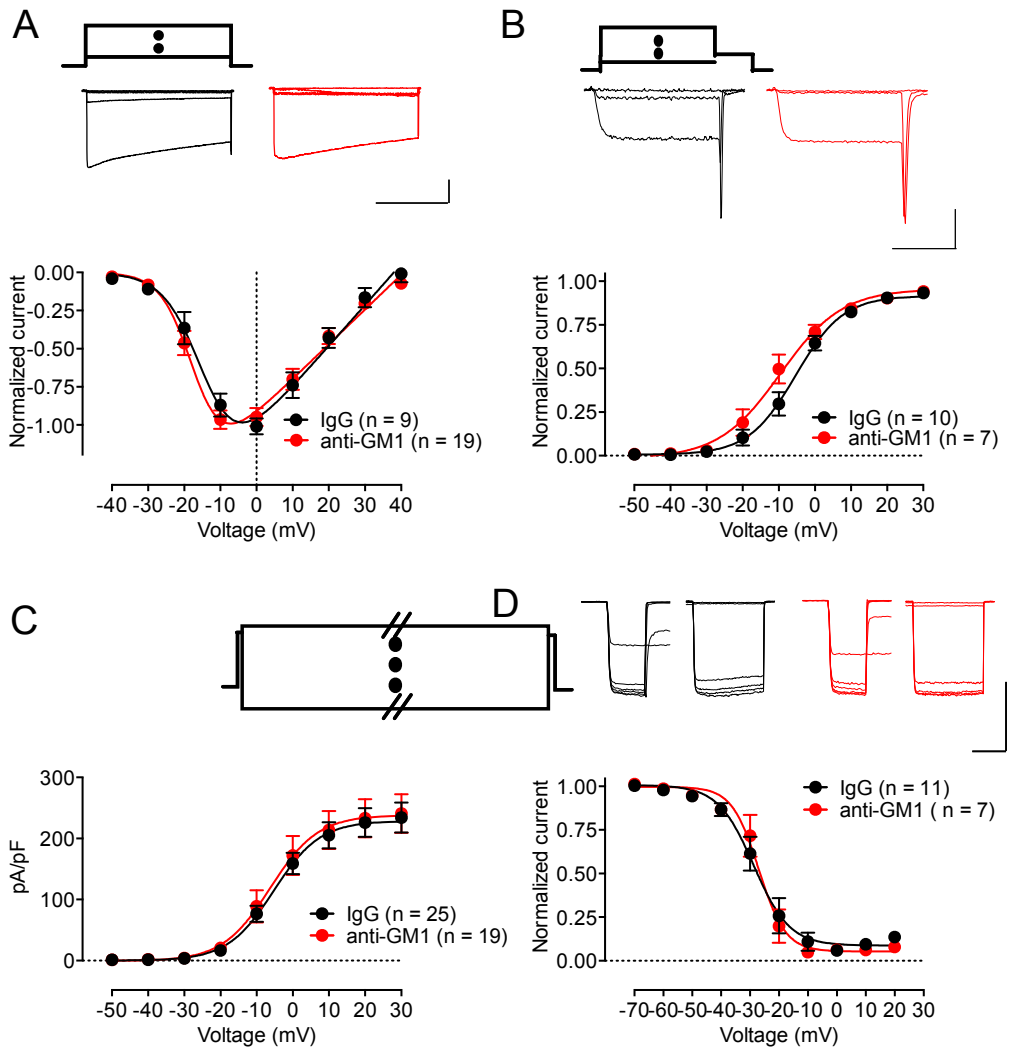

Figure 4.3 Anti-GM1 antibody shifted the activation threshold to hyper-polarized voltage.
A. Normalized I-V curve properties of $Ca_V2.1$ with Anti-GM1 (red) and IgG (black). Anti-GM1 antibody shifted I-V curve of $Ca_V2.1$ to left by 4 mV. *Upper panel,* exemplary trace of Anti-GM1 (red) and IgG (black) were shown. Calibration bar, 500 ms, 1 nA. **B.** Normalized activation curve with Anti-GM1 (red) and IgG (black) recorded by tail protocol. Anti-GM1 antibody shifted the activation curve to $Ca_V2.1$ to left. *Upper panel*, Exemplary trace of Anti-GM1 (red) and IgG (black) were shown. Calibration bar, 20 ms, 1 nA. **C.** The current density of $Ca_V2.1$ with Anti-GM1 (red) and IgG (black) recorded in Tail protocol. Anti-GM1 antibody did not affect the current density of $Ca_V2.1$. **D.** Anti-GM1 antibody did not affect steady-state inactivation. *Upper panel*, Exemplary trace of Anti-GM1 (red) and IgG (black) were shown. Calibration bar, 50 ms, 1 nA.

4.3.2 $\alpha_2\delta$ subunit was involved in the interaction between anti-GM1 antibodies and $Ca_V2.1$

The calcium channel is formed as a hetero-oligomeric complex, which is composed of the α_1-, β- and $\alpha_2\delta$-subunit, in which the $\alpha_2\delta$-subunit is highly glycosylated and attached to the extracellular leaflet of cell membrane (Fig. 4.2). We investigated whether $\alpha_2\delta$-subunit is involved in the interaction between anti-GM1 and $Ca_V2.1$. In this study, we excluded the $\alpha_2\delta$-subunit in the heterogeneous expression system in HEK cell and the $Ca_V2.1$ was still functional (Fig. 4.4A). The $V_{1/2act}$ of IgG group without $\alpha_2\delta$ (-4.48 ± 1.58 mV, n = 10) had no significant difference to that with $\alpha_2\delta$ (-5.33 ± 1.26 mV, n = 10). The current density $Ca_V2.1$ with $\alpha_2\delta$ subunit is slightly bigger than that without $\alpha_2\delta$ subunit (Table 4.1). However, The $V_{1/2act}$ of anti-GM1 without $\alpha_2\delta$ (-9.57 ± 0.93 mV, n =7) is significant lower than that with $\alpha_2\delta$ subunit (-0.37 ± 0.88 mV, n = 9; $p < 0.001$), as shown in figure 4.4, suggesting that without the presence of $\alpha_2\delta$ subunit, the anti-GM1 antibody did not shift the opening threshold to hyperpolarized voltage. These studies indicated that $\alpha_2\delta$ subunit is involved in the interaction between anti-GM1 antibodies and calcium channel.

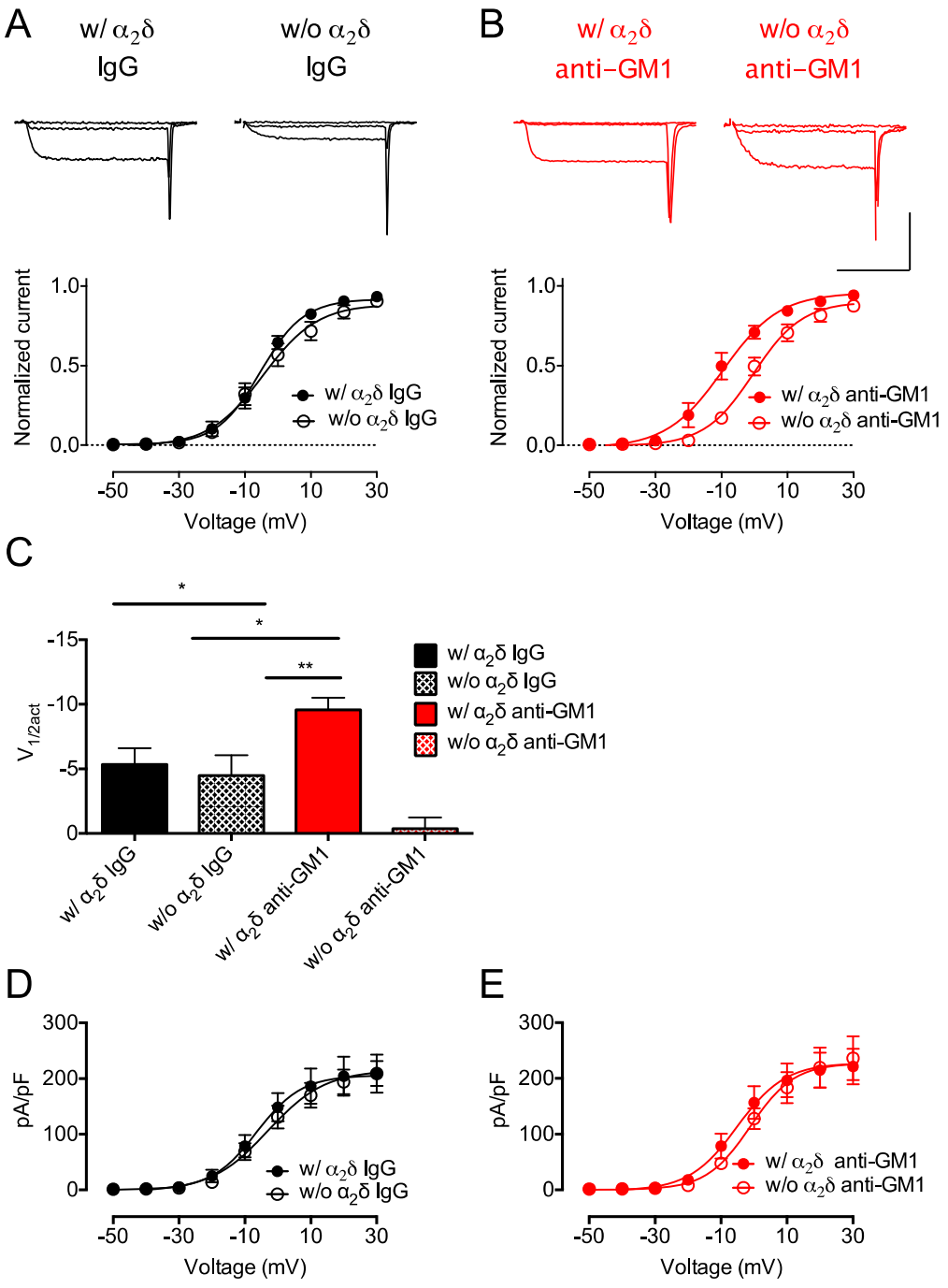

Figure 4.4 $\alpha_2\delta$ subunit abolished the interaction between anti-GM1 and $Ca_V2.1$
A. The activation curves of $Ca_V2.1$ with $\alpha_2\delta$ subunit (filled) and without $\alpha_2\delta$ subunit (open) were shown with IgG incubation. $\alpha_2\delta$ subunit did not affect the activation voltage threshold of $Ca_V2.1$. *Upper panel*, Exemplar current traces of IgG w/ $\alpha_2\delta$, IgG w/o $\alpha_2\delta$. **B.** Anti-GM1 antibody only shifted the activation to left when $\alpha_2\delta$ subunit was present. The activation potentials of $Ca_V2.1$ with $\alpha_2\delta$ subunit (filled) and without $\alpha_2\delta$ subunit (open) are shown with incubation of anti-GM1. *Upper panel*, example traces of anti-GM1 w/ $\alpha_2\delta$ and anti-GM1 w/o $\alpha_2\delta$. Calibration bar. 20 ms, 1nA. **C.** Summary chart showed the detail of $V_{1/2act}$ of $Ca_V2.1$ with or without of $\alpha_2\delta$ subunit or incubation with IgG or anti-GM1 antibodies. **D.** The current densities of $Ca_V2.1$ with $\alpha_2\delta$ subunit (filled) and without $\alpha_2\delta$ subunit (open) are shown with incubation of IgG. **E.** The activation curves of $Ca_V2.1$ with $\alpha_2\delta$ subunit (filled) and without $\alpha_2\delta$ subunit (open) are shown with incubation of anti-GM1. $\alpha_2\delta$ subunit did not affect the current density of $Ca_V2.1$.

4.3.3 Anti-GD1a and anti-GQ1b modulated the calcium channel properties

In comparison with anti-GM1 antibodies, we have also evaluated the function of anti-GD1a and anti-GQ1b antibodies on $Ca_V2.1$ channels. Anti-GD1a is usually found in patient sera of AMAN subtype of GBS along with anti-GM1 antibodies. Both of them affect the transmitter release in neuromuscular junction (NMJ) (Nakatani et al 2007). Our results showed that the anti-GD1a antibodies only decreased the current density (anti-GD1a, 130.8 ± 6.63, n = 8; $p < 0.001$; Figure 4.5B) without affecting the activation potentials (anti-GD1a, -2.90 ± 0.69, n = 8; Figure 4.5A).

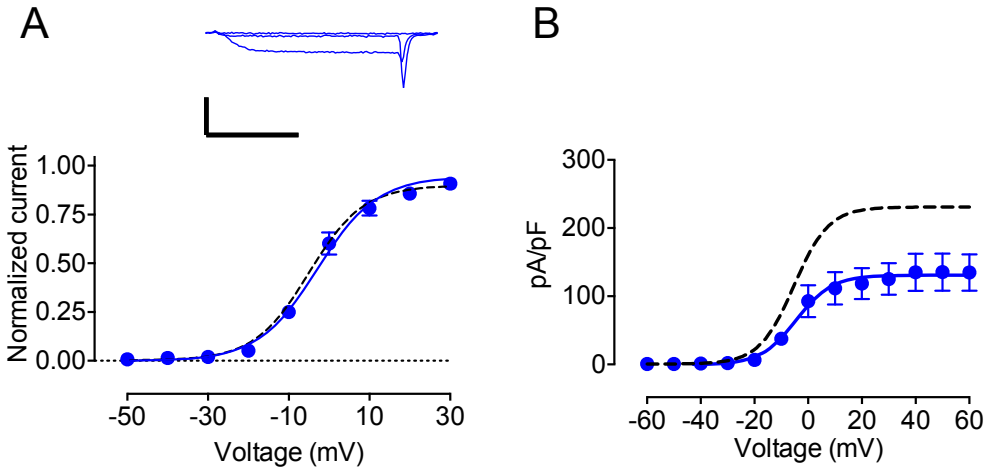

Figure 4.5 Anti-GD1a antibody decreased the current density of $Ca_V2.1$
A. Normalized activation curve with Anti-GD1a (blue) and IgG (black) recorded by tail protocol. Anti-GD1a did not affect $V_{1/2act}$ of the $Ca_V2.1$ *Upper panel*, exemplary trace of Anti-GD1a (blue) Calibration bar, 20 ms, 1 nA. **B.** The current density of $Ca_V2.1$ with Anti-GD1a (blue) and IgG (black, dash) recorded in Tail protocol. Anti-GD1a antibody decreased the current density of $Ca_V2.1$.

The anti-GQ1b antibodies were found at the MFS patient sera and it was reported that anti-GQ1b affected the neuron functions in central nervous systems (Nakatani et al 2009b). In our studies, contrary to the effects of anti-GM1 antibodies, the anti-GQ1b antibodies shifted the activation curve of $Ca_V2.1$ to the hypo-polarized direction (IgG, -5.03 ± 1.06, n = 14; anti-GQ1b, -0.59 ± 0.53, n = 9; $p < 0.001$; Figure 4.6A). The patient sera from MFS exhibited similar effect on $Ca_V2.1$ (IgG, -13.55 ± 1.02, n = 8; anti-GQ1b, -3.61 ± 0.83, n = 8; $p < 0.001$; Figure 4.6B). However, the anti-GQ1b antibody did not affect $C_{aV}2.1$ channel current density (IgG, 230.9 ± 7.07, n = 14; anti-GQ1b, 204.4 ± 9.36, n = 9; Figure 4.6C). These results revealed the diversified function of different anti-ganglioside antibodies on the $Ca_V2.1$ calcium channel function.

Table 4.2 Electrophysiological properties of the $Ca_V2.1$ incubated with anti-GD1a or anti-GQ1b

	IgG	**anti-GD1a**	**anti-GQ1b**
$V_{1/2act}$ (mV)	-5.33 ± 1.26 (10)	-2.90 ± 0.69 (9)	-0.58 ± 0.53* (9)
I_{max} Tail (pA/pF)	215.2 ± 5.2 (25)	130.8 ± 6.6* (9)	204.4 ± 3.3 (8)

The number of experiments is indicated in parentheses. $V_{1/2act}$ represent potential of half activation, which $V_{1/2act}$ was derived from tail-activation curves recorder in Ba^{2+} solution (Fig. 4.5, 4.6). For statistics, *$p < 0.001$, compared with IgG group (Student's t test, unpaired, two tails).

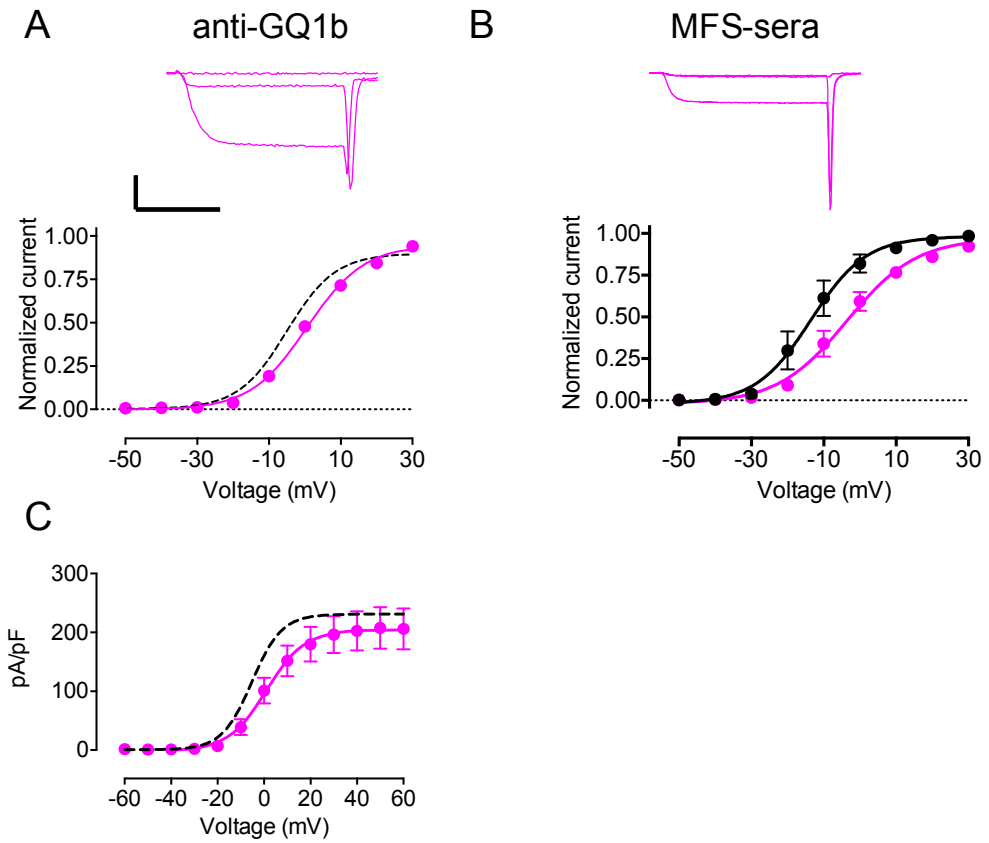

Figure 4.6 Anti-GQ1b antibody shifted the activation potentials of $Ca_V2.1$ to hypo-polarized voltage.
A. Normalized activation curve of GQ1b (cyan) and IgG control (black, dash) recorded by tail protocol were shown. Anti-GQ1b shifted the activation potentials of $Ca_V2.1$ to the right. *Upper panel*, exemplary trace of Anti-GQ1b (Cyan). Calibration bar, 20 ms, 1 nA. **B.** Normalized activation curve of MFS patient sera (cyan) and IgG control sera (black, dash) recorded by tail protocol were shown. MFS patient sera shifted the activation curve of $Ca_V2.1$ to the right. *Upper*, Exemplary trace of MFS patient sera (cyan). **C.** The current density of $Ca_V2.1$ with Anti-GQ1b (cyan) and IgG (black, dash) recorded in Tail protocol. Anti- GQ1b antibody did not affect the current density of $Ca_V2.1$.

4.4 Discussion

4.4.1 Antibody of GM1 interacts with calcium channel.

In this study, we have discovered that antibody against GM1 could modulate the voltage sensing of $Ca_V2.1$ channels and shift the activation potentials of the channels to the hyperpolarized direction. In this way, the calcium channels may open with a relatively lower voltage threshold with anti-GM1 antibodies than that under normal conditions. The inactivation curve of $Ca_V2.1$ was however not changed. Therefore, the channel has relatively large window currents when activated in the presence of anti-GM1 antibodies. Anti-GM1 is found in AMAN patient sera. Studies have shown that anti-GM1 depressed calcium influx and evoked quantal release in NMJ (Buchwald et al 2007). The opening threshold of $Ca_V2.1$ was lower with anti-GM1 than normal conditions. It may lead to excessive calcium influx in NMJ and consequently paralysis on the muscle. Therefore the effect of anti-GM1 on $Ca_V2.1$ voltage sensing might provide one of the potential mechanisms contributing to the muscle weakness in axonal form of GBS.

4.4.2 $\alpha_2\delta$ subunit is involved in the interaction between anti-GM1 antibodies and $Ca_V2.1$

In our studies, we found that the $\alpha_2\delta$-subunit of the $Ca_V2.1$ calcium channel was involved in the interaction between anti-GM1 antibody and $Ca_V2.1$. The $\alpha_2\delta$ subunits integrate the calcium channel into the lipid raft. Davies et al has shown that $\alpha_2\delta$-2 and $Ca_V2.2$ are enriched in the lipid-raft region in mouse cerebellum and tsA-201 cells. Co-localization

of $Ca_V2.2$ and lipid raft marker caveolin requires $\alpha_2\delta$-1 subunit (Peterson et al 2000, Davies et al 2006). The direct interaction between gangliosides and $\alpha_2\delta$ subunit of VGCC has not been shown before. Given that the ganglioside and cholesterol are major components in the rafts, our results suggested that $\alpha_2\delta$ function might be modulated by the gangliosides around the lipid raft regions. It has been shown that the mature $\alpha_2\delta$ subunit can be extensively glycosylated and as such it is possible that these glycosylation sites are important to mediate the interaction between $Ca_V2.1$ channels and anti-ganglioside antibody (Fig. 4.2). It is not clear yet on the details of the molecular interaction between $Ca_V2.1$ channel and anti-GM1 antibody, but we propose two possible hypotheses. One, the anti-ganglioside antibodies could directly bind to the $\alpha_2\delta$ calcium channel and modulate the calcium channel function, or two, the anti-GM1 antibodies could disrupt the interaction between Cav2.1 channels and GM1 and therefore the calcium channel function is altered. Further studies are necessary to elucidate the mechanisms of GM1 and $\alpha_2\delta$ subunit interactions.

4.4.3 Different anti-ganglioside antibodies affect the $Ca_V2.1$ in diversified ways

The GBS could be categorized into demyelinating (AIDP) and axonal subtypes (AMAN), which is associated with various autoantibodies against gangliosides (Yuki & Hartung 2012). Anti-GM1 and GD1a antibodies are found in AMAN patient's sera (Lopez et al 2010), but MFS is distinct to other types of GBS because of its symptoms on

ataxia and association with anti-GQ1b antibodies (Chiba et al 1993, Fisher 1956). In this study, we have examined the effects of anti-GM1, anti-GD1a and anti-GQ1b antibodies on the $Ca_V2.1$ voltage-gated calcium channels. The results revealed the diversified effects of anti-ganglioside antibodies on the calcium channel. Anti-GM1 antibodies shifted the opening threshold to hyperpolarize potential. Anti-GD1a antibodies did not affect the voltage sensing but decrease the calcium channel current. Previous studies using AMAN patient's sera may reflect the combined effects of anti-GM1 and anti-GD1a antibodies (Nakatani et al 2009a). However, our studies suggested that these two auto-antibodies utilized different mechanisms to modulate calcium channel function in contributing to AMAN pathologies. As GM1 and GD1a are highly enriched in the motor and sensory neurons, the diversified effects of anti-GM1 and anti-GD1a may contribute to the degeneration of the motor neurons and neuromuscular junctions.

Anti-GQ1b is associated with MFS. Patients of MFS not only suffer from the limb weakness but also ataxia (Mori et al 1999). It is shown that GQ1b could be found in the cerebellum and is preferentially expressed in the granule cell (Kotani et al 1995, Nakatani et al 2009b). It is reported that $Ca_V2.1$ mutation cause ataxia (Pietrobon 2010). It is possible that the altered calcium channel function may contribute to ataxia in Miller-Fisher syndrome.

The shifting of the activation voltage will affect the open window current of the channels and may cause severe consequence on the nervous

system. Anti-GM1 shifted the activation curve to left and anti-GQ1b shifted the activation curve to right. The voltage sensing of VGCC has been reported to affect the calcium channelopathies. $Ca_V2.1$ mutation V714A and I1815L was associated with FHM1. It is reported that V714A and I1815L shifted the voltage range of activation toward more negative voltage and lead to increase Ca^{2+} influx upon action potential. In this case, the increased vesicle release may increase the neuronal network excitability (Hans et al 1999, Tottene et al 2002). Similarly, the anti-GM1 may induce more Ca^{2+} influx in NMJ and cause muscle paralysis while the anti-GQ1b may lead to less Ca^{2+} influx in central nervous system and contribute to ataxia.

4.4.4 Conclusion and future studies

The study here presented the functional interaction of anti-ganglioside antibodies to $Ca_V2.1$. Anti-GM1 and anti-GD1a are found in AMAN patient sera. Our results showed that anti-GM1 shift the activation curve to hyperpolarized voltage and anti-GD1a decreased the $Ca_V2.1$ channel current. Moreover, the interaction between anti-GM1 and $Ca_V2.1$ was dependent on the auxiliary $\alpha_2\delta$ subunit of calcium channel. The voltage sensing of $Ca_V2.1$ is not affected by anti-GM1 when $\alpha_2\delta$ subunit was removed in the heterologous expression system. On the other hand, anti-GQ1a is associated with the in Miller-Fisher syndrome. The anti-GQ1b increased the activation threshold of $Ca_V2.1$.

Several further studies would be performed to elucidate the interaction between anti-ganglioside antibodies and $Ca_V2.1$ on GBS pathologies.

Firstly, we would like to examine the physiological effects of anti-GM1 on the NMJ. We would like to find out whether the neurotransmitter release is altered in NMJ when applying the anti-GM1 antibodies. Secondly, $\alpha_2\delta$ is extensively glycosylated. It is unknown that whether the glycosylation of $\alpha_2\delta$ is related to the interaction between anti-GM1 and $Ca_V2.1$. We would like to deglycosylate $\alpha_2\delta$ subunit and examine whether it could affect the interaction between anti-GM1 and $Ca_V2.1$.

Reference

Adams PJ, Ben-Johny M, Dick IE, Inoue T, Yue DT. 2014. Apocalmodulin itself promotes ion channel opening and ca(2+) regulation. *Cell* 159: 608-22

Adams PJ, Rungta RL, Garcia E, van den Maagdenberg AM, MacVicar BA, Snutch TP. 2010. Contribution of calcium-dependent facilitation to synaptic plasticity revealed by migraine mutations in the P/Q-type calcium channel. *Proceedings of the National Academy of Sciences of the United States of America* 107: 18694-9

Altier C, Dale CS, Kisilevsky AE, Chapman K, Castiglioni AJ, et al. 2007. Differential role of N-type calcium channel splice isoforms in pain. *J Neurosci* 27: 6363-73

Altier C, Garcia-Caballero A, Simms B, You H, Chen L, et al. 2011. The Cavbeta subunit prevents RFP2-mediated ubiquitination and proteasomal degradation of L-type channels. *Nat Neurosci* 14: 173-80

Anderson RG, Jacobson K. 2002. A role for lipid shells in targeting proteins to caveolae, rafts, and other lipid domains. *Science* 296: 1821-5

Arikkath J, Campbell KP. 2003. Auxiliary subunits: essential components of the voltage-gated calcium channel complex. *Current opinion in neurobiology* 13: 298-307

Arikkath J, Chen CC, Ahern C, Allamand V, Flanagan JD, et al. 2003. Gamma 1 subunit interactions within the skeletal muscle L-type voltage-gated calcium channels. *J Biol Chem* 278: 1212-9

Augustine GJ, Santamaria F, Tanaka K. 2003. Local calcium signaling in neurons. *Neuron* 40: 331-46

Baig SM, Koschak A, Lieb A, Gebhart M, Dafinger C, et al. 2011. Loss of Ca(v)1.3 (CACNA1D) function in a human channelopathy with bradycardia and congenital deafness. *Nat Neurosci* 14: 77-84

Bell TJ, Thaler C, Castiglioni AJ, Helton TD, Lipscombe D. 2004. Cell-Specific Alternative Splicing Increases Calcium Channel Current Density in the Pain Pathway. *Neuron* 41: 127-38

Ben Johny M, Yang PS, Bazzazi H, Yue DT. 2013. Dynamic switching of calmodulin interactions underlies Ca2+ regulation of CaV1.3 channels. *Nature communications* 4: 1717

Bezprozvanny I, Scheller RH, Tsien RW. 1995. Functional impact of syntaxin on gating of N-type and Q-type calcium channels. *Nature* 378: 623-6

Bichet D, Haass FA, Jan LY. 2003. Merging functional studies with structures of inward-rectifier K(+) channels. *Nature reviews. Neuroscience* 4: 957-67

Black DL. 2003. Mechanisms of alternative pre-messenger RNA splicing. *Annual review of biochemistry* 72: 291-336

Borst JG, Sakmann B. 1998. Facilitation of presynaptic calcium currents in the rat brainstem. *J Physiol* 513 (Pt 1): 149-55

Bourinet E, Altier C, Hildebrand ME, Trang T, Salter MW, Zamponi GW. 2014. Calcium-permeable ion channels in pain signaling. *Physiological reviews* 94: 81-140

Bourinet E, Soong TW, Stea A, Snutch TP. 1996. Determinants of the G protein-dependent opioid modulation of neuronal calcium channels. *Proceedings of the National Academy of Sciences of the United States of America* 93: 1486-91

Bourinet E, Soong TW, Sutton K, Slaymaker S, Mathews E, et al. 1999. Splicing of alpha 1A subunit gene generates phenotypic variants of P- and Q-type calcium channels. *Nat Neurosci* 2: 407-15

Brandt A, Khimich D, Moser T. 2005. Few CaV1.3 channels regulate the exocytosis of a synaptic vesicle at the hair cell ribbon synapse. *J Neurosci* 25: 11577-85

Buchwald B, Zhang G, Vogt-Eisele AK, Zhang W, Ahangari R, et al. 2007. Anti-ganglioside antibodies alter presynaptic release and calcium influx. *Neurobiology of disease* 28: 113-21

Bullens RW, O'Hanlon GM, Wagner E, Molenaar PC, Furukawa K, et al. 2003. Roles of complex gangliosides at the neuromuscular junction. *Annals of the New York Academy of Sciences* 998: 401-3

Buraei Z, Yang J. 2010. The ss subunit of voltage-gated Ca2+ channels. *Physiological reviews* 90: 1461-506

Cai Q, Lu L, Tian JH, Zhu YB, Qiao H, Sheng ZH. 2010. Snapin-regulated late endosomal transport is critical for efficient autophagy-lysosomal function in neurons. *Neuron* 68: 73-86

Campbell KP, Leung AT, Sharp AH. 1988. The biochemistry and molecular biology of the dihydropyridine-sensitive calcium channel. *Trends Neurosci* 11: 425-30

Cao YQ, Tsien RW. 2005. Effects of familial hemiplegic migraine type 1 mutations on neuronal P/Q-type Ca2+ channel activity and inhibitory synaptic transmission. *Proceedings of the National Academy of Sciences of the United States of America* 102: 2590-5

Cao YQ, Tsien RW. 2010. Different relationship of N- and P/Q-type Ca2+ channels to channel-interacting slots in controlling neurotransmission at cultured hippocampal synapses. *J Neurosci* 30: 4536-46

Capasso M, Caporale CM, Pomilio F, Gandolfi P, Lugaresi A, Uncini A. 2003. Acute motor conduction block neuropathy Another Guillain-Barre syndrome variant. *Neurology* 61: 617-22

Capasso M, Notturno F, Manzoli C, Uncini A. 2011. Involvement of sensory fibres in axonal subtypes of Guillain-Barre syndrome. *J Neurol Neurosurg Psychiatry* 82: 664-70

Castiglioni AJ, Raingo J, Lipscombe D. 2006. Alternative splicing in the C-terminus of CaV2.2 controls expression and gating of N-type calcium channels. *J Physiol* 576: 119-34

Catterall WA. 2000. Structure and regulation of voltage-gated Ca2+ channels. *Annu Rev Cell Dev Biol* 16: 521-55

Catterall WA, Few AP. 2008. Calcium channel regulation and presynaptic plasticity. *Neuron* 59: 882-901

Chagot B, Potet F, Balser JR, Chazin WJ. 2009. Solution NMR structure of the C-terminal EF-hand domain of human cardiac sodium channel NaV1.5. *J Biol Chem* 284: 6436-45

Chang SY, Yong TF, Yu CY, Liang MC, Pletnikova O, et al. 2007. Age and gender-dependent alternative splicing of P/Q-type calcium channel EF-hand. *Neuroscience* 145: 1026-36

Chapman ER. 2008. How does synaptotagmin trigger neurotransmitter release? *Annual review of biochemistry* 77: 615-41

Chaudhuri D, Chang SY, DeMaria CD, Alvania RS, Soong TW, Yue DT. 2004. Alternative splicing as a molecular switch for Ca2+/calmodulin-dependent facilitation of P/Q-type Ca2+ channels{Chaudhuri, 2007 #114}. *J Neurosci* 24: 6334-42

Chaudhuri D, Issa JB, Yue DT. 2007. Elementary mechanisms producing facilitation of Cav2.1 (P/Q-type) channels. *The Journal of general physiology* 129: 385-401

Chen M, Manley JL. 2009. Mechanisms of alternative splicing regulation: insights from molecular and genomics approaches. *Nature reviews. Molecular cell biology* 10: 741-54

Chheda MG, Ashery U, Thakur P, Rettig J, Sheng ZH. 2001. Phosphorylation of Snapin by PKA modulates its interaction with the SNARE complex. *Nat Cell Biol* 3: 331-8

Chiba A, Kusunoki S, Obata H, Machinami R, Kanazawa I. 1993. Serum anti-GQ1b IgG antibody is associated with ophthalmoplegia in Miller Fisher syndrome and Guillain-Barre syndrome: clinical and immunohistochemical studies. *Neurology* 43: 1911-7

Condliffe SB, Fratangeli A, Munasinghe NR, Saba E, Passafaro M, et al. 2013. The E1015K variant in the synprint region of the CaV2.1 channel alters channel function and is associated with different migraine phenotypes. *J Biol Chem* 288: 33873-83

Davies A, Douglas L, Hendrich J, Wratten J, Tran Van Minh A, et al. 2006. The calcium channel alpha2delta-2 subunit partitions with CaV2.1 into lipid rafts in cerebellum: implications for localization and function. *J Neurosci* 26: 8748-57

Davies A, Hendrich J, Van Minh AT, Wratten J, Douglas L, Dolphin AC. 2007. Functional biology of the alpha(2)delta subunits of voltage-gated calcium channels. *Trends in pharmacological sciences* 28: 220-8

Davies A, Kadurin I, Alvarez-Laviada A, Douglas L, Nieto-Rostro M, et al. 2010. The alpha2delta subunits of voltage-gated calcium channels form GPI-anchored proteins, a posttranslational modification essential for function. *Proceedings of the National Academy of Sciences of the United States of America* 107: 1654-9

Davydova D, Marini C, King C, Klueva J, Bischof F, et al. 2014. Bassoon specifically controls presynaptic P/Q-type Ca(2+) channels via RIM-binding protein. *Neuron* 82: 181-94

de Leon M, Wang Y, Jones L, Perez-Reyes E, Wei X, et al. 1995. Essential Ca(2+)-binding motif for Ca(2+)-sensitive inactivation of L-type Ca2+ channels. *Science* 270: 1502-6

DeMaria CD, Soong TW, Alseikhan BA, Alvania RS, Yue DT. 2001. Calmodulin bifurcates the local Ca2+ signal that modulates P/Q-type Ca2+ channels. *Nature* 411: 484-9

Deng L, Kaeser PS, Xu W, Sudhof TC. 2011. RIM Proteins Activate Vesicle Priming by Reversing Autoinhibitory Homodimerization of Munc13. *Neuron* 69: 317-31

Dolphin AC. 2013. The alpha2delta subunits of voltage-gated calcium channels. *Biochim Biophys Acta* 1828: 1541-9

Ertel EA, Campbell KP, Harpold MM, Hofmann F, Mori Y, et al. 2000. Nomenclature of voltage-gated calcium channels. *Neuron* 25: 533-5

Evans RM, Zamponi GW. 2006. Presynaptic Ca2+ channels--integration centers for neuronal signaling pathways. *Trends Neurosci* 29: 617-24

Fisher M. 1956. An unusual variant of acute idiopathic polyneuritis (syndrome of ophthalmoplegia, ataxia and areflexia). *The New England journal of medicine* 255: 57-65

Fuchs PA. 2005. Time and intensity coding at the hair cell's ribbon synapse. *J Physiol* 566: 7-12

Fuchs PA, Sokolowski BH. 1990. The acquisition during development of Ca-activated potassium currents by cochlear hair cells of the chick. *Proceedings. Biological sciences / The Royal Society* 241: 122-6

Goutman JD. 2012. Transmitter release from cochlear hair cells is phase locked to cyclic stimuli of different intensities and frequencies. *J Neurosci* 32: 17025-35a

Graves TD, Imbrici P, Kors EE, Terwindt GM, Eunson LH, et al. 2008. Premature stop codons in a facilitating EF-hand splice variant of CaV2.1 cause episodic ataxia type 2. *Neurobiology of disease* 32: 10-5

Gray AC, Raingo J, Lipscombe D. 2007. Neuronal calcium channels: splicing for optimal performance. *Cell Calcium* 42: 409-17

Guillain G, Barré JA, Strohl A. 1916. Sur unsyndrome de radiculonévrite avec hyperalbuminose du liquide céphalo-rachidien sans réaction cellulaire: remarques sur les caractères cliniques et graphiques des réflexes tendineux. *Bulletins et mémoires de la Société des Médecins des Hôpitaux de Paris* 40: 1462-70

Hadden RD, Cornblath DR, Hughes RA, Zielasek J, Hartung HP, et al. 1998. Electrophysiological classification of Guillain-Barre syndrome: clinical associations and outcome. Plasma Exchange/Sandoglobulin Guillain-Barre Syndrome Trial Group. *Annals of neurology* 44: 780-8

Hadden RD, Karch H, Hartung HP, Zielasek J, Weissbrich B, et al. 2001. Preceding infections, immune factors, and outcome in Guillain-Barre syndrome. *Neurology* 56: 758-65

Han Y, Kaeser PS, Sudhof TC, Schneggenburger R. 2011. RIM determines Ca(2)+ channel density and vesicle docking at the presynaptic active zone. *Neuron* 69: 304-16

Hans M, Luvisetto S, Williams ME, Spagnolo M, Urrutia A, et al. 1999. Functional consequences of mutations in the human alpha1A calcium channel subunit linked to familial hemiplegic migraine. *J Neurosci* 19: 1610-9

Hatakeyama S, Wakamori M, Ino M, Miyamoto N, Takahashi E, et al. 2001. Differential nociceptive responses in mice lacking the alpha(1B) subunit of N-type Ca(2+) channels. *Neuroreport* 12: 2423-7

Heinemann SH, Terlau H, Stuhmer W, Imoto K, Numa S. 1992. Calcium channel characteristics conferred on the sodium channel by single mutations. *Nature* 356: 441-3

Hiraga A, Mori M, Ogawara K, Hattori T, Kuwabara S. 2003. Differences in patterns of progression in demyelinating and axonal Guillain-Barre syndromes. *Neurology* 61: 471-4

Hoppa MB, Lana B, Margas W, Dolphin AC, Ryan TA. 2012. alpha2delta expression sets presynaptic calcium channel abundance and release probability. *Nature* 486: 122-5

Huang H, Tan BZ, Shen Y, Tao J, Jiang F, et al. 2012. RNA Editing of the IQ Domain in Ca(v)1.3 Channels Modulates Their Ca(2+)-Dependent Inactivation. *Neuron* 73: 304-16

Huang H, Yu D, Soong TW. 2013. C-terminal alternative splicing of CaV1.3 channels distinctively modulates their dihydropyridine sensitivity. *Molecular pharmacology* 84: 643-53

Ikeda SR. 1996. Voltage-dependent modulation of N-type calcium channels by G-protein beta gamma subunits. *Nature* 380: 255-8

Ilardi JM, Mochida S, Sheng ZH. 1999. Snapin: a SNARE-associated protein implicated in synaptic transmission. *Nat Neurosci* 2: 119-24

Inagaki A, Lee A. 2013. Developmental alterations in the biophysical properties of Ca(v) 1.3 Ca(2+) channels in mouse inner hair cells. *Channels (Austin)* 7: 171-81

Irie F, Hidari KI, Tai T, Li YT, Seyama Y, Hirabayashi Y. 1994. Biosynthetic pathway for a new series of gangliosides, GT1a alpha and GQ1b alpha. *FEBS Lett* 351: 291-4

Islam Z, Jacobs BC, van Belkum A, Mohammad QD, Islam MB, et al. 2010. Axonal variant of Guillain-Barre syndrome associated with Campylobacter infection in Bangladesh. *Neurology* 74: 581-7

Jacobs BC, Rothbarth PH, van der Meche FG, Herbrink P, Schmitz PI, et al. 1998. The spectrum of antecedent infections in Guillain-Barre syndrome: a case-control study. *Neurology* 51: 1110-5

Jarvis SE, Zamponi GW. 2001. Distinct molecular determinants govern syntaxin 1A-mediated inactivation and G-protein inhibition of N-type calcium channels. *J Neurosci* 21: 2939-48

Jun K, Piedras-Renteria ES, Smith SM, Wheeler DB, Lee SB, et al. 1999. Ablation of P/Q-type Ca(2+) channel currents, altered synaptic transmission, and progressive ataxia in mice lacking the alpha(1A)-subunit. *Proceedings of the National Academy of Sciences of the United States of America* 96: 15245-50

Kadurin I, Alvarez-Laviada A, Ng SF, Walker-Gray R, D'Arco M, et al. 2012. Calcium currents are enhanced by alpha2delta-1 lacking its membrane anchor. *J Biol Chem* 287: 33554-66

Kaech S, Banker G. 2006. Culturing hippocampal neurons. *Nature protocols* 1: 2406-15

Kaeser PS, Deng L, Wang Y, Dulubova I, Liu X, et al. 2011. RIM proteins tether Ca2+ channels to presynaptic active zones via a direct PDZ-domain interaction. *Cell* 144: 282-95

Kim C, Jun K, Lee T, Kim SS, McEnery MW, et al. 2001. Altered nociceptive response in mice deficient in the alpha(1B) subunit of the voltage-dependent calcium channel. *Mol Cell Neurosci* 18: 235-45

Koga M, Gilbert M, Takahashi M, Li J, Hirata K, et al. 2012. GQ1b-seronegative Fisher syndrome: clinical features and new serological markers. *J Neurol*

Kollmar R, Fak J, Montgomery LG, Hudspeth AJ. 1997a. Hair cell-specific splicing of mRNA for the alpha1D subunit of voltage-gated Ca2+ channels in the chicken's cochlea.

Proceedings of the National Academy of Sciences of the United States of America 94: 14889-93

Kollmar R, Montgomery LG, Fak J, Henry LJ, Hudspeth AJ. 1997b. Predominance of the alpha1D subunit in L-type voltage-gated Ca2+ channels of hair cells in the chicken's cochlea. *Proceedings of the National Academy of Sciences of the United States of America* 94: 14883-8

Kotani M, Terashima T, Tai T. 1995. Developmental changes of ganglioside expressions in postnatal rat cerebellar cortex. *Brain research* 700: 40-58

Krapivinsky G, Mochida S, Krapivinsky L, Cibulsky SM, Clapham DE. 2006. The TRPM7 ion channel functions in cholinergic synaptic vesicles and affects transmitter release. *Neuron* 52: 485-96

Kros CJ, Ruppersberg JP, Rusch A. 1998. Expression of a potassium current in inner hair cells during development of hearing in mice. *Nature* 394: 281-4

Krovetz HS, Helton TD, Crews AL, Horne WA. 2000. C-Terminal alternative splicing changes the gating properties of a human spinal cord calcium channel alpha 1A subunit. *J Neurosci* 20: 7564-70

Kuitwaard K, de Gelder J, Tio-Gillen AP, Hop WC, van Gelder T, et al. 2009. Pharmacokinetics of intravenous immunoglobulin and outcome in Guillain-Barre syndrome. *Annals of neurology* 66: 597-603

Lee A, Scheuer T, Catterall WA. 2000. Ca2+/calmodulin-dependent facilitation and inactivation of P/Q-type Ca2+ channels. *J Neurosci* 20: 6830-8

Letts VA, Felix R, Biddlecome GH, Arikkath J, Mahaffey CL, et al. 1998. The mouse stargazer gene encodes a neuronal Ca2+-channel gamma subunit. *Nat Genet* 19: 340-7

Liang H, DeMaria CD, Erickson MG, Mori MX, Alseikhan BA, Yue DT. 2003. Unified mechanisms of Ca2+ regulation across the Ca2+ channel family. *Neuron* 39: 951-60

Liao P, Yu D, Li G, Yong TF, Soon JL, et al. 2007. A smooth muscle Cav1.2 calcium channel splice variant underlies hyperpolarized window current and enhanced state-dependent inhibition by nifedipine. *J Biol Chem* 282: 35133-42

Liao P, Yu D, Lu S, Tang Z, Liang MC, et al. 2004. Smooth muscle-selective alternatively spliced exon generates functional variation in Cav1.2 calcium channels. *J Biol Chem* 279: 50329-35

Liao P, Zhang HY, Soong TW. 2009. Alternative splicing of voltage-gated calcium channels: from molecular biology to disease. *Pflugers Arch* 458: 481-7

Liu X, Yang PS, Yang W, Yue DT. 2010. Enzyme-inhibitor-like tuning of Ca(2+) channel connectivity with calmodulin. *Nature* 463: 968-72

Lopez PH, Zhang G, Zhang J, Lehmann HC, Griffin JW, et al. 2010. Passive transfer of IgG anti-GM1 antibodies impairs peripheral nerve repair. *J Neurosci* 30: 9533-41

Marangoudakis S, Andrade A, Helton TD, Denome S, Castiglioni AJ, Lipscombe D. 2012. Differential Ubiquitination and Proteasome Regulation of CaV2.2 N-Type Channel Splice Isoforms. *J Neurosci* 32: 10365-9

Martens JR, Navarro-Polanco R, Coppock EA, Nishiyama A, Parshley L, et al. 2000. Differential targeting of Shaker-like potassium channels to lipid rafts. *J Biol Chem* 275: 7443-6

Martens S, Kozlov MM, McMahon HT. 2007. How synaptotagmin promotes membrane fusion. *Science* 316: 1205-8

Maximov A, Bezprozvanny I. 2002. Synaptic targeting of N-type calcium channels in hippocampal neurons. *J Neurosci* 22: 6939-52

McKhann GM, Cornblath DR, Griffin JW, Ho TW, Li CY, et al. 1993. Acute motor axonal neuropathy: a frequent cause of acute flaccid paralysis in China. *Annals of neurology* 33: 333-42

Meir A, Ginsburg S, Butkevich A, Kachalsky SG, Kaiserman I, et al. 1999. Ion channels in presynaptic nerve terminals and control of transmitter release. *Physiological reviews* 79: 1019-88

Minor DL, Jr., Findeisen F. 2010. Progress in the structural understanding of voltage-gated calcium channel (CaV) function and modulation. *Channels (Austin)* 4: 459-74

Mochida S, Sheng ZH, Baker C, Kobayashi H, Catterall WA. 1996. Inhibition of neurotransmission by peptides containing the synaptic protein interaction site of N-type Ca2+ channels. *Neuron* 17: 781-8

Modrek B, Resch A, Grasso C, Lee C. 2001. Genome-wide detection of alternative splicing in expressed sequences of human genes. *Nucleic acids research* 29: 2850-9

Mori M, Kuwabara S, Koga M, Asahina M, Ogawara K, et al. 1999. IgG anti-GQ1b positive acute ataxia without ophthalmoplegia. *J Neurol Neurosurg Psychiatry* 67: 668-70

Mori Y, Friedrich T, Kim MS, Mikami A, Nakai J, et al. 1991. Primary structure and functional expression from complementary DNA of a brain calcium channel. *Nature* 350: 398-402

Nagashima T, Koga M, Odaka M, Hirata K, Yuki N. 2007. Continuous spectrum of pharyngeal-cervical-brachial variant of Guillain-Barre syndrome. *Archives of neurology* 64: 1519-23

Nakatani Y, Hotta S, Utsunomiya I, Tanaka K, Hoshi K, et al. 2009a. Cav2.1 voltage-dependent Ca2+ channel current is inhibited by serum from select patients with Guillain-Barre syndrome. *Neurochemical research* 34: 149-57

Nakatani Y, Murata M, Shibata K, Nagaoka T, Utsunomiya I, et al. 2009b. IgM anti-GQ1b monoclonal antibody inhibits voltage-dependent calcium current in cerebellar granule cells. *Experimental neurology* 219: 74-80

Nakatani Y, Nagaoka T, Hotta S, Utsunomiya I, Yoshino H, et al. 2007. IgG anti-GalNAc-GD1a antibody inhibits the voltage-dependent calcium channel currents in PC12 pheochromocytoma cells. *Experimental neurology* 204: 380-6

Navarro A, Encinar JA, Lopez-Mendez B, Aguado-Llera D, Prieto J, et al. 2012. Mutation of Ser-50 and Cys-66 in Snapin Modulates Protein Structure and Stability. *Biochemistry*

Nishimoto Y, Odaka M, Hirata K, Yuki N. 2004. Usefulness of anti-GQ1b IgG antibody testing in Fisher syndrome compared with cerebrospinal fluid examination. *Journal of neuroimmunology* 148: 200-5

Nowycky MC, Fox AP, Tsien RW. 1985. Three types of neuronal calcium channel with different calcium agonist sensitivity. *Nature* 316: 440-3

Ohmi Y, Ohkawa Y, Yamauchi Y, Tajima O, Furukawa K, Furukawa K. 2012. Essential roles of gangliosides in the formation and maintenance of membrane microdomains in brain tissues. *Neurochemical research* 37: 1185-91

Ophoff RA, Terwindt GM, Vergouwe MN, Van Eijk R, Oefner PJ, et al. 1996. Familial hemiplegic migraine and episodic ataxia type-2 are caused by mutations in the Ca²⁺ channel gene CACNL1A4. *Cell* 87: 543-52

Orlikowski D, Porcher R, Sivadon-Tardy V, Quincampoix JC, Raphael JC, et al. 2011. Guillain-Barre syndrome following primary cytomegalovirus infection: a prospective cohort study. *Clinical infectious diseases : an official publication of the Infectious Diseases Society of America* 52: 837-44

Pan PY, Tian JH, Sheng ZH. 2009. Snapin facilitates the synchronization of synaptic vesicle fusion. *Neuron* 61: 412-24

Pennartz CM, de Jeu MT, Bos NP, Schaap J, Geurtsen AM. 2002. Diurnal modulation of pacemaker potentials and calcium current in the mammalian circadian clock. *Nature* 416: 286-90

Perez-Reyes E. 2003. Molecular physiology of low-voltage-activated t-type calcium channels. *Physiological reviews* 83: 117-61

Peterson BZ, DeMaria CD, Adelman JP, Yue DT. 1999. Calmodulin is the Ca2+ sensor for Ca2+ -dependent inactivation of L-type calcium channels. *Neuron* 22: 549-58

Peterson BZ, Lee JS, Mulle JG, Wang Y, de Leon M, Yue DT. 2000. Critical determinants of Ca(2+)-dependent inactivation within an EF-hand motif of L-type Ca(2+) channels. *Biophys J* 78: 1906-20

Pietrobon D. 2010. CaV2.1 channelopathies. *Pflugers Arch* 460: 375-93

Platzer J, Engel J, Schrott-Fischer A, Stephan K, Bova S, et al. 2000. Congenital deafness and sinoatrial node dysfunction in mice lacking class D L-type Ca2+ channels. *Cell* 102: 89-97

Pragnell M, De Waard M, Mori Y, Tanabe T, Snutch TP, Campbell KP. 1994. Calcium channel beta-subunit binds to a conserved motif in the I-II cytoplasmic linker of the alpha 1-subunit. *Nature* 368: 67-70

Quintero IB, Herrala AM, Araujo CL, Pulkka AE, Hautaniemi S, et al. 2013. Transmembrane prostatic acid phosphatase (TMPAP) interacts with snapin and deficient mice develop prostate adenocarcinoma. *PloS one* 8: e73072

Raingo J, Castiglioni AJ, Lipscombe D. 2007. Alternative splicing controls G protein-dependent inhibition of N-type calcium channels in nociceptors. *Nat Neurosci* 10: 285-92

Rettig J, Sheng ZH, Kim DK, Hodson CD, Snutch TP, Catterall WA. 1996. Isoform-specific interaction of the alpha1A subunits of brain Ca2+ channels with the presynaptic proteins syntaxin and SNAP-25. *Proceedings of the National Academy of Sciences of the United States of America* 93: 7363-8

Robinson P, Etheridge S, Song L, Armenise P, Jones OT, Fitzgerald EM. 2010. Formation of N-type (Cav2.2) voltage-gated calcium channel membrane microdomains: Lipid raft association and clustering. *Cell Calcium* 48: 183-94

Robinson P, Etheridge S, Song L, Shah R, Fitzgerald EM, Jones OT. 2011. Targeting of voltage-gated calcium channel alpha2delta-1 subunit to lipid rafts is independent from a GPI-anchoring motif. *PloS one* 6: e19802

Rousset M, Cens T, Restituito S, Barrere C, Black JL, 3rd, et al. 2001. Functional roles of gamma2, gamma3 and gamma4, three new Ca2+ channel subunits, in P/Q-type Ca2+ channel expressed in Xenopus oocytes. *J Physiol* 532: 583-93

Saegusa H, Wakamori M, Matsuda Y, Wang J, Mori Y, et al. 2007. Properties of human Cav2.1 channel with a spinocerebellar ataxia type 6 mutation expressed in Purkinje cells. *Mol Cell Neurosci* 34: 261-70

Safieddine S, El-Amraoui A, Petit C. 2012. The auditory hair cell ribbon synapse: from assembly to function. *Annual review of neuroscience* 35: 509-28

Sejvar JJ, Baughman AL, Wise M, Morgan OW. 2011. Population incidence of Guillain-Barre syndrome: a systematic review and meta-analysis. *Neuroepidemiology* 36: 123-33

Sekiguchi Y, Uncini A, Yuki N, Misawa S, Notturno F, et al. 2012. Antiganglioside antibodies are associated with axonal Guillain-Barre syndrome: a Japanese-Italian collaborative study. *J Neurol Neurosurg Psychiatry* 83: 23-8

Shen Y, Yu D, Hiel H, Liao P, Yue DT, et al. 2006. Alternative splicing of the Ca(v)1.3 channel IQ domain, a molecular switch for Ca2+-dependent inactivation within auditory hair cells. *J Neurosci* 26: 10690-9

Sheng ZH, Rettig J, Cook T, Catterall WA. 1996. Calcium-dependent interaction of N-type calcium channels with the synaptic core complex. *Nature* 379: 451-4

Sheng ZH, Rettig J, Takahashi M, Catterall WA. 1994. Identification of a syntaxin-binding site on N-type calcium channels. *Neuron* 13: 1303-13

Simms BA, Zamponi GW. 2014. Neuronal voltage-gated calcium channels: structure, function, and dysfunction. *Neuron* 82: 24-45

Snutch TP, Reiner PB. 1992. Ca2+ channels: diversity of form and function. *Current opinion in neurobiology* 2: 247-53

Song H, Nie L, Rodriguez-Contreras A, Sheng ZH, Yamoah EN. 2003. Functional interaction of auxiliary subunits and synaptic proteins with Ca(v)1.3 may impart hair cell Ca2+ current properties. *Journal of neurophysiology* 89: 1143-9

Soong TW, DeMaria CD, Alvania RS, Zweifel LS, Liang MC, et al. 2002. Systematic identification of splice variants in human P/Q-type channel alpha1(2.1) subunits: implications for current density and Ca2+-dependent inactivation. *J Neurosci* 22: 10142-52

Spafford JD, Munno DW, Van Nierop P, Feng ZP, Jarvis SE, et al. 2003. Calcium channel structural determinants of synaptic transmission between identified invertebrate neurons. *J Biol Chem* 278: 4258-67

Splawski I, Timothy KW, Decher N, Kumar P, Sachse FB, et al. 2005. Severe arrhythmia disorder caused by cardiac L-type calcium channel mutations. *Proceedings of the National Academy of Sciences of the United States of America* 102: 8089-96; discussion 86-8

Splawski I, Timothy KW, Priori SG, Napolitano C, Bloise R. 1993. Timothy Syndrome.

Splawski I, Timothy KW, Sharpe LM, Decher N, Kumar P, et al. 2004. Ca(V)1.2 calcium channel dysfunction causes a multisystem disorder including arrhythmia and autism. *Cell* 119: 19-31

Stanley EF. 1997. The calcium channel and the organization of the presynaptic transmitter release face. *Trends Neurosci* 20: 404-9

Starr TV, Prystay W, Snutch TP. 1991. Primary structure of a calcium channel that is highly expressed in the rat cerebellum. *Proceedings of the National Academy of Sciences of the United States of America* 88: 5621-5

Striessnig J, Koschak A. 2008. Exploring the function and pharmacotherapeutic potential of voltage-gated Ca2+ channels with gene knockout models. *Channels (Austin)* 2: 233-51

Tadross MR, Ben Johny M, Yue DT. 2010. Molecular endpoints of Ca2+/calmodulin- and voltage-dependent inactivation of Ca(v)1.3 channels. *The Journal of general physiology* 135: 197-215

Tadross MR, Yue DT. 2010. Systematic mapping of the state dependence of voltage- and Ca2+-dependent inactivation using simple open-channel measurements. *The Journal of general physiology* 135: 217-27

Taguchi K, Utsunomiya I, Ren J, Yoshida N, Aoyagi H, et al. 2004. Effect of rabbit anti-asialo-GM1 (GA1) polyclonal antibodies on neuromuscular transmission and acetylcholine-induced action potentials: neurophysiological and immunohistochemical studies. *Neurochemical research* 29: 953-60

Takahashi M, Seagar MJ, Jones JF, Reber BF, Catterall WA. 1987. Subunit structure of dihydropyridine-sensitive calcium channels from skeletal muscle. *Proceedings of the National Academy of Sciences of the United States of America* 84: 5478-82

Takahashi T, Momiyama A. 1993. Different types of calcium channels mediate central synaptic transmission. *Nature* 366: 156-58

Tan BZ, Jiang F, Tan MY, Yu D, Huang H, et al. 2011. Functional characterization of alternative splicing in the C terminus of L-type CaV1.3 channels. *J Biol Chem* 286: 42725-35

Tan GM, Yu D, Wang J, Soong TW. 2012. Alternative splicing at C terminus of Ca(V)1.4 calcium channel modulates calcium-dependent inactivation, activation potential, and current density. *J Biol Chem* 287: 832-47

Tang ZZ, Liang MC, Lu S, Yu D, Yu CY, et al. 2004. Transcript scanning reveals novel and extensive splice variations in human l-type voltage-gated calcium channel, Cav1.2 alpha1 subunit. *J Biol Chem* 279: 44335-43

Tang ZZ, Liao P, Li G, Jiang FL, Yu D, et al. 2008. Differential splicing patterns of L-type calcium channel Cav1.2 subunit in hearts of Spontaneously Hypertensive Rats and Wistar Kyoto Rats. *Biochim Biophys Acta* 1783: 118-30

Tedford HW, Zamponi GW. 2006. Direct G protein modulation of Cav2 calcium channels. *Pharmacol Rev* 58: 837-62

Tian JH, Wu ZX, Unzicker M, Lu L, Cai Q, et al. 2005. The role of Snapin in neurosecretion: snapin knock-out mice exhibit impaired calcium-dependent exocytosis of large dense-core vesicles in chromaffin cells. *J Neurosci* 25: 10546-55

Toru S, Murakoshi T, Ishikawa K, Saegusa H, Fujigasaki H, et al. 2000. Spinocerebellar ataxia type 6 mutation alters P-type calcium channel function. *J Biol Chem* 275: 10893-8

Tottene A, Fellin T, Pagnutti S, Luvisetto S, Striessnig J, et al. 2002. Familial hemiplegic migraine mutations increase Ca(2+) influx through single human CaV2.1 channels and decrease maximal CaV2.1 current density in neurons. *Proceedings of the National Academy of Sciences of the United States of America* 99: 13284-9

Tsien RW, Lipscombe D, Madison DV, Bley KR, Fox AP. 1988. Multiple types of neuronal calcium channels and their selective modulation. *Trends Neurosci* 11: 431-8

Tsunemi T, Ishikawa K, Jin H, Mizusawa H. 2008. Cell-type-specific alternative splicing in spinocerebellar ataxia type 6. *Neurosci Lett* 447: 78-81

van der Meche FG, Schmitz PI. 1992. A randomized trial comparing intravenous immune globulin and plasma exchange in Guillain-Barre syndrome. Dutch Guillain-Barre Study Group. *The New England journal of medicine* 326: 1123-9

Van Petegem F, Clark KA, Chatelain FC, Minor DL, Jr. 2004. Structure of a complex between a voltage-gated calcium channel beta-subunit and an alpha-subunit domain. *Nature* 429: 671-5

Wang J, Thio SS, Yang SS, Yu D, Yu CY, et al. 2011. Splice variant specific modulation of CaV1.2 calcium channel by galectin-1 regulates arterial constriction. *Circ Res* 109: 1250-8

Watase K, Barrett CF, Miyazaki T, Ishiguro T, Ishikawa K, et al. 2008. Spinocerebellar ataxia type 6 knockin mice develop a progressive neuronal dysfunction with age-dependent accumulation of mutant CaV2.1 channels. *Proceedings of the National Academy of Sciences of the United States of America* 105: 11987-92

Weiss N, Zamponi GW. 2012. Regulation of voltage-gated calcium channels by synaptic proteins. *Advances in experimental medicine and biology* 740: 759-75

Westenbroek RE, Hell JW, Warner C, Dubel SJ, Snutch TP, Catterall WA. 1992. Biochemical properties and subcellular distribution of an N-type calcium channel alpha 1 subunit. *Neuron* 9: 1099-115

Wheeler DB, Randall A, Tsien RW. 1994. Roles of N-type and Q-type Ca2+ channels in supporting hippocampal synaptic transmission. *Science* 264: 107-11

Willison HJ. 2005. The immunobiology of Guillain-Barre syndromes. *Journal of the peripheral nervous system : JPNS* 10: 94-112

Wojcik SM, Brose N. 2007. Regulation of membrane fusion in synaptic excitation-secretion coupling: speed and accuracy matter. *Neuron* 55: 11-24

Wolff S, Stoter M Fau - Giamas G, Giamas G Fau - Piesche M, Piesche M Fau - Henne-Bruns D, Henne-Bruns D Fau - Banting G, et al. 2006. Casein kinase 1 delta (CK1delta) interacts with the SNARE associated protein snapin. *FEBS Lett*

Xu W, Lipscombe D. 2001. Neuronal Ca(V)1.3alpha(1) L-type channels activate at relatively hyperpolarized membrane potentials and are incompletely inhibited by dihydropyridines. *J Neurosci* 21: 5944-51

Yang PS, Alseikhan BA, Hiel H, Grant L, Mori MX, et al. 2006. Switching of Ca2+-dependent inactivation of Ca(v)1.3 channels by calcium binding proteins of auditory hair cells. *J Neurosci* 26: 10677-89

Ye X, Cai Q. 2014. Snapin-mediated BACE1 retrograde transport is essential for its degradation in lysosomes and regulation of APP processing in neurons. *Cell reports* 6: 24-31

Yeo GW, Van Nostrand E, Holste D, Poggio T, Burge CB. 2005. Identification and analysis of alternative splicing events conserved in human and mouse. *Proceedings of the National Academy of Sciences of the United States of America* 102: 2850-5

Yi BA, Jan LY. 2000. Taking apart the gating of voltage-gated K+ channels. *Neuron* 27: 423-5

Yu FH, Yarov-Yarovoy V, Gutman GA, Catterall WA. 2005. Overview of molecular relationships in the voltage-gated ion channel superfamily. *Pharmacol Rev* 57: 387-95

Yuki N, Hartung HP. 2012. Guillain-Barre syndrome. *The New England journal of medicine* 366: 2294-304

Yun HJ, Park J, Ho DH, Kim H, Kim CH, et al. 2013. LRRK2 phosphorylates Snapin and inhibits interaction of Snapin with SNAP-25. *Experimental & molecular medicine* 45: e36

Zampini V, Johnson SL, Franz C, Lawrence ND, Munkner S, et al. 2010. Elementary properties of CaV1.3 Ca(2+) channels expressed in mouse cochlear inner hair cells. *J Physiol* 588: 187-99

Zhang X, Kim-Miller MJ, Fukuda M, Kowalchyk JA, Martin TF. 2002a. Ca2+-dependent synaptotagmin binding to SNAP-25 is essential for Ca2+-triggered exocytosis. *Neuron* 34: 599-611

Zhang Z, Xu Y, Song H, Rodriguez J, Tuteja D, et al. 2002b. Functional Roles of Ca(v)1.3 (alpha(1D)) calcium channel in sinoatrial nodes: insight gained using gene-targeted null mutant mice. *Circ Res* 90: 981-7

Zhou B, Cai Q, Xie Y, Sheng ZH. 2012. Snapin Recruits Dynein to BDNF-TrkB Signaling Endosomes for Retrograde Axonal Transport and Is Essential for Dendrite Growth of Cortical Neurons. *Cell reports* 2: 42-51

Zhuchenko O, Bailey J, Bonnen P, Ashizawa T, Stockton DW, et al. 1997. Autosomal dominant cerebellar ataxia (SCA6) associated with small polyglutamine expansions in the α(1A)-voltage-dependent calcium channel. *Nature Genetics* 15: 62-69

Zuhlke RD, Pitt GS, Deisseroth K, Tsien RW, Reuter H. 1999. Calmodulin supports both inactivation and facilitation of L-type calcium channels. *Nature* 399: 159-62